COO-3072-17

Princeton University
Elementary Particles Laboratory
Department of Physics

A MEASUREMENT OF THE K_S CONTENT OF THE K^o STATE AND THE BRANCHING RATIO BETWEEN THE K_S 2π DECAYS

DAVID J. SAGER

TECHNICAL REPORT NO. 5

December 1972

Contract AT(11-1)-3072

A MEASUREMENT OF THE K_S CONTENT OF THE K^o STATE AND THE BRANCHING RATIO BETWEEN THE K_S 2π DECAYS

David J. Sager

A DISSERTATION

PRESENTED TO THE

FACULTY OF PRINCETON UNIVERSITY

IN CANDIDACY FOR THE DEGREE

OF DOCTOR OF PHILOSOPHY

RECOMMENDED FOR ACCEPTANCE BY THE

DEPARTMENT OF

PHYSICS

December 1972

TABLE OF CONTENTS

ABSTRACT

The K^o meson state is a superposition of the short-lived and long-lived states, K_S and K_L. The K_S component decays principally to charged or neutral pion pairs. By observing the production of an ensemble of K^o's and the decay of the K_S's we determined: (1) the proportion of K_S in the K^o state, and (2) the branching ratio between the charged and neutral two-pion decay modes of the K_S. We found $R(K_S \rightarrow \pi^+\pi^-)/R(K_S \rightarrow \pi^o\pi^o) = 2.22 \pm 0.08$. Within the framework of a phenomenological theory, the amount of K_S overlap with the K^o state is a test of CPT invariance of the weak Hamiltonian. Our results, in excellent agreement with CPT invariance, yield for the usual CPT violating parameter $\mathrm{Re}\ \delta = -0.0014 \pm 0.0075$.

I. INTRODUCTION

What was very likely a K meson was first reported by Leprince-Ringuet in 1944 as a single cosmic ray event observed in a cloud chamber.[1] Two more strange particle events were reported in 1947.[2] The new particles were called "V particles". In 1949 Leprince-Ringuet observed a charged particle which he called tau[3] and Brown, Camerini et al. observed a three-body decay they identified with the tau which they however referred to as "k" within their paper.[4] Estimates of the tau mass and lifetime were soon made and the decay mode to three pions was favored. By 1951 kappa mesons of about the same mass as the tau which decay to a μ and two other particles were identified. V particles were identified as decaying to products lighter than protons and were called V_2^o's. It was soon known that the new particles were produced about 1% as frequently as pions while, amazingly, their mean lives appeared to be of the order of a nanosecond.[7] By 1953 it seemed very likely that some V_2^o's decayed to two pions and had masses in the tau range.[5] These were called θ^o's by suggestion of the Bagneres Congress. In July 1953 at the International Meeting on Cosmic Radiation at Bagneres-de-Bigore, France, the generic name K was given to particles with masses intermediate between the π meson and the nucleon. Individual K's were to have lower case Greek letters for names. By this time remarks had already appeared in print concerning the closeness in mass of the various K's.[6]

In 1952 Pais proposed the concept of strong and weak couplings so that K's and other V particles could be considered to be copiously produced in pairs by the strong coupling which, however, was not effective in dealing with these particles singly, thus the slow decay by the weak coupling.[8] Similarity between the weak coupling and β decay was mentioned.

Experiments in 1953,[9] including the first artificial production of K's at the new Cosmotron at Brookhaven,[10] favored production of V's in pairs only, "associated production".[11] Later in 1953 Gell-Mann[12] and almost simultaneously Nakano and Nishijima[13] proposed the presently accepted extension of the isospin formalism to the new particles. This idea implied associated production and contained the strangeness concept, although the terms "strangeness" and "strange particles" were not used until 1956.[14]

By 1954 there was pressure to place the then known K mesons together as a single isotopic spin doublet but experimental evidence made it appear that the θ and τ mesons could not have the same spin-parity assignments.[15] The K mesons were beginning in their role as the instrument of destruction of great conservation laws. Shortly after, it was pointed out that if the K's contained an isospin doublet composed of a neutral and positive meson, that there must be a distinct antiparticle to the neutral θ^o. In addition the virtual transition $\theta^o \rightarrow \overline{\theta}^o$ is possible and the particle observed decaying is neither the θ^o nor the $\overline{\theta}^o$ but a mixture. In the same way a θ^o is a mixture of θ_1^o and θ_2^o, the particles which should be observed to decay. The θ_1^o and θ_2^o should have different lifetimes and different decay modes. The prediction was made that "not more than half of all θ^o's can undergo the familiar decay into two pions."[16] A simple form of the theory of neutral kaons outlined in Appendix IV was thus in existence. In 1955 Pais and Piccioni predicted that if this was true an initial θ^o beam could be allowed to partially decay to convert it into a long-lived θ_2^o beam due to removal of the θ_1^o component. When the θ_2^o beam subsequently passes through matter it interacts via the strong interaction removing $\overline{\theta}^o$ from the beam which is converted thereby

to a θ^o beam, again containing fast decaying θ_1^o.[17] (In this same paper the experimental advantages of producing θ^o's for study from a θ^+ beam by charge exchange, the method used in the present experiment, were first pointed out.) In 1956 the long-lived neutral kaon with other than two-pion decay modes was observed and its lifetime measured and principal decay modes discovered.[18]

In 1957 Eisler, Plano, Samios, Schwartz, and Steinberger reported an experiment similar to the present one.[30] They confirmed the prediction that one-half of the θ^o's would not decay in short time to two pions. Their result, in fact, was that 51±7.5% of the θ^o's decay in this way. The branching ratio for two-pion decays of the θ^o was reported as $P(\theta_1^o \rightarrow \pi^o\pi^o)/P(\theta_1^o \rightarrow 2\pi) = 0.14\pm0.06$. The present experiment is largely a repetition of theirs, to much better accuracy, and in the light of events in the intervening years.

Although regeneration of θ_1^o's was not actually observed until 1960,[19] the initially confusing behavior of K mesons was by 1956 beginning to seem remarkably well understood, all except for the nagging difficulty with spin-parity assignments. In pursuit of a solution to this problem Lee and Yang concluded that there existed no experimental evidence for conservation of parity in weak interactions.[20] A year later both parity nonconservation and charge conjugation asymmetry were experimentally observed in ^{60}Co β decay[21] and soon after in the π-μ-e sequence.[22] This resolved the θ-τ puzzle. All of the K mesons may indeed be grouped to form an isospin doublet with strangeness +1, and, presumably, a complementary doublet with strangeness -1. One should not, however, try to infer the parity of the doublet from the decays which give apparently contradictory indications due to parity nonconservation. On the other hand the price for solution of the θ-τ difficulty was the refutation of two conservation

principles previously thought to be among the most fundamental and reliable ideas in physics. In 1957 Landau showed that in fact combined parity inversion and charge conjugation (CP) invariance was sufficient to recover a picture of physics containing a sort of space and charge symmetry that would satisfy the old beliefs.[23] The turmoil settled down for five years until Sachs and Treiman suggested a real possibility of nonconservation of CP as well in 1962.[24] K mesons and the neutral kaon in particular caused another upheaval when Christenson, Cronin, Fitch, and Turlay announced observation of the CP violating 2π decay mode of the long-lived neutral kaon in 1964.[25]

Not only has one sacred conservation law, CP, been shown not to hold but this immediately implies that at least one other must fall as well. Either time reversal (T) invariance or the combined CPT invariance. The principle of T invariance has been considered almost above question all the way back to classical mechanics. Similarly, the CPT theorem of Luders and Pauli[26] shows that, loosely speaking, CPT invariance is a consequence of our very approach to the formulation of theories of elementary particles.

The present experimental situation favors CPT being an exact symmetry while T is not. K^+ and K^- have been shown to have the same lifetimes to within 0.2%[27] which supports CPT invariance in their decays. An analysis of the currently available experimental data reached the conclusion that in the K^o system CP invariance violations are completely compensated by time reversal invariance violations leaving CPT an exact symmetry.[28] Some approximations and reasoning were employed, however. Attempts to directly observe asymmetry under time reversal have failed.[29]

The present experiment tests one consequence of CPT invariance, a

prediction for the fraction of an initially pure K^o sample to decay in a given time, in this case, six mean lives of the short-lived neutral kaon. In addition this test is made with decays of the same particles used to show CP invariance violations. Although, due to the accuracy achieved, the present experiment does not settle the question of CPT invariance, it does represent essentially the only measurement of one of the K^o propagation parameters (see Appendix IV).

In essence, the strangeness concept was invented so that certain decays of strange particles would have to be $\Delta I = 1/2$ transitions while stronger interactions could only induce whole integer isotopic spin changes. The weak interaction provided the half integer isotopic spin changes. Right from the beginning it was very easy to think of a $\Delta I = 1/2$ selection rule for weak decays as at least a first approximation. As more details were learned about weak decays this selection rule seemed more and more to be an accurate description. Only a very small violation of the $\Delta I = 1/2$ rule was evident from the presence of $K^+ \rightarrow 2\pi$ decay. The rule immediately predicts that the rates for $K^o \rightarrow 2\pi^o$ and $K^o \rightarrow \pi^+\pi^-$ are in the ratio of 1:2 (see Appendix V). The experiment of Eisler et al. in 1957 gave very large departure from this prediction. Another experiment in 1959 disagreed with Eisler and found $\Delta I = 1/2$ to be good.[31]

In the first four years of the 1960's several more experiments measuring the branching ratio of neutral 2π decays of the K^o were reported.[32-35] The best of these reported $\pm 4.2\%$ accuracy. The agreement between the experiments left much to be desired but it was clear that the $\Delta I = 1/2$ rule was at least a good approximation for these decays but that a slight admixture of $\Delta I = 3/2$ transitions may be

indicated. Two of the experiments[33,34] also reported values for the fraction of K^o decaying to two pions, substantially improving on the accuracy reported by Eisler et al.[30] The world average was then 0.505 ± 0.016. Three recent measurements of the K_S^o branching ratio,[36-38] which has come to be expressed as $R(K_S^o \rightarrow \pi^+\pi^-)/R(K_S^o \rightarrow \pi^o\pi^o)$, have been made with improved accuracy but the agreement between experiments was still not good.

A brief description of the entire experiment will next be given as an orientation before entering into a detailed discussion of each part.

A separated K^+ beam at 620 MeV/c from the AGS was brought into the 30-inch BNL bubble chamber. A portion of the beam charge exchanged with the deuterium filling the chamber ($K^+d \rightarrow ppK^o$). Due to strangeness conservation in this reaction a pure K^o state was produced. The K^o did not emerge with a momentum much higher than the K^+ momentum so that the mean length of flight of the K_S component was limited to several centimeters. Only a small fraction of the K_S produced in the defined fiducial region could escape the chamber, but almost all of the K_L produced anywhere in the chamber escaped. The K_S decays most frequently to π^+ and π^- and about half as frequently to $2\pi^o$'s. The few other reported decay modes are relatively rare (fraction of decays to other products is $< 3.1 \times 10^{-3}$).[64]

Potential K^o production events were found by visually scanning the film for the two proton signature (allowing for the possible invisibility of one proton track) and productions were verified by kinematical reconstructions combined with visual estimates of the relative bubble densities of the tracks. Frames in which a K^o production had been verified were rescanned for a nearby characteristic V indicating a decay to

π^+ and π^-. Since the other principal decay mode usually leads to only neutral particles (4 gammas) it is not directly observable in a bubble chamber. The neutral decays were indirectly detectable because the chamber had been fitted with a pair of coaxial stainless steel cones. Gammas penetrating the stainless steel had a useful probability of producing electron pairs observable in the bubble chamber. An independent search was made for electron pairs that could have been produced as a result of the neutral mode decays of the identified K^o's. The electron tracks were measured to determine the energy of each gamma and its trajectory, allowing elimination of many background events. The total number of neutral decays was determined statistically from the gamma information.

Since about half of the K_S neutral decays actually resulted in one or more observed electron pair gamma conversions, the problem of the detection efficiency of this apparatus is crucial. Accordingly, film was taken while using a 400 MeV/c positive pion beam. A fraction of the beam penetrating the chamber charge exchanged with the deuterium producing neutral pions which immediately decayed to pairs of gammas and by the $\gamma e^+ e^-$ (Dalitz) mode. The two-proton signature of the charge exchange is similar to the signature for kaon charge exchange and π^o productions were found and verified in close analogy with the kaon case. By design, the γ's produced and the resulting electron pair conversions were also similar to the ones produced by the kaon exposure. The pion exposure film was scanned for electron pairs potentially the result of decay of π^o's from the identified charge exchanges. Measurement of the electron tracks allowed elimination of most of the already small number of background γ's and indicated the accuracy with which the direction of origin

and energy of a γ could be determined. A Monte Carlo simulation program was written so that with minor modification the production of conversion electrons either from the pion beam initiated events or from the kaon beam initiated events could be simulated. The program was adjusted to accurately reproduce the statistical properties of the pion beam subexperiment and was then used to simulate the kaon beam subexperiment, to determine the detection efficiency for K_S to two neutral pions decays.

Table I summarizes the computation of the results. It is useful to refer to this Table as the various individual details are discussed to see the role of each detail in obtaining the final results. In the discussion of the experimental methods certain results from the theory of the conversion of γ rays, such as the fact that the resulting electrons indicate the direction of the γ, are implicit. An outline of this theory appears in Appendix III.

II. APPARATUS AND METHODS

A. K^+ and π^+ Beams

Beam was used from the Alternating Gradient Synchrotron at Brookhaven National Laboratory in several runs between January and August 1968. Momentum and mass selection took place in the low energy 1A beam transport[39] leading directly into the 30-inch BNL bubble chamber (see Appendix I for details of the beam line).

1. The K^+ Beam

Good momentum resolution in the beam entering the chamber is important in achieving accurate kinematical reconstructions and mass purity is essential. Either protons or pions in the incoming beam could produce events with one or two protons emerging as the only visible particles -- events which might be mistaken for K^o productions. The 1A beam transport was carefully studied and tuned and counters with the appropriate electronics were installed to monitor performance (details in Appendix I). The careful computation of beam trajectories, neglecting multiple scattering, indicated that all particles with momentum 0.5% or more off the tuned momentum and all π's and protons originating in the target would be easily excluded. Multiple scattering does indeed take place, however, and the target to chamber distance of about 22 meters is 4.7 mean decay lengths of K^+ at the beam transport momentum so that a substantial π and μ flux is generated in the transport itself, much of it in the first half where the particle density was high. Time-of-flight studies over the second half of the beam line during the entire run indicated 1.2±0.6% light particles entering the beam port of the chamber. The light particles should have been pions, muons, and electrons.

Since most of the light particles result from decay in the beam line (largely from π decay and $K\mu$ and $K\pi$ decays), it is thought that a large number of these light particles were relatively innocuous muons. A time-of-flight spectrum taken midway in the run is presented in Fig. 1. The K's and light particles are readily distinguished by time of flight.

Looking again at the time-of-flight spectrum (Fig. 1), assuming the light particle peak to be produced by particles of pion mass at the same momentum as the kaons, one observes that the separation of the peaks gives 608±21 MeV/c for the mean transport momentum. The assumption that the light particles are of muon mass leads to a mean beam momentum of 621±21 MeV/c. This is in better agreement with the momentum from the beam magnet excitation data (632 MeV/c) and the momentum determined from a study of τ decays (615 MeV/c plus an estimated 10 MeV/c loss in penetrating the chamber window for a total of 625 MeV/c in the transport) but the large errors in the time-of-flight figures limits the usefulness of this as evidence that the light particles were muons and not pions. The width of the K peak represents 25 MeV/c FWHM but this is dominated by the time-of-flight system resolution. Figure 2 is a range curve taken in copper near the chamber beam port, selecting the K peak by time of flight. One can expect little attenuation of the beam until the copper is thick enough to stop secondary particles (e.g., protons) from interactions. The flat part of the curve up to about 2.5 cm of copper (range of about 525 MeV/c protons) is expected. The curve from 2.5 cm to the knee at about 12 cm suggests an exponential attenuation with about 30 cm interaction length which is reasonable for positive kaons. The range is 12.37±0.2 cm. This would be expected for a mean beam momentum of 624 MeV/c. The sudden drop in counting rate in an interval about 0.4 cm wide from 12.17 cm to

12.57 cm shows that most of the particles were in a momentum bite 10 MeV/c wide at worst.

2. The π^+ Beam

Exactly the same apparatus was used for the 400-MeV/c pion beam but the separation requirements were a little different. Selection of the numerous pions and rejection of the rarer kaons were much easier than obtaining a kaon beam free of pions and were all the easier due to the lower momentum. No attempt was made to reject muons. A pion beam of this low a momentum from the AGS is however likely to be accompanied by a deluge of electrons which shower to produce many electron pairs in the chamber. The electrons were avoided by taking the proton spill on the target early in the AGS acceleration cycle (at 400 msec) when the circulating proton energy was low (about 13 BeV).

As discussed in paragraph C, the τ decays in the kaon beam can be used to determine the beam momentum but no such simple means is available to accurately calibrate the pion beam momentum. For the pion beam the bending magnet currents were carefully scaled from the tuned values for the kaon exposure according to the nonlinear magnet excitation characteristics[40] so the pion beam momentum would be known in terms of the accurately calibrated kaon beam momentum.

B. The Bubble Chamber

The 30-inch BNL bubble chamber was run filled with deuterium so that the positive meson beams would charge exchange with it. The required γ detection efficiency was achieved through the placement of metal converters in the chamber and extensive modification of the optical system (see Fig. 3).[41]

Two stainless steel cone sections were placed in the chamber such that they were coaxial with the chamber and their apices were coincident at the camera optical plane. Refraction of light at the various media interfaces was taken into account so that a camera placed on chamber axis viewed the entire active volume (with obvious insignificant exceptions; see Appendix II). The optical system was composed of "Scotchlite"[42] retrodirective reflector on the flat chamber bottom plate and cone base rings, polished silver reflective plating on all cone surfaces, and a new camera plate with four 70-mm cameras. One camera was on cone axis (camera 4) and the other three were placed symmetrically around it. Ring flash tubes around each camera lens were used. In this way essentially all the volume of the chamber was visible in some pair of views and 95% was visible in a pair excluding view 4. The cones were approximately 0.42 cm thick each, which is about 1/4 radiation length. Considerable attention was paid to the cyrogenic and optical properties of silver-plated stainless steel, thermal expansion effects on the cone mountings and the possibility of induced bubbling in deuterium at points on the cones and mountings. Experience showed that the electrical properties of the cones were important in the event of a rapid change in the chamber magnetic field. Engineering data on the cones and optical system is available in Appendix II.

A right-handed coordinate system was defined in the chamber which is implicitly used throughout this presentation. The chamber fiducials were scribed on the inside surface of the chamber window (in contact with the deuterium) and this surface is the XY (Z = 0) plane. The origin is defined as the center fiducial and is very nearly on chamber axis. The X axis is defined in terms of certain other fiducials. All points

in the deuterium have negative Z values. The positive Y axis points toward the expansion piston. The beam enters near the negative X axis curving to leave the chamber at positive X and Y.

The deuterium filling the bubble chamber may not have been completely pure. Hydrogen contamination is relatively unimportant since any background reactions it could cause could also occur as deuterium reactions anyway. Troublesome concentrations of heavier nuclei were not present since the film would have contained characteristic reactions with extra protons and only about five such events were seen in film containing 10,000 charge exchanges.

C. Operating Parameters

Many of the optical parameters of the 30-inch chamber such as window thickness and indices of refraction were taken from BNL engineering measurement reports. The camera lens to fiducial plane distance and the distances between cameras were taken from engineering reports on the new four-camera optical board. The remaining optical parameters are two coordinates for the four-camera assembly, an angle of rotation of the assembly and the index of refraction of deuterium at camera flash time. Careful measurement of the front and back fiducials in the four views on film determined the rotation angle. The camera assembly coordinates were adjusted from nominal values to minimize error estimates from the reconstruction programs. The index of refraction of deuterium was adjusted to reconstruct the nominal depth of the back fiducial. The optical parameters were independently determined for each of three assemblies and fillings of the chamber involved in the run. Resulting camera assembly positions varied by less than 2 mm in the three determinations.

The rotation angle varied by 0.08 radians. The absolute error in coordinates of a point in the chamber is proportional to the error in camera assembly coordinates with a proportionality factor ranging from 0 at the fiducial plane to about 0.2 at the bottom of the chamber. However, since few events extend over the entire depth of the chamber this is a generous limit on resulting event distortion. Values of optical parameters are available in Appendix II.

The chamber magnetic field was carefully mapped and fit with a set of 30 polynomials to an overall accuracy of about ±0.2% over the entire chamber volume several months before the film-taking runs.[43] Fifty-seven τ decays were easily identified in a portion of the K^+ beam film. These were carefully measured and kinematically reconstructed. The fit to the shape of the chamber field with an overall adjustable factor was used for the field and the overall factor was varied so that the combined mass of the π's measured 493.82. The best value for the overall factor was one so that the field actually used corresponds exactly to the mapped field in the case of the K^+ beam film. Having established the magnetic field in the chamber, we computed the beam momentum from the decay product momenta for the 57 τ's. Energy loss in deuterium was allowed for at the rate of 0.540 MeV/cm to determine the momentum of the beam entering the chamber (at $X = -35.0$ cm in our coordinate system to be exact). The momentum was found to be 615 MeV/c with a standard deviation of 7 MeV/c. This is in good agreement with the time-of-flight value and the range data if account is taken of loss in penetrating the entrance window of the chamber.

For the π exposure the chamber magnet current was brought to 2/3 the value for the K exposure so that beam curvature would be approximately

the same. The actual field strength was determined from the curvature of beam tracks and their momentum which was determined from the bending magnet currents. The currents themselves were determined by scaling from the kaon beam values according to measured nonlinear excitation characteristics for the magnets.[40]

D. Scanning and Measuring

Film from the four cameras is on four separate 70-mm rolls of Kodak Recordak Microfile with mylar base -- about 2300 frames per roll. The views were conventionally numbered with the chamber-cone axis view numbered 4 and the surrounding cameras numbered 1 (over entrance port), 2 (over expansion piston opening), and 3.

Scanning was done on three-view Prevost scanning tables with overall magnification to the fiducial plane of just over one. Since camera 4 views the entire chamber, scanning was done principally with view 4, using two of the remaining three views more for examining specific features in a different perspective than for searching. Measuring was done in a selection of three of the four views. Three types of measuring machines were used: the Mangiospago image plane digitizers had a least count of about 5 microns on film which is about 60 microns in the chamber, and an overall magnification to the fiducial plane near unity. These machines were controlled by an on-line computer system which supervised the measuring operations and collected data. The Vanguard film plane digitizers had a least count of about 2.5 microns on film corresponding to 29 microns in the chamber and a magnification of about 1.4 overall to the fiducial plane. Versions of the Vanguard were used both on-line to the same computer system as the Mangiospagos and operating directly into

a card punch. Most measuring was done with views 123 on the machines. When possible, points were taken in all three views. At times, more often when measuring electron pairs from γ conversions in the cones, measurements of particular tracks could be made in only two views. Again due to the obscuring of tracks in certain views by the cones, it was occasionally necessary to replace one of the views 123 with view 4 and measure in view 4 and one or two of the remaining views.

Reconstruction and event fitting was first done on various models of IBM system 360 computers with the CERN bubble chamber program package THRESH-GRIND. Later the reconstruction and fitting was done on a CDC 6400 with the Berkeley programs TVGP-SQUAW. Both of the reconstruction-fitting packages were modified to allow for momentum loss when tracks penetrated the stainless steel cones. Extensive use was made of both computing systems with programming specifically written for this experiment for data processing subsequent to reconstruction and fitting and for Monte Carlo simulations.

Only the region of the bubble chamber inside of the inside surface of the large cone was searched for charge exchanges. In addition the scanners did not look for or accept potential charge exchanges produced by beam tracks far outside of the beam region, by beam tracks entering the chamber at a much different angle than the majority or with a much different curvature. Perhaps 5% of the beam was discounted in this way. Interactions that could be seen to have taken place in the metal of the small cone were ineligible for consideration as charge exchanges. After potential charge exchanges were found, measured, reconstructed and fitted they were reviewed by an experiment-specific post fitting program. Checks were made for adequate measurement quality and successful reconstruction.

The interaction point was required to have Z coordinate between -21.0 and -12.0 cm. The beam track was required to have a dip between -0.10 and +0.11 (radian) and to be parallel to the mean beam track in the XY plane to $\pm 3^{o}$. All nonstopping secondary tracks were required to have dips less than 60 degrees, so that accurate bubble density estimates could be made.

III. THE PION BEAM SUBEXPERIMENT

A. The Charge Exchange Vertex

The 400 MeV/c pion beam probably contained a large muon contamination and there may also have been some electrons. Protons at 400 MeV/c would stop in the chamber and produce tracks with high bubble density. Very few high bubble density or high momentum tracks were seen and no events initiated by such beam tracks were accepted as charge exchanges. The muons and electrons have such a low cross section for producing anything that might be confused with a $\pi^+ d$ charge exchange that they would be no serious cause of background even if they outnumbered the pions. A kaon contamination in the beam can be ruled out because of the ratio of pions to kaons at the target in this momentum range (which is known to be several hundred to one), the fact that the beam transport is about seven times the mean free path of kaons at this momentum, and by the absence of typical V decays associated with charge exchanges.

Recalling, in addition, the description of the bubble chamber, we can assume that a pure π^+ beam interacted with a pure deuterium target. The 400-MeV/c beam momentum is above threshold for single pion production only. The reactions with significant cross sections which might look like $\pi^+ d$ charge exchange are:

0.	$\pi^+ d \rightarrow pp\pi^o$	21 mb (Ref. 44)
I.	$\pi^+ d \rightarrow pp\pi^o\pi^o$	0.3 mb (Ref. 45)
II.	$\pi^+ d \rightarrow pp\gamma$	0.19 mb (Ref. 46)
III.	$\pi^+ d \rightarrow pp$	2.8 mb (Ref. 47)
	$\pi^+ d$ total	105 mb (Ref. 48)

No reactions with charged pions in the final state are considered since

the identification of the charged pion as a light particle was readily made to reject such events. For each of the four reactions the corresponding reaction with, in addition, photons in the final state is possible. The cross sections for such reactions are very small unless the photons are of low energy, and rise rapidly as the photon energies approach zero. If any effects due to such photons were significant the numbers of detected photons would show a rise at low photon energy observable in Fig. 22 to be discussed below and no such effect was seen. Furthermore, even reaction III is not a background since it is distinctive kinematically and could rarely be confused with the desired charge exchange. The minimum proton momentum in reaction III is 443 MeV/c and can occur only with that proton going backwards in the lab. In the case of the charge exchange, reaction 0, the spectator proton has a momentum greater than 350 MeV/c only 1% of the time and when the slow proton is this fast it must go forward in the lab. In the case of reaction III, both protons should usually leave the chamber without stopping, while in the case of reaction 0, one proton will nearly always stop.

From the cross sections presented it is found that the probability of any interaction is about 0.52 per meter of track length. With a nominal ten tracks per frame and a 0.5-meter track length within the fiducial volume, 2.6 interactions should be expected per frame with a charge exchange occurring about once in two frames. The sample of identified charge exchanges will contain 97.7% simple charge exchange (reaction 0), 1.4% of reaction I which produces twice as many γ's, and 0.88% of reaction II which produces only one γ.

Ten rolls (23,000 frames) were triple scanned for charge exchanges and 10,983 charge exchanges were identified (Table I, line 1). Approxi-

mately 880 examples of reaction III were noticed and were not included in the charge exchange sample. Physicists examined the sample of charge exchanges at the same time that the searches were made for electron pairs.

The events found in the first two rolls were measured, reconstructed and fitted to the charge exchange and elastic scattering hypotheses. The post fitting program checked fits for consistency between visually estimated relative ionization of each track and $1/\beta^2$ for that track. In the remaining eight rolls charge exchanges were measured only when electron pairs were associated.

B. The Detection of the γ's

The frame in which each event in the sample of $\pi^+ d$ charge exchanges occurs was carefully examined by physicists for γ conversions in three separate passes. Electron pairs produced in the liquid anywhere in the chamber were acceptable. For conversions in the metal cones, at least one positron was required to be identified along with whatever negatrons were present, or, if there was no positron at least two negatrons were required. Conversions in the metal were not acceptable if they occurred in the rings at the bottom of the cones which formed part of the structure mounting the cones to the chamber back plate or in the legs attached to the rings. Further, conversions in the thin strips of metal remaining when the large rectangular expansion holes were cut in the cones were not acceptable.

A 400-MeV/c pion charge exchanging with deuterium results in γ's with momenta in the range from 11.4 MeV/c to 412 MeV/c. The average laboratory energy of the γ's was 168 MeV and the average energy loss due to

the electrons penetrating the metal was 33 MeV. Thus the total emerging energy in a γ conversion averaged about 135 MeV, shared randomly between two electrons in the usual case. The efficiency for detecting electrons emerging from the metal dropped off as the momentum of the electrons went below about 1 MeV. It was not even attempted to find all the conversions with total emerging energy of all electrons less than 5 MeV. The presence of all γ's was recorded except when the directions of the emerging electrons left no hope of their pointing back to within some eight centimeters of the charge exchange. About 3800 γ's were recorded.

The charge exchange events with associated conversions and the electrons resulting from the conversions were measured and reconstructed. The main vertex was fitted to the charge exchange hypothesis (one constraint) to compute the neutral pion trajectory. From this information four parameters relating to the degree to which the γ appeared to come from the charge exchange were computed. The direction of the γ trajectory was first estimated as the sum of the electron momenta, which together with the conversion point determined a line. The distance of closest approach of this line to the charge exchange is termed "DL". If the line segment along which DL is measured is projected onto the fiducial plane (XY plane), the length of the projection is "DLXY". The distance between the point of closest approach to the charge exchange and the conversion point is "L". The γ energy was estimated as the total electron energy emerging from the conversion plus a nominal energy loss due to ionization. The thickness of metal intersected by the γ trajectory was halved to get an estimate, correct on the average, of the distance the electrons traveled through the metal. An ionization loss of 15.82 MeV per centimeter was ascribed. The γ direction was again computed,

this time as the direction from the charge exchange to the conversion point except when the distance between these points was less than 5 cm, in which case the previously described estimate was used. The fourth parameter to be computed was the γ energy in the neutral pion center of mass.

Figure 8 shows the momentum distribution in the neutral pion center of mass obtained as described in the previous paragraph. The distribution is plotted separately for conversions in the stainless steel cones and in the liquid (including Dalitz mode decays). In both cases the peak occurs at 67 MeV/c and the frequency falls off more slowly on the low momentum side than on the high side. On the high momentum side the rate is down to 50% at 12 MeV/c above the peak for the conversions in the metal, and the fall off is only slightly faster for the conversions in the liquid.

Figures 9a,b,c present the frequency distribution of DL and of DLXY as described above. The distributions include all values of L and are broken down into four ranges of laboratory γ energy for γ's converted in the metal converters, and conversions in the liquid are represented in a fifth category. The DL distribution for conversions in the metal for γ energies above 150 MeV shows a strong peak for DL less than 1.2 cm. DLXY is much less affected by the poorer accuracy of depth measurements (Z coordinate) than is DL and depends almost exclusively on the more precisely measurable XY coordinates. This parameter shows a strong, sharp frequency peak below 1 cm with very little tail above 1 cm. The distributions of DL and DLXY for conversions in the liquid are similar but the peaks are still sharper and narrower. For the conversions in the metal the peaks in the DL and DLXY frequency distributions become

progressively broader and flatter as the γ laboratory energy decreases. Finally, for γ's with energies less than 50 MeV, the frequencies rise almost linearly as DL or DLXY is reduced from 6 or 7 cm to zero.

A detailed study of the two-dimensional frequency distributions of L and DL and of L and DLXY broken into the same five categories of γ energy and conversion in metal or liquid was made. For each category two piecewise linear functions were decided upon to be limits on DL and DLXY for a given value of L. The functions were chosen to include the frequency peaks with room to spare and to only exclude a fairly flat background of about 1% of the events. These functions are represented in Fig. 10. A γ was considered correlated with a charge exchange only if the corresponding values of DL and DLXY were both less than the limit for the value of L. The γ's with momenta more than 115 MeV/c in the neutral pion center of mass were closely studied and if the reason for the high momentum could not be found (incorrect or inaccurate electron measurement or poor fit to the charge exchange hypothesis at the main vertex, for some examples) the γ was considered not correlated with the charge exchange.

C. γ Background

Frames containing no charge exchanges selected from the π exposure film were scanned for elastic scatters and then for γ's, just as if the elastic scatters were charge exchanges. We studied 7572 elastic scatters. In those cases where γ's were found, the scatter vertex and the conversion electrons were measured in the same standard way as for pion charge exchange events. The parameters L, DL, and DLXY were computed, and, if the DL and DLXY were not within the limits used for the primary events (Fig. 10), the γ was taken to not be correlated with the

event. For those scatters with a γ remaining, neutral pion momenta and directions were simulated to go along with the measured vertex point to completely simulate pion charge exchange. The γ energy in the simulated neutral pion center of mass was computed in the conventional manner. For each elastic scatter, 1000 neutral pions were randomly generated to determine the probability that the γ momentum in the center of mass would be less than 115 MeV/c. Each γ was given a weight equal to this probability and the weighted sum was divided by the number of scatters studied to determine the γ background rate. The background rate was found to be 0.54% background γ's per charge exchange. In the same way each γ was weighted according to the probability that it would have a momentum greater than 115 MeV/c. The rate for high momentum background is 0.71% γ's per charge exchange. The high momentum background is not really a background because high momentum γ's were deleted from the sample of charge exchange correlated γ's. Rather, it is a check on the method of measuring the low momentum background. The observed number of γ's matched with real charge exchanges, with DL and DLXY parameters within limits, but with center-of-mass momenta higher than 115 MeV/c, was 80, giving a rate of 0.73% high momentum γ's per charge exchange in excellent agreement with the background determining analysis.

D. Results

A total of 3781 γ's were correlated with the 10,983 events charge exchange sample (Table I, line 2). Of these γ's 60 were background (10,983 charge exchanges times the 0.54% background rate described in paragraph C) (Table I, line 3). Since 1.4% of the charge exchanges produced two extra

γ's, and 0.88% produced only one (from paragraph A), a total of 0.96% excess γ's were produced. The data is equivalent to 3686 γ's detected from an ideal sample of 10,983 charge exchanges (Table I, line 5). The overall γ detection efficiency was then 16.8%. This is the result of both triple scanning for charge exchange vertices and searching for γ conversions three times. The result after only double scanning for both features differed by only 0.2% from the triple scan result. The statistical error on the γ detection efficiency is 1.5%, computed according to binomial distribution formulas (Appendix VII), and other errors are insignificant at this statistical level.

IV. THE KAON BEAM SUBEXPERIMENT

A. The Charge Exchange Vertex

It is known that although the 620 MeV/c K^+ beam entering the chamber may have been contaminated with protons, pions, and muons, the total contamination was not more than 2% at worst (see Section II, paragraph A). A small muon contamination is totally harmless due to the very low cross section for muon interactions. A specific search was made for pion interactions and this will be discussed in the following paragraphs. The proton contamination was found to be negligible but it is more convenient to support this point in a later paragraph.

Considering then the reaction of 620 MeV/c positive kaons with deuterium with faith in the conservation of strangeness and baryon number, we observe that the final state must consist of two nucleons, a kaon and possibly a pion. The possible reactions are:

0.	$K^+d \rightarrow ppK^o$	6.6 mb (Ref. 49)
I.	$\rightarrow ppK^o\pi^o$	0.1 mb (Ref. 50)
II.	$\rightarrow ppK^+\pi^-$	0.1 mb (Ref. 50)
III.	$\rightarrow pnK^+$ or dK^+	19.3 mb (Ref. 51)
IV.	$\rightarrow pnK^+\pi^o$ or $dK^+\pi^o$	0.05 mb (Ref. 52)
V.	$\rightarrow pnK^o\pi^+$ or $dK^o\pi^+$	0.14 mb (Ref. 52)
VI.	$\rightarrow nnK^+\pi^+$	0.008 mb (Ref. 53)
	K^+d total	27 mb (Ref. 49)

In addition there is the possibility of photons in the final state as well. The cross section for each of the reactions, with photons in the final state as well, is very small unless the photon energy is low. Reaction I can be thought of as the desired reaction producing a K^o but in addition producing a pair of high energy photons from decay of the π^o. Thus reaction I, and the small probability of photon production (with energy above 1 MeV) along with a charge exchange, just add a background γ flux to the γ's originating from decay of K^o's. A highly effective treatment of the background γ flux, equally applicable to γ's from charge exchanges with pion or γ production or to an external γ flux, will be presented.

Reaction II might be mistaken for reaction 0 with very quick decay of K^o to π^+ and π^-. Besides the low cross section of reaction II compared with 0, the number of events described by reaction II in our charge exchange sample would be further reduced since many would not kinematically fit simple charge exchange. For reaction II, the maximum K^+ momentum is 350 MeV/c and at this momentum a kaon leaves a bubble density three times as high as a pion. Kaons and pions are separable by track ionization down to well below 100 MeV/c but at these low momenta the kaon track should always end in the chamber. K^+ and π^+ decays were readily distinguished.

Reactions V and VI each have two charged tracks, both positive and one track is a pion. The pion track was easily distinguished from a proton track to eliminate examples of these reactions from consideration as charge exchanges. It remains to select charge exchange, reaction 0, from reactions III and IV. The problem resolves itself into selecting those reactions with only one or two proton tracks

visible from those occurring about three times as often with a charged kaon emerging.

A track ending in the chamber, when intelligently examined, can be called a proton and not a kaon with almost complete confidence, for the purposes of this experiment. Consider the probability of error in such a case. If a kaon track ends in the chamber, it must either charge exchange at the endpoint or else decay. A K^+ decay is readily recognized so that a secondary K^+ track that ends in the chamber and is mistaken for a proton must be charge exchanging at the endpoint. In addition the track must be of low momentum near the endpoint, below about 200 MeV/c if the track ends in the liquid or below about 300 MeV/c if it ends in the metal cones, or it could not be mistaken for a stopping proton. First, although there are three times as many events with K^+ secondary tracks to be separated from events with only proton secondary tracks, phase space favors higher momentum kaons. Secondary K^+'s with such a low momentum occur less than half as frequently as stopping protons. Secondly, a K^+ with this low a momentum should decay rather than charge exchange with a probability greater than 99% (the CE cross section is about 1 mb or less). In addition charge exchanging kaons have associated V's in 1/3 of the cases. Thus, if V decays are not looked for in deciding whether a track ending in the chamber is a K or a proton, then a later search for V's associated with endpoints can determine the level of accuracy of the decision process. Only two events were found where such a V was seen.

The more difficult decision is to determine the nature of the faster, often nonstopping track. As a simple model of the problem with which to study kinematics, consider K^+n charge exchange compared

with K^+n scattering. Figure 11 presents the momentum of the outgoing charged track in terms of its angle with respect to the incoming 615 MeV/c K^+ beam for the two reactions. The curves cross at 470 MeV/c. For a track in the vicinity of 470 MeV/c it is not possible to discriminate between scatters and charge exchanges on a kinematical basis alone.

Figure 12 presents the expected bubble densities of K^+ and proton tracks in terms of momentum. Bubble densities may be judged visually, by comparison with the beam track, over the range from minimum (1) to about five times minimum, and with experience to a resolution of about a factor of 1.5, quite reliably. For tracks with a momentum above 275 MeV/c identification by bubble density is practical, while lower momentum tracks should stop if they are protons. Figure 13 presents the momentum loss in penetrating 5 mm of stainless steel for a K^+ and for a proton in terms of momentum. The amount of momentum change, as evidenced by bubble density changes and curvature changes, when a track penetrates the cone was of great help in identifying tracks. The presence of the cones also increased the probability of tracks stopping in the chamber.

About 35 rolls of the K^+ exposure film were triple scanned for charge exchanges by the scanning staff. The scanners looked for all one and two prong vertices with only protons emerging, or three prongs with one proton emerging or four prongs with two protons. The scanners rejected vertices with a definitely identified K^+ in the final state. Those vertices with two proton tracks which both leave the chamber were rejected. There was therefore always at least one stopping secondary track that could be identified with great confidence, and its momentum

was known from range as well as curvature. The scanners were carefully trained to use track curvature and relative bubble densities to distinguish protons from kaons but were instructed to call the track a proton in a case of real doubt. All tracks ending in the chamber and showing no sign of decay were taken as protons. Considerable attention was devoted to insuring that the scanners did not realize the significance of V decays or γ conversions.

All of the potential charge exchanges found by the scanners were measured (and remeasured several times when necessary) to get a kinematical reconstruction. The fitting programs tried the K scatter and K charge exchange hypotheses. A post fitting program tested all fits for consistency with visually estimated ionizations and proton range. Checks were made that supposed stopping points were inside the chamber.

Physicist scan requests were generated for all events consistent with the charge exchange hypothesis even when the K scatter hypothesis was more likely. About 14% of the events were not actually charge exchanges -- most of them having been marked as suspicious by the post fitting program. Physicists looked at each of the supposed charge exchanges to make a final decision as to whether it really was a charge exchange or not. In making this decision the physicist had the benefit of complete kinematical information for the charge exchange hypothesis and for the scatter hypothesis if a fit could be made to scattering. Using this information the physicist checked for correct measuring technique, double checked bubble densities, and checked for momentum loss along tracks, especially where tracks penetrated the metal. Supposed stopping points were scrutinized. Most of the 14% background in the event sample was readily removed. In less than 1% of the cases was the

physicist unsure of his decision. A second pass was made by physicists on the film to check the decisions made on the first pass.

From the charge exchange cross section it is expected that the about 75,000 frames scanned would contain about 1 charge exchange per 5 frames (with a nominal 0.5-meter per track in the fiducial volume and 10 tracks per frame), for a total of 15,000 events. Table A summarizes the nature of the identified charge exchanges. From the original sample of 23,143 events found by the scanners, the post fitting program rejected 7382. Rejection was most often due to inconsistency with our defined limits on track dips, beam direction, etc., and sometimes because the event fitted well to the scatter hypothesis (including identification of stopping tracks as protons and using ionization and range data) and did not fit charge exchange. The physicists then rejected another 2158 to give the final sample of 13,603 charge exchanges. Ideally no charge exchanges with two nonstopping proton tracks should appear, but in fact 94 such events were found to be in the final sample.

Table A

Total charge exchanges	13603
One proton visible	8163
Proton nonstopping	4382
Proton stopping	3781
Two protons visible	5440
One proton stopping	2934
Two protons stopping	2412
Residual two protons nonstopping events	94
Events consistent with K scatter according to post fitting program	439
Events already rejected by post fitting program	7382
Events already rejected by physicists	2158

B. K^o Decays

At the same time the charge exchange vertices were being checked the physicist searched for possible K^o decay products. The fitted direction of the K^o was at hand and the mean length of flight of the K_S was 2.14 cm. When a V decay was identified the distance from the charge exchange vertex to the V vertex was measured with a ruler. The physicist scanned the entire chamber for converted γ's just as in the pion beam subexperiment, but account was taken of the possibility of a K^o length of flight of 10 cm or more, so that a conversion pair need only point to somewhere along the trajectory, not necessarily to the charge exchange vertex. A conversion pair was not recorded if there was no hope of its pointing to within 8 cm of the reconstructed K^o trajectory. The same rules of acceptability were imposed on the conversion pairs as in the pion beam subexperiment. Either a positron must have been identified or a minimum of two negatrons. Conversions in the rings at the bottoms of the cones were not accepted, etc. Laboratory energies of γ's from K^o decay were in the range from 7.2 MeV to 630 MeV. The mean energy was 160 MeV and the mean energy lost by electrons in penetrating the steel was 30 MeV so that the emerging energy averaged 130 MeV shared randomly between 2 electrons in most cases. For each γ conversion recorded the physicist scanned the chamber for possible alternative sources of the γ. These took the form of K^+ decays and pion charge exchanges from K^+ decays or from K^o V decays. All charge exchange events were scanned for conversion γ's in the same way irrespective of an identified V decay. Scanner's reports were punched on cards. The reports were redundant and programs made consistency checks to reduce the chance of keypunch errors. The scanner's reports were added to

the charge exchange vertex fit data and checks were made to insure that each event had been looked at and that each event was represented in the data only once in spite of possible duplicate measurements. The programs then generated decay product measurement requests for those events with reported γ conversions. Each event was scanned twice in this manner by physicists.

Table B presents a summary of the results of the scans for decay products.

Table B

Charge exchanges	12970
Events with no V decay	8410
With no V but with γ's	2235
Events with V decay	4560
With V and with γ	620
Total γ's	3617
Total γ's possibly from a K^+ decay	1761

Note: the last two rolls of film have not been processed for decay products and do not appear here but were included in Table A.

The 620 events with both V decay and γ's reported to first approximation could not have actually produced γ's, so that a substantial background γ flux is evident in the raw scanning results. This is again shown by the fact that nearly half of the reported γ's have an alternative possible source identified.

The reported γ conversions and K^+ decays, which could alternatively have been the source of the γ's, were measured and kinematically reconstructed. In scanning, one-prong events initiated by a beam track were selected for measurement as possible K decays. These events would be K^+n scatters, $K_{\mu 2}$ and $K_{\pi 2}$ decays and three-body decays including K_{e3}, $K_{\pi 3}$, and $K_{\mu 3}$. A scatter or $K_{\mu 2}$ decay does not lead to γ production but $K_{\pi 2}$ and various of the three-body decays do result in neutral pions and therefore γ's. In the single case of the $K_{\pi 2}$ decay the neutral pion momentum is reconstructable from the decay vertex. The supposed decays were fitted to K^+ scatter, $K_{\pi 2}$, and $K_{\mu 2}$ hypothesis. In case there was a fit but there was no $K_{\pi 2}$ fit, the decay was marked non-γ producing. This information was combined with the charge exchange vertex and physicist scanning information. A program checked the decay product measurement data against the physicist's description and if there was a discrepancy or if there was poor reconstruction of an element a request was made for additional measurements of the unsatisfactory parts. Another program chose the best measurements when a conversion pair or decay had been measured more than once and assigned each γ to a source (the main charge exchange and subsequent K^o decay, K^+ decay, or external background).

The final processing program, as described, was responsible for deciding the source of each γ. For each γ the program first investigated each measured K^+ decay as a possible source. The parameters L, DL, and DLXY were computed exactly as described in the section on the pion beam subexperiment. Slightly tighter limits of acceptability were used than those described there. If the DL and DLXY parameters were larger than acceptable the decay was eliminated as a possible source.

If the decay was marked non-γ producing it was eliminated. If a $K_{\pi 2}$ fit was made the γ momentum in the center of mass of the neutral pion was computed, exactly as previously described, and was required to be less than 111 MeV/c. If a match between a γ and a decay was not eliminated by these methods, the γ was assigned to come from a decay and the decay that seemed to fit best was chosen as the source. The program then checked the main K^o producing event as a source for the γ's. The significant length of flight of the K^o makes the geometry involved in matching a γ with the main event more complicated. The parameters L, DL, and DLXY were again used but were defined differently. The fitted K^o direction and charge exchange vertex determine a line, the K^o trajectory. The distance of closest approach between this line and the γ trajectory, reconstructed as usual from the pair conversion point and the total electron momentum, is DL. The closest approach of the two lines defines a second point on each trajectory. L is therefore defined as the distance between the two points along the γ trajectory, and the apparent length of flight of the K^o is the distance defined along the K^o trajectory. To be exact, DL was computed by minimization within the constraints that the lengths of flights of the K^o and of the γ were non-negative and that the length of flight of the K^o was not more than six mean decay lengths. DLXY was computed by similarly minimizing the distance between the K^o and γ trajectories under the constraint that the lengths of flight were non-negative but this time as a two-dimensional system using only the fiducial plane coordinates X, Y. It is apparent that in two dimensions the trajectories must cross, and DLXY would always be zero if it were not for the constraints. Even so DLXY was usually zero. DL and DLXY were required to be within limits for the

γ's to be considered as originating from the main event, but the limits were not exactly those previously described. In addition, the momentum of the γ's in the K^o center of mass was required to be less than 300 MeV/c. The kinematical limits on γ momentum from K^o to $2\pi^o$ decay are 20 MeV/c and 229 MeV/c. The center-of-mass momentum was computed from the total emerging electron energy. The γ direction was computed as the line joining the conversion point with the apparent K^o decay point when L was greater than 5 cm, and as the direction of the total electron momentum when L was less than 5 cm. If the γ was not already assigned to K^+ decay and if it passed the requirements for a match with the main K^o decay, it was assigned to main. Gammas not assigned to decay or main were assigned to the external γ flux. In addition, conversion pairs with a total emerging energy of less than 10 MeV were assigned to the external γ flux regardless of any other factor. This has the effect of defining an acceptance cut.

The K^o trajectory was not known perfectly since it was reconstructed from a fit to the charge exchange. A sample of 1228 charge exchanges, found by specifically looking for V decays, was measured in the usual fashion and the K^o directions were reconstructed. The V's were also measured to provide much more accurate K^o directions. Figure 14 shows the frequency distribution of the angle between the K^o directions determined in the two ways. Error in the K^o direction was taken into consideration in setting the limit of acceptability on DL for a match between a γ and the main K^o decay. If the apparent length of flight of the K^o was less than three mean decay lengths, the apparent length of flight times the rms of the errors in dip and azimuth of the K^o as supplied by the fitting program were added to the DL limit computed according

to the pion beam subexperiment recipe. If the apparent length of flight was more than three mean decay lengths, then the addition to the limit on DL was figured on a length of flight of three mean decay lengths. The rms of the estimated angular errors was typically 0.1. The limit on DLXY was the same as for the pion beam subexperiment.

Finally, a physicist looked at the complete analysis of each event with reported γ's and the film frame to verify the computer program's decisions. The physicist could work with the program in a primitive sort of conversational manner. In events with several γ's or several decays, when there were many measurements of each part, the computer program sometimes became confused and gave up its attempt to find the best unique set of measurements. The physicist could set it right. The program indicated suspicious cases, for example, when two γ's were assigned to the same K^o decay but gave K^o lengths of flight differing by more than a computed reasonable error estimate. The physicist could then look for the reason for the difficulty (a γ may have been improperly measured, or it may be possible to substantiate the idea that one of the γ's comes from somewhere else). Additional information may be available about possible K^+ decays on sight, such as the fact that an event that had fit the K scatter hypothesis and had therefore been marked non-γ producing was in fact a K decay, since the prong could be identified as a pion by its decay. In certain cases one comparatively low energy electron track from a γ conversion may not have reconstructed properly so that the accuracy of the reconstruction of the γ may be improved by including hand measurements or sight estimates of the electron track parameters (this would be a small perturbation since the reconstructed γ parameters would be dominated by the well measured

higher energy electron). A Monte Carlo simulation was done to investigate the probability of a γ originating from the main K^o decay being falsely assigned to a K^+ decay. The result of the study is that 26 additional charge exchanges should have had an assigned γ. In the course of this review of the data, physicists chose approximately 25 γ's that the program had assigned to K^+ decays and designated them to be from K^o decay instead. The physicist's side of the conversation was punched on cards and in a new run the processing program redid the analysis. Possibly physicist intervention would again be required. Throughout the entire processing no distinction was made between charge exchanges with or without associated V decays.

Table C presents a summary of the results emerging from the final processing program.

Table C

Total charge exchanges	12970
Events with no V decay	8410
Events with no V but with γ's associated	1284
Events with a V decay	4560
Events with a V decay and with γ's associated	164
Total γ's measured	3379
Assigned to main	1772
Assigned to K^+ decay	922
Assigned to external	685
Assigned to decay but also acceptable for main	387
Events with unreconstructed γ's which appear to fit main	10

C. Background Studies

There was a recognized possibility of a small pion contamination in the K^+ beam. If there were pions in the beam, some of them should have reacted according to:

I.	$\pi^+ d \rightarrow \pi^+ \pi^- pp$	29%	
II.	$\rightarrow \pi^o pp$	56%	
III.	$\rightarrow \pi^o \pi^o pp$	12%	
IV.	$\rightarrow \pi^o \pi^o \pi^o pp$	0.6%	
V.	$\rightarrow \gamma pp$	1%	
VI.	$\rightarrow \pi^+ \pi^- \pi^o pp$	1%	(Ref. 54)

(figures indicate distribution of cross section among the channels given). Occurrences of I and VI would have been accepted by our processing as charge exchanges with V's. From the sample of supposed charge exchanges with V decays were selected those events with a reported K^o length of flight projected on the fiducial plane of 0.5 mm or less. The two charged pion tracks were measured for each event. A frequency distribution of the two charged pion combined mass for these events appears in Fig. 15. The phase space for reaction I at 600 MeV/c appears in Fig. 16 in terms of the combined mass of the two pions. If the event was a kaon charge exchange, the combined mass of the pions is expected to be the K^o mass, 498 MeV. The combined mass peak near 500 MeV is clearly evident. Those events with combined mass less than 425 MeV were selected for further study. Each of these events was examined by a physicist to insure correct measurement and to check the general appearance of the event (the physicist could check to make sure it was not a charge exchange and K^o decay to π^+ and π^- with a pion scattering very near the K^o decay point, for example). About 65% of the film was treated in this fashion

to find nine of these events, so all of the data is expected to contain 14. The assumption was made that the combined mass of the charged pion pairs from reactions I and VI is distributed the same as the phase space for reaction I (observe that reaction VI occurs less frequently than I). 68.8% of this phase space is below 425 MeV (fig. 16), so that the total number of occurrences of reactions I and VI is expected to be 20.

A second study of the background also involved the previous identification of V decays. Ideally the ratio of the number of events, selected on the basis of some property of the charge exchange vertex, with no V decay to all with that property should not depend on the selection of the events. The variation of the ratio R of events with no V decay to all events with many different parameters was studied. A few of these are displayed in Figs. 17 and 18. In examining the plot of R in terms of the radius of the charge exchange in the fiducial plane it is seen that there is an abnormality at a radius of about 15 cm. This is approximately the radius of the small γ converter cone at the beam depth. About 150 of the identified charge exchanges appear to have been events taking place in the steel. The analysis program was directed to read the comments section of the physicist's scanning report and to pass over those 150 events that were in the metal or in the beam slit of the small cone. These events are not included in any of the other tables or figures presented. The sensitivity of this test for abnormalities can be appreciated when it is seen how clearly this 150 events sample, containing bias to the extent of about 40 events, was picked out of a total of 14,000 events. Again, looking at the plot of R vs the ionization and stopping characteristics of the two-prong charge exchange protons, one can see that the residual 94 events with both protons nonstopping must

contain background. The background was estimated to be 0.2% and again shows the sensitivity of the test. No further significant indication of abnormality could be found.

Since the plot of R vs the momentum of the fast proton indicated no abnormality in the data even up to a momentum of 700 MeV/c, we were able to distinguish protons from kaons at the beam momentum by bubble density, at least to a fair confidence level, say 50%. Some entering beam tracks were identified, in passing, as probably being protons. Most of these tracks were outside the limits on beam angle and, therefore, could not be considered for charge exchanges. Of the events first found by the scanning staff, not more than 60 were later recognized by physicists as being produced by proton beam tracks. These were not included in the final data but perhaps an equal number escaped recognition and do appear in the data.

D. Results

Figure 23 presents the lifetime distribution for K^o to two charged particle decays. Also plotted is a straight line with slope corresponding to the K_S mean lifetime. The experimental data lie very nearly on the straight line for decay times less than four short lifetimes, and rise above for longer decay times, approaching a constant decay rate of about 7 to 10 decays per K_S mean lifetime. A naive model, in which the K^o has a lifetime distribution consisting of an equal sum of two exponentials with the known long and short lifetimes, fits the data well giving a near constant rate of about 9 decays per short lifetime at decay times longer than 9 short lifetimes. The indications are that the efficiency for detecting V decays remains good out to lengths of flight at which

the decays are dominated by K_L's. The reconstructed momentum and dip of the K^o were required for the computation of the decay time so that this further indicates that K^o reconstructions from the measured charge exchanges were substantially correct.

Figures 24 and 25 give the distributions of the DL parameter separately for four different laboratory γ momentum ranges and for charge exchanges with and without a V decay. All are conversions in the metal, and all γ's with momenta below 300 MeV/c in the K^o rest system are included. The hatched distribution is for the charge exchanges with V decays. The unit in which DL was measured was the limit of acceptability of this parameter, as used in the final processing program, and varies from one momentum range to another and with the L parameter of each γ (Fig. 10). The hatched distributions must represent the background γ flux, since few events with V decays could have actually produced γ's. The distributions are fairly flat, decreasing a bit at large DL. The DL limits generously include the peaks in the distributions for events with no V decays and do not exclude the small shelves of events with DL a little larger. The fairly flat tails, similar to the distributions for events with V decays, do lie beyond the acceptable range of DL.

Figure 26 presents the frequency distribution of the γ momentum in the neutral pion rest frame, for those γ's assigned to a K^+ decay with a $K_{\pi 2}$ fit. The frequency rises to a peak near 64 MeV/c and falls to half maximum on the high momentum side at about 74 MeV/c.

The pion beam induced reactions in the charge exchange sample contained the following (as was listed previously):

I.	$\pi + d \rightarrow \pi^+\pi^- pp$	29%
II.	$\rightarrow \pi^o pp$	56%
III.	$\rightarrow \pi^o\pi^o pp$	12%
IV.	$\rightarrow \pi^o\pi^o\pi^o pp$	0.6%
V.	$\rightarrow \gamma pp$	1%
VI.	$\rightarrow \pi^+\pi^-\pi^o pp$	1%

The 20 events with $\pi^+\pi^-$ in the final state (from paragraph C) represent 30.7% of the cross section for π^+d interactions that would have appeared in the K^+ charge exchange sample. Assuming that the acceptance efficiencies for reactions I to VI in this sample are all the same we expect a total of 65 pion beam induced events in the kaon charge exchange sample. The sample also contained an estimated 30±30 proton beam events and 0.2% scatters (Table I, lines 11, 12). The number of charge exchanges was then 12849±50 (Table I, line 13). Twenty events must be subtracted from the events with V decays to yield 4540 charged mode K^o decays (Table I, lines 15, 16). With the approximate γ detection efficiency of 16.8%, about 16 of the pion beam events should have had detected γ's (Table I, line 19).

The 164 events with both a V decay and associated γ's is expected to contain zero pion beam events with a γ originating from the event (only reaction VI above has a possibility of producing such a case and only one instance of reaction VI is expected to have occurred), two K^o decays to two pions and a γ, and two K^o-to-three-pion decays. Thus 160 events should have been kaon charge exchanges with γ's not originating from a K^o decay. Both cases of γ's arising from the charge exchange vertex itself, such as neutral pion production, and cases of false correlation with unrelated γ's are included. Since four events with V decays actually

produced observed γ's, 4556 events out of the 4560 events with V's had a chance to be falsely correlated with a γ. The rate for false correlations between a charge exchange and a γ conversion is 160 out of 4556 or 3.5%. Since the decay of the K^o had nothing to do with the origin of the γ, 3.5% of the charge exchanges with no V decay must also have one or more γ's with which they are falsely associated. However, if a charge exchange is correctly associated with a conversion, it may also be falsely associated with another without producing any error. The number of charge exchanges with a correctly associated γ is then given by the equation:

$$N = NOBS - 0.035(NOV - N)$$

N = events with true detected γ

NOBS = events with observed γ

NOV = all charge exchanges with no V decay

or $$N = (NOBS - 0.035\ NOV)/(1 - 0.035)\ .$$

Thus, 1027 events have correctly associated γ's out of the 1284 emerging from the processing programs with γ's. The addition of 10 events with unreconstructed conversions and deduction of the 16 pion beam events leaves 1021 K^o decays yielding detected γ's. This computation is outlined in Table I, lines 17-21.

The method of removing the background is more general. Any subsample of events may be taken based on properties of the charge exchange. If the events with V decays and without are treated the same, the true number of K^o decays in the subsample with associated γ conversions may be computed with the same formula. Alternatively, the γ's may be studied instead of the events with γ's. In this case,

$G = GNOV - NOV \cdot GV/V$

G = number of γ's from main K^o decay with property A

GNOV = number of γ's with property A assigned to main when there was no V decay

GV = number of γ's with property A assigned to main when there was a V decay

V = number of events with a V decay

NOV = number of events with no V decay

The V decay and no V decay data may be used in a bin-by-bin application of the method to histogram distributions of the true K^o decay originating γ's.

Figure 27 presents a lifetime distribution for neutral decays. The distribution is reasonably exponential out to about 4.5 short lifetimes, with the exception of one data point, but a characteristic time somewhat longer than the short lifetime is indicated. The data points at 5.2 and 6 short lifetimes are entirely too high. A study of events with multiple γ's detected showed that the standard deviation in the measurement of the K^o length of flight determined from the γ's was 1.6 cm, which averages more than half a short lifetime. The fact that the resolution in determining length of flight is comparable to the mean length of flight has the effect of increasing the apparent lifetime as observed. The high rates near six mean lives is due to the piling up of events with longer actual lifetimes, or longer apparent lifetimes due to the random measurement error, since the processing program forced the computed lifetimes to be six mean lives or less. Since the histogramming of the apparent decay lifetime does not fall into one of

the two categories described above; that is, it is neither the selection of groups of events by a property of the charge exchange, nor is it a selection of γ's by a property of the γ (the lifetime is a joint property of all the γ's when the event has more than one), the methods of subtraction of background γ effects described above are not really applicable. The second formula was used for background subtraction anyway. This is correct to first order but cannot be expected to give the correct result to high accuracy. Since the number of events per bin varies in the distribution by a factor of 30, small errors due to the incorrect handling of background can have a large effect.

Least it be doubted that there is any practical case to which the formulas for subtraction of the effect of the background γ flux are applicable see Figs. 29 and 30. These distributions are free of background effects except for the slightly increased random error.

The main results are summarized in Table D. Since the data are presented in terms of numbers of events observed, no statistical error is given with the numbers, the quoted errors being due solely to corrections and background subtraction.

Table D

Actual number of K^o productions observed	12849±50
K^o decays to charged pions observed	4540±7
K^o decays yielding observed γ's but not charged pions	1021±30

V. MATCHING THE SUBEXPERIMENTS -- THE MONTE CARLO

To a first approximation it can be seen that the pion beam subexperiment and the kaon beam subexperiment should produce similar samples of γ's. The overall efficiency for neutral pion detection could be taken from the calibration subexperiment and used immediately in the kaon subexperiment. For a high precision result, though, small differences between the two subexperiments should not be left unaccounted for.

A package of subroutines was written to simulate a γ in the chamber originating from a given point with a given momentum. The routines are equally useful for the simulation of either subexperiment with the addition of routines to simulate one or the other up to the point of γ production. For the theory on which the simulation is based refer to Appendix III. The exact forms of the calculations in the program (which involves some numerical approximations to the theoretical formulas) are described in this section.

The γ simulating program first determined the mean free path in radiation lengths (for stainless steel since this is still slightly material dependent) from the γ momentum and the Messel function (Fig. 4). Then an actual pathlength in radiation lengths was generated randomly according to an exponential distribution. The path of the γ was traced through the various lengths of deuterium and stainless steel (if it intersected a cone) until it had either accumulated the determined number of radiation lengths or else left the chamber. If the required number of radiation lengths were reached a conversion took place and its actual location was found. If conversion was in the liquid the simulation was complete. If it was in the metal the energies of the

two electrons were generated randomly. The kinetic energy per available energy (γ energy minus two electron masses), X, was distributed according to

$$[1 - \exp(-\alpha X)](1 - \beta X) \qquad 0 \leq X \leq 0.5$$

$$\alpha = 22.3 \log_{10}(P_\gamma)$$

$$\beta_o = 0.331 \log_{10}(P_\gamma) - 0.385$$

$$\beta = \beta_o \quad \text{for} \quad \beta_o \geq 0$$

$$\beta = 0 \quad \text{for} \quad \beta_o < 0$$

(P_γ in MeV/c)

and an even chance was given for this to be either the positron or the negatron, with the other energy by conservation of energy. The positron then propagated to the surface of the metal under the influence of ionization loss (a fixed 15.82 MeV per centimeter), bremsstrahlung and annihilation. The negatron was treated the same but there was no annihilation. When simulated bremsstrahlung or annihilation resulted in high energy γ's (above 10 MeV) they were taken as going straight forward and the possibility of reconversion was accounted for.

In simulating bremsstrahlung, the computations were made using the formulas of Bethe and Heitler made more suitable for Monte Carlo methods by some empirical curve fitting. The probability for an electron to radiate less than 1% of its energy in a samll penetration of steel was roughly treated while the radiation of more energy was carefully computed. For stainless steel, the probability of radiating more than 1% of the electrons energy per cm was well fit by

$$2.83 - 1.468\ U^{-0.544}$$

U = electron energy in electron masses

over the range of electron energy encountered in the experiment. If V is the fraction of the electron energy radiated the shape of the distribution is given by

$$(1/V)\beta(\ell n\,(2U(1 - V)/V) - 0.5 - C) \quad \text{for } \gamma > 2 \text{ and } V > 0.01$$

$$C = 2.762/(\gamma + 1.627)^2$$

$$(U/V)\beta(F_f/4 - 1.1) \quad \text{for } \gamma \leq 2 \text{ and } V > 0.01$$

$$F_f = 20.2 - 2.45\,\gamma$$

where $\beta = U + (1 - V)^2 - 2(1 - V)/3$

$$\gamma = 33.33V/(U(1 - V))$$

and by

$$V^{-5/6} \quad \text{for } V < 0.01 \ .$$

Bremsstrahlung loss in a real thickness of stainless steel was simulated by randomly generating an energy loss in each of many small steps. The step size was usually much less than 1 mm which is 0.06 radiation lengths. For each step it was randomly decided if the energy loss was to be more or less than 1% and then the exact energy loss was found by choosing a number according to the appropriate distribution.

For positrons, the annihilation probability per cm in stainless steel was computed by

$$(0.555/(U + 1))((U^2 + 4U + 1)/(U^2 - 1)A - (U + 3)/F)$$

$$F = \sqrt{U^2 - 1}$$

$$A = \ell n\,(U + F)$$

In the Monte Carlo an emerging electron was required to have an energy of 1 MeV to be visible and the total emerging energy was required to be 8 MeV for a γ to be seen.

A. Modeling the Pion Beam Subexperiment

About 100,000 pion beam events were simulated with Monte Carlo methods. The beam parameter distributions were Gaussian with the observed means and standard deviations. A point along the beam track was randomly chosen to be the charge exchange point and the fiducial constraints were imposed. The neutron momentum in the deuteron was computed randomly using the Hulthén distribution.[55] The spectator momentum is equal and opposite. The spectator energy was deducted from the deuteron mass to give the neutron energy (the neutron, of course, is usually a little off the mass shell). A scattered neutral pion direction was chosen randomly according to the experimental distribution in the pion-neutron center of mass, and the energy and momentum balance made for the emerging real proton and neutral pion. The neutral pion decays immediately into two oppositely directed γ's of half-pion-mass energy in its own center of mass, one of them in a randomly chosen direction. The resulting charge exchange point and γ vector momenta for each simulated event were written on tape and later analyzed by the general γ simulating program.

A sample of 2364 identified pion charge exchanges were measured and analyzed to provide both the beam parameters and the angular distribution for the simulation. The lower momentum reconstructed proton was taken to be the spectator. The neutron momentum and energy within the deuteron were calculated. The incoming pion and fitted outgoing neutral pion could then be transformed into the pion-neutron center of mass for computation of the scattering angle. Figure 19 is a frequency distribution of the cosine of this scattering angle.

Table E presents the general features of the pion subexperiment

data, amended by the background subtraction, compared with the Monte Carlo simulation data for ten times as many charge exchanges, scaled to the experimental number. The agreement is excellent.

Table E

COMPARISON OF DATA AND MONTE CARLO

Monte Carlo = 109,830 C.E. events

	Data	Back-ground		Monte Carlo
Total #	3746	60	3686	3749
Liquid	267	1	266	271
Dalitz pairs	129	0	129	139
# inner cone	1771	31	1740	1764
# outer cone	1579	28	1551	1574
# e^+ only	161	2	159	159
# 2 γ's (total)	320	10	310	312
# 2 γ's (cone)	261	8	253	246
# 2 γ's (liquid, cone)	37	1	36	42
# 2 γ's (Dalitz, cone)	16	1	15	19
# 2 γ's (liquid)	2	-	2	2
# 2 γ's (liquid, Dalitz)	3	-	3	2
# 2 γ's (Dalitz)	1	-	1	1

In order to fit the experimental data the radiation lengths of the steel and liquid deuterium were considered adjustable parameters. This data was produced with the radiation lengths set to 1.721 cm and 1100.0 cm respectively. For stainless steel the value computed from the definition is 1.70 cm. The difference is a little over 1% but it must be

remembered that the cone material is not homogeneous, and that the variations in thicknesses are of the order of a percent. The value for deuterium is somewhat higher than reported values but there is considerable uncertainty in the density at beam spill time. Also the probabilities for conversion in the liquid were computed from the mean free path for conversion in radiation lengths for steel not for deuterium. Since the mean free path in radiation lengths is a little material dependent it is expected that a slight compensating error in the value for the radiation length of deuterium would be necessary for the correct overall conversion probability.

Figure 20 presents the frequency distributions of the Z of γ's converted in the two cones, both for the Monte Carlo and for the actual data. Notice that even the positions of the beam ports are apparent in the range of Z between -13 and -16 cm where their presence reduces the conversion probability. There is very good agreement between the simulation and the data. Figure 21 similarly presents a comparison of the simulation with the data on the basis of the radial angle of γ's converted in the two cones. The agreement is good and the expansion holes are sharply delineated in the data. In the experiment the actual γ momentum was known since the neutral pion vector momentum was known and the γ angle was known when a conversion pair was seen. Figure 22 shows the close agreement between simulation and experiment on the frequency distribution of the γ production momentum of the observed γ's. This shows that the simulation produced the correct γ momentum distribution and that the γ momentum dependence of the simulated detection is correct.

In Table E it can be seen that the Monte Carlo is slightly too high

in detection efficiency so that an overall correction of about 1.3% is required in the detection efficiency computed with this Monte Carlo as is described in the next paragraph. A possibility for understanding this small error in the Monte Carlo was identified: Compton scattering was not accounted for in the simulation but may be significant (see Figs. 5 and 6).

B. Modeling the Kaon Beam Subexperiment

Actual data from measured, identified charge exchanges -- the same sample of charge exchanges used in the final analysis -- was used in the simulation up to the charge exchange coordinates and vector momentum of the K^o. A length of flight of the K^o was then generated randomly using the K_S lifetime. In the K^o center of mass two oppositely directed neutral pions were generated in a random direction and in each neutral pion center of mass two oppositely directed γ's were generated in a random direction. The general γ-simulating routines then were used to find the fate of the four γ's. Regardless of whether any γ's were detected a simulated physicist's scanning report record was generated, and if γ's were detected, a simulated γ measurement record was generated. All data was written on a tape. The tape was then processed as if it were the real experimental data. Thus any imposed acceptance cuts (for example, the requirement for the emerging electron energy to be more than 10 MeV) were automatically the same for both the real and the simulated data. The final number of events with one or more accepted γ's divided by the total number of charge exchanges is the neutral decay detection efficiency.

Table F summarizes a comparison between the actual data and the

simulation. The agreement in the numbers of γ's converted in the liquid and in the metal is excellent. The Monte Carlo was here normalized to about the same total number of γ's. The agreement in the numbers of events with various numbers of γ's detected is less striking. Figure 28 presents the distribution of the combined mass of pairs of γ's using all possible pairings, for those events with more than one detected γ. The agreement between the Monte Carlo and the data is good except at the very lowest combined mass region (below about 25 MeV). In this region the real data shows more events than the simulated data. This is likely to be due to γ's from the event converting in one cone and the resulting electrons producing a high energy photon by bremsstrahlung (or possibly by annihilation). This photon also converts in the other cone. Since this happens only when the neutral decay is detected due to the primary conversion, no error in the detection probability for neutral decays is associated with the effect. Figure 29 shows very good agreement between the simulation and observation in the frequency distribution of the observed γ energy. The polar angles of the conversion points in the fiducial plane likewise had a well-simulated distribution (Fig. 30).

In the simulation, 13,603 charge exchanges yielded 6999 events with detected γ's. This must be corrected by deducting 1.3%, since the pion subexperiment simulation resulted in 1.7% too many detected γ's compared with observation (1.7% change in the single γ efficiency corresponds to 1.3% change in the efficiency for detecting one or more out of four γ's). Statistical errors must be computed for the pion beam subexperiment and for two Monte Carlo simulations (binomial distribution, see Appendix VII). The error in the detection efficiency of a

Table F

	Exp.	Simulation
Number γ's converted in metal	1121	1120
Number of γ's converted in liquid	128	134
Events with:		
1 γ	818	770
2 γ's	202	235
3 γ's	16	31
4 γ's	1	2

γ reported for the pion beam subexperiment was 1.5%. For the pion beam subexperiment simulation 0.9% error was added in quadrature to give 1.7%. The relative error in the efficiency for detecting one or more out of four γ's is only 77% of the relative error in the efficiency for detecting one out of one γ. Thus there is a 1.3% contribution to the relative error in the efficiency for detecting a K^o neutral decay. We added 1.7% error in quadrature for the kaon beam simulation to obtain 2.1% for the expected relative error in the detection efficiency for K_S neutral decay. The statistical error estimates for each simulation were approximately doubled to generously allow for imperfect properties of the random number generator. The efficiency for detecting K short to two-neutral-pion decays is 50.8±1.1% (Table I, line 7). The observed cases of K^o neutral decay should have been nearly all K^o decays to two pions and, as was seen from the lifetime study, they are mostly distributed according to the K_S decay time characteristic. The determined detection efficiency for two pion decay of 50.8±1.1% must be very

nearly the fraction of the neutral decays observed. Crudely estimated the neutral decays should have been 99.4% two-pion decays and 0.6% three-pion decays. The net detection efficiency should then have been a little higher, 50.9±1.1% (Table I, line 9).

VI. RESULTS

Out of 12,849 K^o productions, 1021 K^o neutral decays were observed (from Table I, line 21). These neutral decays occurred within six K_S lifetimes due to the effective cut at this length of flight in the processing program. The detection efficiency for neutral mode decays was determined to be 50.9±1.1% (from Table I, line 9). A division yields the total number of neutral mode decays occurring within six K_S mean lifetimes, 2006 (Table I, line 22). The primary numbers from the experiment are now contained in Table I, lines 13, 16, and 22.

A. Analysis for the Branching Ratio Result

Of the 4540 observed charged mode decays (Table I, line 16), 74 decays occurred after observed lengths of flight equivalent to more than six K_S mean lifetimes. The number of K_S expected to decay after six mean lives but within the chamber was roughly calculated and subtracted from the 74 decays observed after six mean lives. Thus, naively, 63 K_L charged mode decays were observed in this long decay time range while the expected number of K_L's to decay in the chamber after six short mean lives was 62±7. The tail of the charged mode decay lifetime distribution (Fig. 23) agrees very well with simple calculations. In the same way it was estimated that the total number of K_L charged mode decays observed was 112 while two K_S's escaped the chamber before undergoing charged mode decay (Table I, lines 24 and 25). There were therefore 4430 K_S charged mode decays but 0.1% of them should have been leptonic. The fraction of K_S charged mode decays producing γ's of over 50 MeV energy ($R(K_S \rightarrow \pi^+\pi^-\gamma)/R(K_S \rightarrow \pi^+\pi^-)$, essentially) was found experimentally to be $3.3\pm1.2 \times 10^{-3}$.[56] The fraction with energy

greater than 10 MeV may be somewhat greater, 4.0×10^{-3} will be used. After deleting the 0.5% other mode decays (Table I, line 26) we conclude that 4408 K_S decays to $\pi^+\pi^-$ and possibly soft photons were observed (Table I, line 27).

We observed 2006 neutral decays (from Table I, line 22). Three K_S neutral decays should be expected at decay times longer than six mean lives while 14 K_L neutral decays should be deducted (Table I, lines 29 and 30). Evidently 1995 K_S decays to two neutral pions were observed (Table I, line 31). Thus the branching ratio is measured to be 2.21 (Table I, line 32).

B. Analysis for the Fraction of All K^o's Decaying in 6 K_S Mean Lifetimes

Out of 12,849 K^o productions 4540 charged mode decays were observed (from Table I, lines 13, 16) but 74 decays had lifetimes longer than six short mean lives (Table I, line 45). Thus 4466 charged mode decays were observed with decay times less than six K_S mean lifetimes (Table I, line 46). The total number of decays occurring before six K_S mean lifetimes, 6472, is obtained by adding the 2006 neutral decays (Table I, line 48). By division, the fraction of all K^o states decaying in this time is 0.5038 (Table I, line 49).

C. Error Analysis

An analytic evaluation of the statistical errors in the two results (viz., the fraction of all K^o's decaying in less than six K_S lifetimes, and the charged vs neutral mode branching ratio for decay of K_S) is rather involved since the primary numbers obtained from the experiment (number of charge exchanges, the number of events with V decays, the number of events with associated V's and γ's, and the number of events with associated γ's but no V's) are not statistically independent.

Therefore an error analysis by simulation of experiments was undertaken.

An experiment was simulated by an ensemble of 12,849 charge exchanges. For each charge exchange it was randomly decided if there would be a background γ, with a 3.5% probability that there would be (this is the actual background γ rate -- see Sec. IV, paragraph D). A random choice was then made with exactly 50% probability to see if the event would be a K_S. Thus in the simulation the "true" value for the fraction of K_S in a K^o state was known to be 0.50 by direct arrangement with the Creator. If the event was a K_L the simulation was complete. If it was a K_S then a random choice was made giving exactly a 68.75% chance that there would be a V decay, so that again by direct arrangement with the Creator, the branching ratio in question was known to have a "true" value of 2.20. If the event had a V decay the simulation was complete. If not then the event was assumed to decay to neutral pions and then to γ's. A random choice was made with a 50% probability exactly, to see if the γ's were detected. Thus in the simulation it is assumed that the detection efficiency is exactly 50% and this fact is infused knowledge -- the efficiency need not be measured. Only the statistical errors in the experiment itself were being investigated; errors associated with the calibration of apparatus are not included. An event would have γ's associated if it had a background γ, or if it were a K_S decay in the neutral mode with γ's detected, or both. Depending on the pattern of random choices the appropriate counters were incremented. Counters were kept for the number of charge exchanges, the number of events with V's, the number of events with V's and γ's, and the number of events with γ's but no V's -- just the numbers produced by the actual experiment. Upon completion of the simulation of 12,849

charge exchanges the counters were used, along with 50% for the γ detection efficiency, to compute the two experimental results in the same way as was actually done. The experiment was simulated 100 times.

The mean value of all the experiments comes out to be the "true" value to within a small fraction of a standard deviation for each of the two experimental results, as should be expected. The rms deviations from the mean values were computed from the distributions and are the sought for statistical error estimates. The statistical errors are found to be ±0.0067 for the fraction of K^o's decaying to all modes within six short lifetimes (0.5038), and ±0.10 for the charged vs neutral mode K_S branching ratio (2.21). The other significant independent error to be combined with these is due to the determination of the K^o neutral decay detection efficiency (2.1% relative error).

D. Conclusions

The principal results are finally:

Fraction of K^o decaying to all modes	
before six short mean lives	0.5038±0.0075
$(\text{rate}(K_S \rightarrow \pi^+\pi^-(\gamma < 10 \text{ MeV})))/(\text{rate}(K_S \rightarrow \pi^o\pi^o))$	2.21±0.11

Consideration was given to the possibility of error in these results due to regeneration (Appendix VI). It was concluded that the extent of these effects was much less than our statistical errors.

From theory, the value for the fraction of initial K^o states decaying in six short mean lives is (see Appendix IV)

$$0.5052 + 0.99 \text{ Re } \delta$$

where δ is the so-called CPT violating parameter. It can be seen that

the consistency with $\delta = 0$ is embarrassingly good. In fact we have

$$\text{Re } \delta = - 0.0014 \pm 0.0075 \ .$$

If the assumption is made that Re $\delta = 0.0$, a more accurate value for the branching ratio may be had. This must be an assumption however, since the accuracy of the determined value of Re δ will not permit a better value for the branching ratio than was already presented, which is the best that can be done without additional assumptions. If Re $\delta = 0.0$ then the short lifetime component of K^o is

$$0.5 - \text{Re } \epsilon = 0.4984$$

of the total flux (Appendix IV), and the 12,849 K^o's must have included 6404±57 K shorts (Table I, lines 34, 35). This includes 22 K shorts decaying to $\pi^+\pi^-\gamma$ (> 10 MeV) or by leptonic modes (Table I, line 36). Evidently 6382±57 events decayed to pion pairs (Table I, line 37). The branching ratio may now be determined separately using only the charged mode decay observations or only the neutral mode observations (as is summarized in Table I, lines 38-41):

$$\text{BR} = \text{NV}/(6382 - \text{NV}) = 2.23 \pm 0.084$$

$$\text{BR} = (6382 - \text{NG})/\text{NG} = 2.20 \pm 0.15$$

NV = number of events with $\pi^+\pi^-$ decay (Table I, line 27)

NG = number of events with $\pi^o\pi^o$ decay (Table I, line 31)

The errors were found by simulation much as described above. The weighted average of these two results may be taken to find

$$\text{BR} = 2.22 \pm 0.080 \quad \text{(Table I, line 42)}.$$

There is very little improvement in the error over that obtained using only the charged mode data since these two results are by no means

independent determinations of the branching ratio -- the errors are highly correlated. We find then, no substantial change in the value itself which may be taken equally well to be 2.21 or 2.22. The error estimate however is ±0.08 if $\mathrm{Re}\ \delta = 0.00$ is believed to be established (for example by unshakable faith in the CPT invariance of the weak interaction) or ±0.11 if $\mathrm{Re}\ \delta = 0.0$ is not accepted a priori.

From the theoretical formula for the K_S branching ratio (Appendix V) it can be deduced that

$$\mathrm{Re}(A_2/A_0)\ \cos(\delta_2 - \delta_0) = 0.026 \pm 0.013\ (\pm 0.010)\ .$$

(In this paragraph the larger error on the branching ratio will be used with the smaller one in parenthesis.) As shown in Appendix V, with certain assumptions concerning the absence of the $\Delta I = 5/2$ transitions and the nature of the A parameters, $|\mathrm{Re}(A_2/A_0)|$ can be estimated from the rate for the decay $K^+ \to \pi^+\pi^0$ to be about 4.5%. Then

$$|\delta_2 - \delta_0| = 55^{+18}_{-25}\quad (^{+11}_{-18})^{\circ}\ .$$

This can be compared with $\pi\pi$ phase shifts computed from pion-nucleon scattering data: $\delta_0 = (30 \pm 10)^{\circ}$ (Refs. 57, 58) and $\delta_2 = (-12 \pm 4)^{\circ}$ (Ref. 58) (the agreement between the two determinations of δ_0 is not as good as might be desired). $|\delta_2 - \delta_0|$ then is $42 \pm 10^{\circ}$. Alternatively, $\delta_2 - \delta_0$ may be taken as known and then $\mathrm{Re}(A_2/A_0)$ is found to be $0.036 \pm 0.019\ (\pm 0.015)$.

Three recent measurements of the K_S charged mode vs neutral mode two-pion decay branching ratio have been reported: 2.12±0.17 (Ref. 36), 2.285±0.055 (Ref. 37), and 2.10±0.06 (Ref. 38). The previously existing world average was 2.165±0.10 (Ref. 59). The weighted average of all values including 2.22±0.08 for our value is

2.200 ± 0.033

with a χ^2 of 5.57 for 5 points.

ACKNOWLEDGMENTS

I would like to express my thanks to Professor Uriel Nauenberg, my thesis advisor, who, by his encouragement and many long hours of work, sustained me and the experiment through many difficult times. It is a pleasure to thank Drs. A. P. Colleraine, R. Morse, A. Goshaw, and D. Hutchinson for their generously-given and much needed help.

I am grateful to Dr. A. Prodell and Mr. J. Koehler who implemented modifications to the BNL 30-inch bubble chamber. I thank Mr. Ken Wright and Mr. Rolf Brocker for their help in constructing the γ converter cones. I thank Dr. D. Berley for his help with the beam line.

I gratefully acknowledge the help of Mr. V. Bearg with the computer programing. My thanks go to Dr. E. Bierman for her organization of the film scanning and measuring effort at Princeton.

Finally, I would like to thank the BNL 30-inch bubble chamber crew and the film scanning and measuring staffs at Princeton University and the University of Colorado.

APPENDICES

Appendix I - The Beam Line

Figure 31 presents a simplified schematic of the beam layout -- not to scale.[39] The secondary beam was taken at 12° from the beryllium target in the circulating beam at the F20A position and the first septum dipole bent it out farther away from the AGS. The first pair produced a double image of the target at the first mass-momentum slits which are in the aperture of Q3. The second pair produced a double image of the first mass-momentum slits at the second mass momentum slits. Q3 images the collimators in the first pair on the collimators in the second pair in the horizontal plane and has little effect in the vertical plane. Q6 shapes the beam into a narrow vertical sheet in the chamber, broadside toward the cameras. D2 provides for momentum separation at the first momentum slit. The momentum dispersed beam passing the first momentum slit is compressed back together again by D3 in the second stage. The mass separators in the two stages S1 and S2 however do not recompress the mass bite so that any off-mass particles managing to pass the first mass slit would be deflected again by the second separator.

A 1.5 × 0.5 × 0.125-inch scintillator was installed at the first focus with the beam entering a 1.5 × 0.125-inch face. Since the mass-momentum slits were within the aperture of Q3 and vacuum pipe extended from Q3 to S2, there was no choice but to place the counter in front of the slits. A 3 × 3 × 1/16-inch counter and a 4 × 4 × 0.125-inch counter were placed between Q6 and the entrance to the bubble chamber. These counters were about 12 inches apart and, for range studies, accurately machined copper blocks were placed between them. All

counters were coupled through light pipe to 56AVP photomultipliers. The counters were used for beam tuneup and afterwards to monitor performance. Particles entering the chamber were considered to be coincidences between all three counters, taking into consideration time of flight between these counters at beam momentum over the mass range from somewhat below the pion mass to about the proton mass. For each triple coincidence the time of flight was taken from counters 1 to 3. Counters 1 and 3 fed two coincidence circuits timed to accept kaons and pions separately. In addition they fed a time-to-height converter and a pulse-height analyzer to monitor the entire mass spectrum. Due to the very high rates at counter 1, it was impossible to monitor performance while using the rapid beam deflector and its 100 μsec spill to take pictures. At the completion of each roll of film we switched to long spill, without changing any other parameters, and took a time-of-flight spectrum and pion-to-kaon ratio with the counters. While taking pictures the counter at the first focus was remotely moved out of the beam path.

The beam line is 850 inches from target to center of chamber and the distance between counters 1 and 3 was about 400 inches. At 620 MeV/c this provides just less than 9 nanoseconds difference in the pion and kaon time of flight. The pulse-height analyzer calibration was 0.164 nanoseconds/channel giving 54 channels separation between the masses (see Fig. 1).

A new insert was machined for the first momentum slit to provide a 0.6-inch aperture. The momentum dispersion here was about 1.7 inches/% and simulation with a monochromatic beam gave an image that was about 0.5-inch FWHM. The mass slit at this position had a 0.125-inch aperture.

The pion-kaon separation was 0.45 inch with 500-500 kV on the separators but much of the run used 450-450 kV. The image was 0.18-inch FWHM. Figure 32 presents the measured beam profile at the first mass slit. The pion rejection at the chamber was much improved by surrounding the aperture in the second slit assembly with heavy metal shielding.

The beam line was studied with the BNL beam optics program and account was taken of magnet aberrations[40] but not of multiple scattering. This was made more difficult by the presence of the septum dipole D1, a 15C30, and the special N8Q12 quadrupole, Q1. These magnets are nonstandard and do not possess the usual symmetries for dipoles and quadrupoles. Accurate data on their calibration and unusual aberrations is not so readily available. Magnet currents for optimum beam performance were found to about the precent level.

From the study of the beam a step-by-step procedure for attaining the best tuning was worked out. This beam line is not of unusual design and, although our tuning procedure was worked out independently and specifically for this beam, it also is fairly typical of beam tuning procedures for two stage beam lines. First, convergence is much faster and the correct tuning point can be found more accurately and with less chance of false maxima if the quadrupoles are adjusted in pairs so as to maintain constant performance in the vertical plane while varying the horizontal parameters and vice versa. Contours of constant vertical or constant horizontal focus were computed in the two-dimensional current plane for the two pairs of quadrupoles ahead of time. Secondly for efficient tuning a kind of bootstrap procedure was used to make each stage the instrument for tuning the other. The second stage is particularly useful in the tuning of the first since it would be

impossible to tune the first stage in the horizontal plane without a momentum analyzing detector. When the first stage has been tuned it in turn becomes a monochromatic source for tuning the second. The final magnet currents after tuning were within 2.2% of the computed values (worst case).

Appendix II - The Bubble Chamber and γ Converters

The bubble chamber is roughly cylindrical with diameter of the Scotchlite-covered back plate about 72.5 cm. The fiducial plane (Z = 0) is the inside surface of the window. The back plate was at Z = -33.94 cm. Two cones were mounted to the back plate (Fig. 3). The cones each had a ring at the bottom covered with Scotchlite, to which feet were attached for mounting to the back plate. There was therefore space at the bottom for deuterium to flow at expansion time. The cones do not extend all the way to the glass window so another flow path was available near the window. In addition, a large rectangular hole was cut in each cone on the side facing the piston. The holes extended nearly the whole axial length of each cone so that only a narrow strip of steel (about 2 cm) remains at the top and the mounting ring at the bottom. The cones were cut at this point and reconnected with nylon bolts and insulation to avoid placing a large electrically conducting loop in the chamber magnetic field. Slits 4 cm wide in the Z direction were cut to allow the beam to pass through the cone arrangement without penetrating the steel.

Cone Parameters

	Small Cone	Large Cone
Z of apex inside surface	170.62 cm	172.16 cm
Slope	0.0789	0.136
Approximate radius (Z = -16)	15 cm	25 cm
Average thickness	0.418 cm	0.433 cm
Maximum thickness-minimum thickness	0.014 cm	0.014 cm
Z of top	-1.63 cm	-1.63 cm
Z of bottom not including mounting ring	-31.45	-31.45
Expansion hole Y > 0 and	$-5.88 < X < 5.88$	$-9.02 < X < 9.02$
Entrance port	$-16.98 < Z < -12.98$	$-16.98 < Z < -12.98$
	$3.141 < \varphi < 4.223$	$3.239 < \varphi < 3.797$
Exit port	$-16.53 < Z < -12.53$	$-16.53 < Z < -12.53$
	$-0.424 < \varphi < 0.662$	$0.033 < \varphi < 0.543$

Composition of Cones

Cryogenic stainless steel No. 305, 0.42-cm thick with 0.0094 cm silver coating (total of both sides):

97% × Fe 67.3%
Cr 18%
Ni 11.5%
Mn 2%
Si 1%
Other (C, S, etc.) 0.2%

+ 3% Ag

Density at 22° C, 7.91±0.02 Density at 22° K, 7.99

Beam Path in the Chamber (K Beam, π Beam was similar)

	Mean	Standard Deviation
Radius of curvature	158.5 cm	
Beam axis		
X	-48.722 cm	3.707 cm
Y	147.30 cm	2.468 cm
Z at X = 0	-16.177 cm	0.964 cm
Dip	-0.017	0.024

It can be seen that the beam was in the form of a sheet some 2 cm or a little more thick in Z and about 7 cm wide, broadside facing the cameras. The beam enters near $Y = 0$ at $X < 0$ and proceeds toward $X > 0$, bending toward $Y > 0$. It passes almost exactly through $X = 0$, $Y = 0$, in the mean. The tracks were parallel to about $\pm 2^{o}$.

A small amount of turbulence was present near the corners of the beam ports and between the expansion holes and the piston but these were places where the track density was low. Most of the volume of the chamber especially in important areas was free of turbulence and no difficulty was experienced due to turbulence. In spite of careful design, there was some bubbling in the chamber but this too caused no difficulty.

The Scotchlite[42] on the chamber back has the property of returning a high proportion of the light falling on it to the incident direction with small angular spread. This remains true for incident directions up to about 30^{o} from normal. Light from the ring flashtube surrounding a camera lens is always reflected back to the camera lens by the

Scotchlite, so the Scotchlite appears to be an evenly luminous surface. The cones were plated with silver and polished. Since the cameras viewed the cone surfaces at a small angle, the flashtube light reflected to the Scotchlite at a point not far from the base of the cone at an incident angle within the retrodirecting range and after reflecting at the Scotchlite surface, it returned along the same path to the camera. A camera viewing the cone side also saw an evenly luminous surface -- a curved and distorted virtual image of the real Scotchlite. But curved and distorted Scotchlite appears the same as flat Scotchlite so this appearance of the cones is independent of their shape, in particular of the curvature of the surfaces. It is important to the design that in the worst case the flastube light reflected off the side of a cone hits the backplate within the Scotchlite covered area. The reflectivity of silver at the violet end of the visible spectrum is significantly less than unity, so the virtual Scotchlite seen behind the cone surfaces

Optical Parameters

	X	Y	Z
Camera coordinates	-25.6755	1.3777	157.713
	+12.6693	22.8655	157.713
	+12.4500	-22.9834	157.713
	+0.2900	0.000	157.713
Total glass thickness		13.805 cm	
Average index of refraction		1.501	
Approx. opitcal distance to fiducial plane		153.17	
Stereo ratio camera 4 and another		0.17	
Stereo ratio not camera 4		0.29	

was apparently not as well illuminated as the real Scotchlite backing but tracks were still adequately visible against this background. The cones were in fact sometimes helpful, since when a track penetrated a cone the track's reflection and shadow were often visible, meeting the track at the cone surface, so that the approximate depth of the track could be determined by sight. In particular the depth of a γ conversion point was usually obvious.

Although this arrangement provides visibility in practically all of the chamber volume it is clear that there are several small volumes that are obscured. For example, the small volume between the mounting ring at the base of each cone and the chamber back plate which serves as a flow path for the deuterium is invisible. In addition, in windows in the cones, some of that volume in a 4-mm wide strip which would have been occupied by the cut away metal may be obscured. These volumes are very small and unimportant and are only mentioned to qualify the statement that the entire volume was visible.

Appendix III - Theory of γ Detection

When a γ with large energy compared to the electron mass propagates through matter two processes take place, Compton scattering and pair production.

Define the formal conversion cross section for an atom to be

$$4Z(Z + \xi)r_o^2 \alpha \ell n (183Z^{-1/3})$$

with $\xi = \ell n (1440Z^{-2/3})/\ell n (183Z^{-1/3})$

Z = nuclear charge number

r_o = the classical radius of the electron

(r_o^2 is about 79.3 mb)

α = the fine structure constant

(α is about 1/137.04)

Formal conversion cross sections for various species of atoms (barns):

Fe	6.77
Cr	5.83
Ni	7.79
Mn	6.29
Si	2.13
Ag	20.5

The bulk formal cross section for a homogeneous, but not necessarily homonuclear, material is defined as the sum of the formal cross sections for all atoms in a unit volume and the radiation length is defined as the inverse of the bulk cross section.

Although the cones are not homogeneous (they are stainless steel plated with silver), the plating amounts to 3% or less of the total mass and the situation is approximated by using a radiation length as

if the material were homogeneous. The radiation length at liquid deuterium temperatures was computed to be 1.70 cm. The composition and density of the cones can be found in Appendix II.

Messel et al. present a theoretical formula based on the Bethe-Heitler cross section with screening and with corrections to the Born approximation for the pair production probability per radiation length[60]:

$$\int_{1/U}^{1-1/U} \varphi(U,\epsilon)d\epsilon$$

where

$$\varphi(U,\epsilon) = \delta[(\frac{2}{3} - \frac{1}{36\gamma})C + (\frac{4}{3} + \frac{1}{9\gamma})A(\epsilon - \frac{1}{2})^2]$$

$$A = \frac{3f_1(X) - f_2(X) + 8[\ell n\, Z^{-1/3} - f]}{3f_1(0) - f_2(0) + 8[\ell n\, Z^{-1/3} - f]}$$

$$C = \frac{3f_1(X) + f_2(X) + 16[\ell n\, Z^{-1/3} - f]}{3f_1(0) + f_2(0) + 16[\ell n\, Z^{-1/3} - f]}$$

$$\left.\begin{aligned} f_1(W) &= 20.867 - 3.242W + 0.625W^2 \\ f_2(W) &= 20.209 - 1.930W - 0.086W^2 \end{aligned}\right\} \quad \text{for} \quad W \leq 1$$

$$f_1(W) = f_2(W) = 21.12 - 4.184\, \ell n\,(W + 0.952) \quad \text{for} \quad W > 1$$

$$X = 136Z^{-1/3}\frac{1}{U\epsilon(1 - \epsilon)}$$

$$\delta = \gamma/\beta \;; \quad \gamma = \beta - f \;; \quad \beta = \ell n\,(183Z^{-1/3})$$

$$f = (\frac{Z}{137})^2 \sum_{\mu=1}^{\infty} \{\mu[\mu^2 + (\frac{Z}{137})^2]\}^{-1}$$

U = γ energy in electron masses

The probability is approximately independent of the nature of the material, the radiation length having been defined to roughly account for the nature

of the material. The conversion probability per radiation length computed for iron and various γ energies is given in Fig. 4.

In the formulas above, $\varphi(U,\epsilon)$ is actually the differential probability of conversion with the positron having energy ϵU in electron masses. The kinetic energy of the positron is equally likely to be any value between zero and the available energy, as a first approximation. More accurately the distribution of energy varies somewhat with incident γ energy. The distribution drops off at the very extremes of one electron or the other having all the available energy and at high incident γ energy there is a broad shallow dip at symmetric energy sharing.

Jost, Luttinger, and Slotnick have theoretically computed the pair production differential cross section in terms of the recoil nucleus momentum.[61] Their results indicate that the cross section peaks close to the kinematical minimum recoil momentum and falls rapidly at higher momenta. The cross section is down to 30% of the peak when the product of incident γ momentum and nuclear momentum is 14 MeV^2 at the worst case. This corresponds to a recoil momentum of 140 keV/c for a 100 MeV/c γ. Since for γ's in the 100 MeV energy range the recoil nucleus almost always has less than 1% of the incident momentum, the sum of the electron momenta is very nearly the incident momentum in magnitude and direction.

The Klein-Nishina formula was used to compute the Compton scattering cross section.[62] The total cross section is:

$$2\pi r_o^2 \left\{\frac{A}{U^3}\left[\frac{2UA}{B} - \ell n\, B\right] + \frac{1}{2U}\ell n\, B - \frac{1+3U}{B^2}\right\}$$

$$A = 1 + U \quad , \qquad B = 1 + 2U$$

U = incident γ energy in electron masses .

The differential cross section for Compton scattering with a final γ energy E is:

$$\frac{\pi r_o^2 m_e}{E_o^2}\left[\frac{E_o}{E} + \frac{E}{E_o} + \left(\frac{m_e}{E} - \frac{m_e}{E_o}\right)^2 - 2m_e\left(\frac{1}{E} - \frac{1}{E_o}\right)\right]$$

E_o = incident γ energy .

Figure 5 presents the fraction of Compton scatters per interaction (Compton or pair production) computed for stainless steel. The fraction is several percent in the region of hundreds of MeV and rises as the incident γ energy decreases, reaching about 20% at 25 MeV. Figure 6 gives the probability that a γ with a given initial energy emerges with less than 25 MeV or less than 10 MeV after Compton scattering. It can be seen that any γ in the energy range of hundreds of MeV or less has a high probability of being low energy -- in the range of tens of MeV -- after scattering.

As positrons propagate through matter their behavior is described by the processes of bremsstrahlung, annihilation, ionization loss, and multiple scattering. Negatrons behave similarly except for annihilation.

The Bethe-Heitler formula indicates that the differential probability for a fractional energy loss V per radiation length by bremsstrahlung is about 1/V. The average fractional energy loss per radiation length is then 1. An individual electron has a wide range of possible emerging energies. It may lose nearly all of its energy very rapidly or it can penetrate several radiation lengths without large losses. Much more refined theoretical calculations of bremsstrahlung

energy loss probabilities are available.[63] The probability density for an electron to radiate a fraction V of its energy per centimeter in a homogeneous material is $\frac{F(U,V)}{LV}$, where U is the electron energy in electron masses.

$$L = \frac{A}{4\alpha Z^2 r_o^2 ND}$$

(L is about equal to the radiation length)

N = Avogradro's number

D = density

A = atomic mass

F is defined in two ranges of a parameter γ:

$$\gamma = 100 \frac{1}{U} \frac{V}{1 - V} Z^{-1/3}$$

for $\gamma < 2$

$$F(U,V) = [1 + (1 - V)^2][\frac{f_1(\gamma)}{4} - \frac{1}{3} \ln Z] - \frac{2}{3}(1 - V)[\frac{f_2(\gamma)}{4} - \frac{1}{3} \ln Z]$$

for $2 < \gamma < 15$

$$F(U,V) = [1 + (1 - V)^2 - \frac{2}{3}(1 - V)][\ln (2U \frac{1 - V}{V}) - \frac{1}{2} - C(\gamma)]$$

f_1, f_2 and C are described in tabular form:

γ	$f_1(\gamma)$	$f_2(\gamma)$
0	20.9	20.2
0.4	19.3	19.2
0.8	18.0	
1.2	17.2	
1.6	16.3	
2.0	15.7	

γ	$C(\gamma)$
2	0.21
2.5	0.16
3	0.13
4	0.09
5	0.065
6	0.05
8	0.03
10	0.02
15	0.01

Positron annihilation is important only for low energy positrons as can be seen in Fig. 7. The probability of annihilation per radiation length is plotted for various positron energies for stainless steel. The unit of length was chosen to be convenient for comparison with other quantities such as the bremsstrahlung probability. The plot was made from the annihilation cross section[62]:

$$\pi r_o^2 \frac{1}{U+1}\left[\frac{U^2+4U+1}{U^2-1}\ln\left\{U+\sqrt{U^2-1}\right\}-\frac{U+3}{\sqrt{U^2-1}}\right]$$

U = positron energy in electron masses.

Bremsstrahlung and annihilation can produce high energy γ's that may again convert to pairs (shower). In annihilation, a resultant γ can have high energy only if the positron has high energy, and then it must go forward in the laboratory. The theoretical treatment of bremsstrahlung is similar to the treatment of conversion and the nuclear recoil is of similarly low momentum. The sum of the resultant γ momentum and the electron momentum is essentially the incident momentum. In

either case, if the γ again converts, all the electrons together still represent the original incident γ direction and energy.

The ionization loss was computed to be 26.9 MeV per radiation length for electrons in stainless steel. Multiple scattering was computed from a simple formula[64] to produce a mean squared deflection of 0.18 per radiation length, for a 50 MeV electron and varies as $1/\text{momentum}^2$. For a penetration of 1/4 radiation length an rms deflection of about 0.21 is indicated, while two 50 MeV electrons from a γ give an rms deviation of 0.15.

Appendix IV - Theory of K^o States

The interpretation of the results was done within the theoretical framework presented by Lee and Wu.[65] The time development of a system is taken to be produced by a Hamiltonian which is composed of two terms, H(weak) and H(everything else). H(everything else) is CPT invariant. The states K^o and $\overline{K}^o$ are eigenstates of H(everything else) with

$$\overline{K}^o = CPT\ K^o \quad .$$

Since the development of the K^o state, for example, into the $\overline{K}^o$ state is not forbidden and since this transition would be an undetected transition from one single particle state to another (in contrast with a single particle state decay to an expanding two particle state), the K^o need not decay exponentially. The K^o and $\overline{K}^o$ must be treated together.

At least to the extent that a treatment of the K^o system decay in a perturbation theory with H(weak) being treated as a perturbation on H(everything else) is correct, the rates of change of the K^o and $\overline{K}^o$ amplitudes are linearly related to those amplitudes. Thus the vector ψ may be defined in terms of the two amplitudes A_{K^o}, $A_{\overline{K}^o}$:

$$\psi = (A_{K^o}, A_{\overline{K}^o})$$

and

$$-\frac{d\psi}{d\tau} = V\psi \quad .$$

For some 2×2 matrix V gives the time development of ψ. If H(weak) is CPT invariant perturbation theory may be used to show

$$\text{I.} \quad V(1,1) = V(2,2) \ .$$

and if H(weak) is T invariant perturbation theory shows

$$\text{II.} \quad V(1,2) = V(2,1) \ .$$

Relations I and II together are sufficient to show that V has two linearly independent eigenvectors. Since we wish to proceed without the assumption of CPT or T invariance, it is assumed instead that V does have two linearly independent eigenvectors. Since the long and short lived kaon states are familiar from observation only matrices with two independent eigenvectors can be used for V to accurately describe the neutral kaon system. Two linearly independent two-dimensional eigenvectors can of course be parameterized with the two parameters ϵ,δ:

$$K_S = [2(1 + |\epsilon + \delta|^2)]^{-1/2} \quad \begin{pmatrix} 1 + \epsilon + \delta \\ 1 - \epsilon - \delta \end{pmatrix}$$

$$K_L = [2(1 + |\epsilon - \delta|^2)]^{-1/2} \quad \begin{pmatrix} 1 + \epsilon - \delta \\ -1 + \epsilon - \delta \end{pmatrix}$$

with the completely general representations of their eigenvalues:

$$\tfrac{1}{2}\gamma_S + im_S \quad \text{and} \quad \tfrac{1}{2}\gamma_L + im_L \text{ , respectively.}$$

The matrix V is uniquely determined by its eigenvectors and eigenvalues and we have:

III. $$V_{11} = \tfrac{1}{D}[(1 + \epsilon + \delta)(-1 + \epsilon - \delta)(\tfrac{1}{2}\gamma_S + im_S) - (1 - \epsilon - \delta)(1 + \epsilon - \delta)(\tfrac{1}{2}\gamma_L + im_L)]$$

$$V_{12} = -\tfrac{1}{D}[(1 + \epsilon + \delta)(1 + \epsilon - \delta)(\tfrac{1}{2}(\gamma_S - \gamma_L) + i(m_S - m_L))]$$

$$V_{21} = \tfrac{1}{D}[(-1 + \epsilon - \delta)(1 - \epsilon - \delta)(\tfrac{1}{2}(\gamma_S - \gamma_L) + i(m_S - m_L))]$$

$$V_{22} = -\tfrac{1}{D}[(1 - \epsilon - \delta)(1 + \epsilon - \delta)(\tfrac{1}{2}\gamma_S + im_S) - (-1 + \epsilon - \delta)(1 + \epsilon + \delta)(\tfrac{1}{2}\gamma_L + im_L)$$

$$D = (1 + \epsilon + \delta)(-1 + \epsilon - \delta) - (1 - \epsilon - \delta)(1 + \epsilon - \delta)$$

If CPT invariance of H(weak) is assumed then relation I can be expanded using III to establish $\delta = 0$, while if T invariance is assumed relation

II expanded using III shows $\epsilon = 0$. If H(weak) is CP invariant then K_S and K_L would be eigenstates of the unitary CP operator and hence orthogonal. With

$$\xi = \langle K_S | K_L \rangle \approx 2(\mathrm{Re}\ \epsilon - i\ \mathrm{Im}\ \delta)$$

CP invariance violation is measured by the deviation of ξ from zero.

The eigenstates K_S and K_L of V of course have simple exponential time developments:

IV. $$e^{-(\frac{1}{2}\gamma_S + im_S)\tau} K_S \quad ; \quad e^{-(\frac{1}{2}\gamma_L + im_L)\tau} K_L$$

while the intensities develop as $e^{-\gamma_S \tau}$ and $e^{-\gamma_L \tau}$, respectively. Evidently the experimentally known particles which propagate unchanged through free space until they decay are to be identified with the states K_S and K_L and γ_S and γ_L must be the experimentally measured decay rates. m_S and m_L are the observed particle masses. All solutions to the time development equation

$$-(d\psi/d\tau) = V\psi$$

are found as linear combinations of the two functions given in IV.

Suppose that some means were found by which one could test for the presence of the K_S state. The amount of K_S in the K^o state would then be given by

$$|\langle K_S | K^o \rangle|^2 = \frac{|1 + \epsilon + \delta|^2}{2(1 + |\epsilon + \delta|^2)} \approx \frac{1}{2} + \mathrm{Re}\ \epsilon + \mathrm{Re}\ \delta$$

with the approximation made assuming ϵ and δ are small.

Alternatively, consider the total decay rate at time τ of a system that was a pure K^o state at time zero, which is computed from the known time developments IV:

$$|A|^2 \gamma_S e^{-\gamma_S \tau} + |B|^2 \gamma_L e^{-\gamma_L \tau} + 2 \text{ Re } \{A^* B \langle K_S | K_L \rangle$$

$$(\tfrac{1}{2}(\gamma_S + \gamma_L) + i(m_L - m_S))\exp[-\tfrac{1}{2}(\gamma_S + \gamma_L)\tau - i(m_L - m_S)\tau]\}$$

where $K^o = AK_S + BK_L$,

$$|A|^2 = \frac{(1 + |\epsilon + \delta|^2)|1 - \epsilon + \delta|^2}{2|1 - \epsilon^2 + \delta^2|^2} \approx \frac{1}{2} - \text{Re } \epsilon + \text{Re } \delta$$

$$|B|^2 = \frac{(1 + |\epsilon - \delta|^2)|1 - \epsilon - \delta|^2}{2|1 - \epsilon^2 + \delta^2|^2} \approx \frac{1}{2} - \text{Re } \epsilon - \text{Re } \delta$$

$$A^* B \langle K_S | K_L \rangle = \frac{(\epsilon^* + \delta^* + \epsilon - \delta)(1 - \epsilon^* + \delta^*)(1 - \epsilon - \delta)}{2|1 - \epsilon^2 + \delta^2|^2} \approx \text{Re } \epsilon - i \text{ Im } \delta$$

It can be seen that the first term gives a pure exponential decay with the short lifetime. If the decay component with the short lifetime is taken as the definition of the amount of K short in the K^o state, then this quantity is

$$|A|^2 \approx \frac{1}{2} - \text{Re } \epsilon + \text{Re } \delta$$

and differs by about 2 Re ϵ from $|\langle K_S | K^o \rangle|^2$. The question how much K_S is in K^o can have different answers. Care must be taken to state the question unambiguously.

It is not clear how to go about detecting the presence of the K_S state. The careful fitting of an entire decay rate function to the three terms to find the best coefficient for the short lifetime exponential term was also considered inconvenient. It was decided to interpret the experiment in terms of the total fraction of a pure sample of K^o's decaying by any mode in less than six short lifetimes. This should be given by

$$\text{V.}\quad 1 - |A|^2 e^{-6} - |B|^2 e^{-6\gamma_L/\gamma_S} - 2\,\mathrm{Re}\,\{A^*B(K_S|K_L)\exp[-\frac{3(\gamma_S+\gamma_L)}{\gamma_S} - 6i\frac{(m_L - m_S)}{\gamma_S}]\}$$

An explicit value for the 2 × 2 complex matrix V constitutes a complete description of the free space propagation of the neutral kaon system within this phenomenological theory. It is more convenient to consider explicit values for the two eigenvalues and eigenvectors from which V can be easily computed. Thus the real numbers m_S, m_L, γ_S, γ_L together with the complex numbers ϵ,δ completely characterize the system (relations III). The four real numbers corresponding to observed masses and lifetimes are all known to well better than ±1%.[27]

$$\left.\begin{matrix} m_S \\ m_L \end{matrix}\right\} \quad 497.79\pm0.15\ \text{MeV}$$

$$\gamma_S \quad (1.160\pm0.008)\times 10^{10}\ \text{sec}^{-1}$$

$$\gamma_L \quad (1.933\pm0.016)\times 10^{7}\ \text{sec}^{-1}$$

$$\frac{m_L - m_S}{\gamma_S} \quad 0.4653\pm0.0042$$

The parameters ϵ,δ are not so directly connected with observation. If CPT invariance is assumed then Re ϵ is obtainable to good accuracy from charge asymmetry in leptonic decays together with a value for the $\Delta S - \Delta Q$ violating parameter. CPT invariance also allows direct computation of ϵ as a combination of η_{+-} and η_{oo} where

$$\eta_{+-} = \frac{A(K_L \to \pi^+\pi^-)}{A(K_S \to \pi^+\pi^-)}$$

and

$$\eta_{oo} = \frac{A(K_L \rightarrow \pi^o\pi^o)}{A(K_S \rightarrow \pi^o\pi^o)}$$

There is agreement on Re ϵ assuming CPT invariance, with the more accurate charge asymmetry result being Re $\epsilon = (1.64\pm0.24) \times 10^{-3}$ (Ref. 27) and the phases of both η_{+-} and η_{oo} being 44 ± 3^o and 51 ± 30^o, respectively,[27] indicates that Im ϵ is about the same as Re ϵ, if CPT invariance is good.

A more involved analysis not assuming CPT or CP invariance has yielded values for ϵ and Im δ (Ref. 28):

$$\text{Re } \epsilon = (1.68\pm0.30) \times 10^{-3}$$

$$\text{Im } \epsilon = (1.45\pm0.30) \times 10^{-3}$$

$$\text{Im } \delta = (-\ 0.30\pm0.45) \times 10^{-3}$$

A sum rule based on unitarity and isospin arguments were used. In addition, there were assumptions of the absence of $\Delta I = 5/2$ currents, and that CP violation in leptonic decays is independent of spin orientation and position in the Dalitz plot. Many experimentally measured quantities were used notably η_{+-}, η_{oo}, time distributions of leptonic decays, and the famous $K_S - K_L$ mass difference. Re δ was not determined as it was not separable from a CPT violating parameter in the transition matrix.

Using the known parameters the fraction of a sample of K^o's decaying before six short lifetimes (expression V) can be evaluated as

VI. $\quad (0.5052\pm0.0003) + (0.9876\pm0.0001)\text{Re } \delta$

assuming Re δ is small. A measurement of the fraction of K^o's decaying before six short lifetimes therefore provides a measurement of the one K^o propagation parameter so far unmeasured: Re δ.

Appendix V - Theory of the Modes of K_S Decay

Since the neutral kaon has spin-0, Bose statistics for pions dictates that the only two-pion states that it can decay to are $I = 0$ and $I = 2$. The two states are:

$$(0,0) = \frac{1}{\sqrt{3}} (\pi^-\pi^+ - \pi^o\pi^o + \pi^+\pi^-)$$

$$(2,0) = \frac{1}{\sqrt{6}} (\pi^-\pi^+ + 2\pi^o\pi^o + \pi^+\pi^-)$$

The properly symmetrized 2π states are:

$$\frac{1}{\sqrt{2}} (\pi^+\pi^- + \pi^-\pi^+) = C$$

$$\pi^o\pi^o = N$$

which can be expressed in terms of the isospin states:

$$C = \sqrt{2/3}\ (0,0) + \frac{1}{\sqrt{3}}\ (2,0)$$

$$N = -\frac{1}{\sqrt{3}}\ (0,0) + \sqrt{2/3}\ (2,0)$$

The $\Delta I = 1/2$ transition produces only the $(0,0)$ state while the $(2,0)$ state may result from $\Delta I = 3/2$ or $\Delta I = 5/2$ transitions. Notice that if only the $\Delta I = 1/2$ transitions take place, then the branching ratio

$$\frac{\Gamma(K_S \rightarrow \pi^+\pi^-)}{\Gamma(K_S \rightarrow \pi^o\pi^o)} = 2 \quad ,$$

apart from small electromagnetic and phase space corrections (less than a 1% correction, total), just by inspection of the expansion of $(0,0)$. We assume CPT invariance at this point so that $\delta = 0$. The analysis not assuming CPT invariance is similar but with more algebraic complication. We then have

$$K_S = \frac{1}{\sqrt{2(1 + \epsilon\epsilon^*)}} \begin{pmatrix} 1 + \epsilon \\ 1 - \epsilon \end{pmatrix} .$$

Define

$$A_0 = \langle (0,0) | H_{weak} | K^o \rangle$$

$$A_2 = \langle (2,0) | H_{weak} | K^o \rangle$$

and observe that if H(weak) is CPT invariant then

$$A_0^* = \langle (0,0) | H_{weak} | \bar{K}^o \rangle$$

$$A_2^* = \langle (2,0) | H_{weak} | \bar{K}^o \rangle$$

one phase factor is arbitrary and, following Lee and Wu,[65] A_0 is chosen to be real.

$$H_{weak} K_S = \frac{1}{\sqrt{2(1 + \epsilon\epsilon^*)}} [((1 + \epsilon)A_0 + (1 - \epsilon)A_0^*)(0,0)$$

$$+ ((1 + \epsilon)A_2 + (1 - \epsilon)A_2^*)(2,0)] .$$

In addition, the final state strong interaction introduces phase shifts in the isospin-0 and -2 states, respectively. The wave function ψ resulting from K_S decay is given by:

$$\frac{1}{\sqrt{2(1 + \epsilon\epsilon^*)}} [((1 + \epsilon)A_0 + (1 - \epsilon)A_0^*)e^{i\delta_0}(0,0)$$

$$+ ((1 + \epsilon)A_2 + (1 - \epsilon)A_2^*)e^{i\delta_2}(2,0)] .$$

The branching ratio can then be written

$$\frac{\Gamma(K_S \to \pi^+\pi^-)}{\Gamma(K_S \to \pi^o\pi^o)} = \frac{\rho_{+-}}{\rho_{oo}} \cdot \frac{|\langle C|\psi\rangle|^2}{|\langle N|\psi\rangle|^2}$$

where ρ_{+-} and ρ_{oo} are density of states factors. This is easily evaluated to give

$$\frac{\Gamma(K_S \to \pi^+\pi^-)}{\Gamma(K_S \to \pi^0\pi^0)} =$$

$$2\,\frac{\rho_{+-}}{\rho_{00}}\left|\frac{1 + 2^{-1/2}e^{i(\delta_2-\delta_0)}\,\mathrm{Re}(A_2/A_0) + 2^{-1/2}\epsilon i\,\mathrm{Im}(A_2/A_0)e^{i(\delta_2-\delta_0)}}{1 - 2^{1/2}e^{i(\delta_2-\delta_0)}\,\mathrm{Re}(A_2/A_0) - 2^{1/2}ei\,\mathrm{Im}(A_2/A_0)e^{i(\delta_2-\delta_0)}}\right|^2$$

Dropping the terms containing ϵ Im A_2 and further approximating by assuming A_2 is small compared to A_0,

$$\frac{\Gamma(K_S \to \pi^+\pi^-)}{\Gamma(K_S \to \pi^0\pi^0)} \approx \frac{\rho_{+-}}{\rho_{00}}\,(2 + 6\sqrt{2}\ \mathrm{Re}(\frac{A_2}{A_0})\cos(\delta_2 - \delta_0))$$

$$\frac{\rho_{+-}}{\rho_{00}} \approx 0.986 \quad .$$

Electromagnetic corrections need to be made to this formula and allowance for soft photon emission. Allowing up to 10 MeV γ's to accompany the decay, the effects have been calculated by Nachtmann and Rafael.[66] The correction was found to be somewhat less than 1% and roughly cancels the phase space factors. They give the corrected relation

VII. $$\frac{\Gamma(K_S \to \pi^+\pi^-\gamma \text{ up to } 10 \text{ MeV})}{\Gamma(K_S \to \pi^0\pi^0)} = 2 + 6\sqrt{2}\ \mathrm{Re}(\frac{A_2}{A_0})\cos(\delta_2 - \delta_0) - 0.006$$

Experimental measurement has shown that $|\mathrm{Im}(A_2)/\mathrm{Re}(A_2)| \leq 0.06$ with some evidence that this upper limit may be safely halved.[67] Thus, to more than adequate accuracy, $\mathrm{Re}(A_2/A_0) = A_2/A_0$. Further, if CP is conserved A_2 would be real to lowest order in the weak interactions, and CP conservation is apparently a good approximation although not exactly true. Both A_2 and the rate $(K^+ \to \pi^+\pi^0)$ contain contributions, in different proportions, from $|\Delta I| = 3/2$ and $|\Delta I| = 5/2$ transitions.

If it is assumed that only the $|\Delta I| = 3/2$ amplitude is important then $|A_2/A_0|$ and therefore $|\mathrm{Re}(A_2/A_0)|$ can be estimated from the K^+ decay rate to be about 4.5%.[65]

Appendix VI - Propagation of Neutral Kaons Through Matter

A particle that is initially a K^o at 600 MeV/c or less traveling through matter, due to strangeness and baryon conservation, may in the beginning only scatter, charge exchange, or induce pion production. If the situation is first approximated as propagation in free space, then from Appendix IV it is seen that a $\overline{K}^o$ component will appear and grow. In fact (still approximating the case as free space propagation), the wave function will eventually become a pure K_L state which is approximately 50% $\overline{K}^o$. Due to strangeness conservation the strong interactions cause no mixing of the K^o and $\overline{K}^o$ states so that these states may be considered individually in their interactions with the medium. The $\overline{K}^o$ component of the wave may enter in reactions producing Σ's or Λ's, as well as participate in reactions such as scattering, charge exchanging, and pion production which are also possible for the K^o component.

As the beam proceeds through matter both debris of various kinds and a scattered K wave are left in the wake and an ever diminishing K component continues in the forward direction. Since the K^o and $\overline{K}^o$ components interact differently with matter, there is a readjustment of the K_S - K_L composition of both the scattered and forward K waves. This leads to the reappearance of decays characteristic of the K_S component in both waves even at times very long compared with the K_S mean lifetime.

To gain an idea of the possible magnitude of these effects when the medium is liquid deuterium, consider the following simplified model. The forward wave is a pure K^o state from the initial time up until one mean K_S lifetime has elapsed. After one mean K_S lifetime the forward wave is a pure K_L state.

First, consider the initial part of the trajectory up until one short lifetime when the forward wave is pure K^o. Over the range of momentum from zero to 600 MeV/c the kaon-nucleon total cross section in the $I = 0$ state ranges between 0 and about 16.5 mb, while in the $I = 1$ state the cross section is more nearly constant at about 12 mb.[68] 23 mb may be taken as an estimate of the K^od total cross section over this range of momenta. This would give a K^o interaction rate of about 1.2×10^{-3} per cm in liquid deuterium. With a mean length of flight of about 3 cm before the observation of K_S decay the loss of forward K^o flux should average several tenths of a percent up until this time.

At longer times the model provides that the forward wave is pure K_L. An extrapolation of the measured cross section in hydrogen for the reaction $K_L p \rightarrow K_S p$ (Ref. 69) indicates that in the range of momenta below 600 MeV/c the cross section for this reaction is about 7 mb. Assuming the neutron contributes the same to regeneration in the scattered wave, the rate for such regeneration in deuterium would be about 7×10^{-4} per cm. With a mean path in deuterium of 13 cm, 0.9% of the K_L flux would produce K_S's in the scattered wave. The $\bar{K}^o N$ total cross section in the $I = 0$ state below 600 MeV/c ranges up to 100 mb while in the $I = 1$ state it is near 20 mb.[68] Thus the $\bar{K}^o$d total cross section over the range of momenta in this experiment may be typically represented as 80 mb. The simplest view of regeneration in the scattered wave, which comes from considering that only the $\bar{K}^o$ interacts with matter, would lead to the estimate that the cross section for such regeneration should be one-fourth of the $\bar{K}^o$ elastic and inelastic cross section. A substantial amount of the $\bar{K}^o$d total cross section is not elastic or inelastic so this would lead to a regeneration cross section

substantially below 20 mb. This is in agreement with the 14 mb estimated above (give or take a factor of 2). Averaging the $\bar{K}^o d$ and $K^o d$ total cross sections yields 50 mb as the estimated $K_L d$ total cross section. The rate for the production of other debris such as Λ's, pions, recoils from scatters not causing regeneration, etc., may thus be expected to be 1-2% of the K_L flux for a path length of 13 cm.

The problem of K_S regeneration in the forward wave, usually called coherent regeneration has been of much interest. A formalism analogous to that in Appendix IV has been developed describing this effect.[65] Essentially, an additional term characteristic of the medium is added to the time development matrix. The resultant two eigenvectors of this matrix, analogous to the K_S and K_L eigenvectors of the free space development matrix, are the two states which propagate without mixing and with simple exponential decay in the medium. In terms of the K_S and K_L states the eigenstates in the medium are approximately

$$|K_1'\rangle = |K_S\rangle - r|K_L\rangle$$

and

$$|K_2'\rangle = |K_L\rangle + r|K_S\rangle$$

with

$$r = - \frac{i\pi N\Lambda(\bar{f}(0) - f(0))}{k(\frac{1}{2} + i\mu)}$$

N = number of nuclei/unit volume

$f(0), \bar{f}(0)$ are the forward elastic scattering amplitudes for $K^o, \bar{K}^o$

k = particle momentum

Λ is approximately the K_S mean path length before decay

μ is the ratio of eigenstate mass difference to decay rate difference

If μ is of the same order of magnitude as the analogous quantity in free space, which is of the order of magnitude 1, then to sufficient accuracy

for our purposes

$$\left|\left(\frac{1}{2} + i\mu\right)\right| = 1$$

$f(0)$ and $\bar{f}(0)$ can be approximated as being purely imaginary and then they can be related to the K^o and $\bar{K}^o$ total cross sections:

$$\frac{4\pi}{k} \text{ Im } f(0) = \sigma_{K^o} \approx 20 \text{ mb}$$

$$\frac{4\pi}{k} \text{ Im } \bar{f}(0) = \sigma_{\bar{K}^o} \approx 80 \text{ mb}$$

With these approximations $|r|$ is found to be

$$1.9 \times 10^{-3}$$

The long-lived part of the wave in the medium will contain a K_S flux (besides that due to CP nonconservation) amounting to $|r|^2$ or about 4×10^{-6} of the total. The mean path before decay of a K_S is about 2.5 cm so that about 2×10^{-6} K_S decays/cm should appear to be regenerated per K_L in the beam. For a 13 cm path length 2.5×10^{-5} K shorts are expected to be regenerated per K_L. Even if, due to the approximations, these estimates were in error by two orders of magnitude the rate for coherent regeneration could not be significant.

Probably most of the perhaps 0.3% of the original K^o flux that interacts before 1 K_S mean life represents a true loss of flux -- let us say 0.2% is lost. 0.9% of the K_L flux is expected to incoherently regenerate. Since these K shorts, when they decay, will often be kinematically much different from what would have been expected for simple K_S or K_L decay (the regeneration is accompanied by changes in angle and momentum) and they occur evenly distributed over 13 cm or more length of flight, not all are likely to have been detected as decays. It is reasonable to suppose that half were detected. The approximately 1%

of the K_L flux engaging in other interactions, such as Λ production, should most of the time not have been confused with K decay and should not be a significant factor. Coherent regeneration was seen to not be significant. The net effect of the medium should have resulted in a 0.25% increase in the total number of K^o decays before six short mean lives as compared with propagation in vacuum. The branching ratio could only have been affected by the 0.3% of the K^o flux interacting before one short mean lifetime. Even at that the effect is only due to the perhaps 0.1% which interacted and were detected anyway, and depends on the differences in detection efficiency between the two decay modes after a K^o interaction.

The metal cones represent an additional complication. The expectation value for thickness of penetration of steel for a K^o is of the order of 1% of the track length, generously estimated. The density of the steel is 50 times that of the deuterium. Effects other than coherent regeneration scale with the density if the nucleons interact independently. The cones should therefore increase the effects calculated for the liquid by 50%, so there should be a total increase in the decay rate up to six short mean lives by 0.4% relative to propagation in vacuum, considering both liquid and metal. Although the total coherent regeneration is increased by a factor of 25 over that computed for the liquid alone, it is still insignificant.

Appendix VII - Errors with a Binomial Distribution

In a physical situation in which events are occurring randomly, however the number of opportunities for the random events to occur is well defined (for example, random occurrence of heads up at the flip of a coin), binomial distribution formulas are believed to be applicable. If a coin is flipped N times and heads up occurs M times, then the statistical error on the number M can be estimated as

$$\sqrt{M(1 - \frac{M}{N})} \quad .$$

The random error is analogously computed for such measurements as the number of K_S's that decay to $\pi^+\pi^-$ or the fraction of γ's that convert in a metal plate. This situation may be contrasted with the other familiar case of measuring random rates. For example, if M cosmic rays enter an apparatus in a fixed time interval there is no well defined number of opportunities for this to happen and the random error is estimated as

$$\sqrt{M} \quad .$$

REFERENCES AND NOTES

1. L. Leprince-Ringuet and M. Lheritier, Compt. Rend. 219, 618 (1944).

2. G. D. Rochester and C. C. Butler, Nature 160, 855 (1947).

3. L. Leprince-Ringuet, Revs. Mod. Phys. 21, 42 (1949).

4. R. Brown, U. Camerini, P. H. Fowler, H. Muirhead, C. F. Powell, P. M. Ritson, Nature 163, 82 (1949).

5. Review article: L. Leprince-Ringuet, Ann. Rev. Nucl. Sci. 3, 39 (1953).

6. R. W. Thompson, A. V. Buskirk, L. R. Etter, C. J. Karzmark, and R. H. Rediker, Phys. Rev. 90, 329 (1953); note particularly Footnote 12.

7. For example: Proceedings of the Third Annual Rochester Conference, 1952, p. 43 and following.

8. A. Pais, Phys. Rev. 86, 663 (1952).

9. R. L. Garwin, Phys. Rev. 90, 274 (1953).

10. W. B. Fowler, R. P. Shutt, A. M. Thorndike, and W. L. Whittemore, Phys. Rev. 91, 1287 (1953).

11. M. Gell-Mann attributes this term to M. G. K. Menon, Nuovo Cimento Suppl. 4, 2, 853 (1956).

12. M. Gell-Mann, Phys. Rev. 92, 833 (1953).

13. T. Nakano and K. Nishijima, Prog. Teor. Phys. (Kyoto) 10, 581 (1953).

14. M. Gell-Mann, Nuovo Cimento Suppl. 4, 2, 848 (1956).

15. M. Gell-Mann and A. Pais, Proceedings of the 1954 Glasgow Conference on Nuclear and Meson Physics, p. 342.

16. M. Gell-Mann and A. Pais, Phys. Rev. 97, 1387 (1955).

17. A. Pais and O. Piccioni, Phys. Rev. 100, 1487 (1955).

18. K. Lande, E. T. Booth, J. Impeduglia, L. M. Lederman, W. Chinowsky, Phys. Rev. 103, 1901 (1956). The following paper (W. E. Fry, J. Schneps, M. S. Swami) on page 1904 submitted a few days earlier is also of interest. A more complete account of the Lande experiment is to be found in M. Bardon, K. Lande, and L. M. Lederman, Ann. Physics 5, 156 (1958).

19. F. Muller, R. W. Birge, W. B. Fowler, R. H. Good, W. Hirsch, R. P. Matsen, L. Oswald, W. M. Powell, H. S. White, and O. Piccioni, Phys. Rev. Letters 4, 418 (1960) and R. H. Good, R. P. Matsen, F. Muller, O. Piccioni, W. M. Powell, H. S. White, W. B. Fowler, and R. W. Birge, Phys. Rev. 124, 1223 (1961).

20. T. D. Lee and C. N. Yang, Phys. Rev. 104, 254 (1956).

21. C. S. Wu, E. Ambler, R. W. Hayward, D. D. Hoppes, and R. P. Hudson, Phys. Rev. 105, 1413 (1957).

22. R. L. Garwin, L. M. Lederman, and M. Weinrich, Phys. Rev. 105, 1415 (1957).

23. L. Landau, Nucl. Physics 3, 127 (1957).

24. R. G. Sachs, and S. B. Treiman, Phys. Rev. Letters 8, 137 (1962).

25. J. K. Christenson, J. W. Cronin, V. L. Fitch, and R. Turlay, Phys. Rev. Letters 13, 138 (1964).

26. G. Luders, Ann. Physics 2, 1 (1957) and W. Pauli, Niels Bohr and the Development of Physics, W. Pauli (editor), New York 1955, p. 30.

27. A. Rittenberg, A. Barbaro-Galtieri, T. Lasinski, A. H. Rosenfeld, T. G. Trippe, M. Roos, C. Bricman, P. Soding, N. Barash-Schmidt, and C. G. Wohl, Revs. Mod. Phys. 43, S1 (1971).

28. K. R. Schubert, B. Wolff, J. C. Chollet, J.-M. Gaillard, M. R. Jane, T. J. Ratcliffe, and J.-P. Repellin, Phys. Letters 31B, 662 (1970).

29. D. F. Bartlett, C. E. Friedberg, P. E. Goldhagen, and K. Goulianos, Phys. Rev. Letters 27, 881 (1971).

30. F. Eisler, R. Plano, N. Samios, M. Schwartz, and J. Steinberger, Nuovo Cimento 5, 1700 (1957).

31. F. S. Crawford, Jr., M. Cresti, R. L. Douglass, M. L. Good, G. R. Kalbfleisch, M. L. Stevenson, and H. K. Ticho, Phys. Rev. Letters 2, 266 (1959).

32. C. Baglin, M. Bloch, V. Brisson, J. Hennessy, A. Lagarrigue, P. Mittner, P. Musset, A. Orkin-Lecourtois, P. Rancon, A. Rousset, A. M. Sarius, X. Sauteron, and J. Six, Nuovo Cimento 18, 1043 (1960).

33. J. L. Brown, H. C. Bryant, R. A. Burnstein, D. A. Glaser, R. Hartung, J. A. Kadyk, J. D. Van Putten, D. Sinclair, G. H. Trilling, and J. C. Vander Velde, Nuovo Cimento 19, 1155 (1961).

34. J. L. Brown, J. A. Kadyk, G. H. Trilling, B. P. Roe, D. Sinclair, and J. C. Vander Velde, Phys. Rev. 130, 769 (1963).

35. M. Chretien, V. K. Fischer, H. R. Crouch, Jr., R. E. Lanou, Jr., J. T. Massimo, A. M. Shapiro, J. P. Averell, A. E. Brenner, D. R. Firth, L. G. Hyman, M. E. Law, R. H. Milburn, E. E. Ronat, K. Strauch, J. C. Street, J. J. Szymanski, L. Guerriero, I. A. Pless, L. Rosenson, and G. A. Salandin, Phys. Rev. 131, 2208 (1963).

36. G. Bozoki, E. Fenyves, E. Gombosi, E. Nagy, G. Suranyi, F. Telbisz, and G. Vesztergombi, Phys. Letters 30B, 498 (1969).

37. B. Gobbi, D. Green, W. Hakel, R. Moffett, and J. Rosen, Phys. Rev. Letters 22, 682 (1969).

38. J. Morfin, D. Sinclair, Phys. Rev. Letters 23, 660 (1969).

39. D. Berley, Brookhaven National Laboratory AGS Division Technical Note 25.

40. G. T. Danby, Brookhaven National Laboratory AGS Internal Report GTD-2 and G. T. Danby, J. W. Jackson, and S. T. Lin, BNL AGS Internal Report GTD/JWJ/STL-1.

41. E. Bierman, A. Goshaw, D. Sager, A. Colleraine, J. Koehler, A. Prodell, and U. Nauenberg, Proceedings of International Conference on Bubble Chamber Technology, Argonne National Laboratory, 1970, p. 555.

42. Trademark of 3M Company.

43. J. Maynard, U. Nauenberg, D. Berley, D. Campbell, A. Kasden, J. Koehler, R. Majestic, and G. Radlhamer, Brookhaven National Laboratory Internal Report EP+S DIV 68-1 (1968).

44. From $\pi^- p \rightarrow N\pi^o$, CERN/HERA 70-7, Compilation of Cross Sections VI. π-Induced Reactions (1970).

45. M. Olsson, Ph. D. Thesis, University of Maryland, Technical Report No. 379 (1964).

46. To obtain the cross section $\pi^+ d \rightarrow pp\gamma$, detailed balance arguments and the cross section for $\gamma p \rightarrow N\pi^+$ were used. See CERN/HERA 70-1, A Collection of Pion Photoproduction Data.

47. Estimated from inverse by detailed balancing. CERN/HERA 70-2, Compilation of Cross Sections I - Proton Induced Reactions (1970).

48. Estimated from $\pi^+ p$ and $\pi^- p$ total cross sections. CERN/HERA 70-5 and 70-7, Compilation of Cross Sections IV - π^+ Induced Reactions and VI - π^- Induced Reactions.

49. CERN/HERA 70-4, Compilation of Cross Sections III - K^+ Induced Reactions (1970).

50. Estimated by extrapolating cross section at 810 MeV/c linearly to zero at threshold. CERN/HERA 70-4, Compilation of Cross Sections

III - K^+ Induced Reactions (1970).

51. A. K. Ray, Ph. D. Thesis, Carnegie-Mellon University (1968), p. 60.

52. Estimated by extrapolating cross section at 863 MeV/c linearly to zero threshold. UCRL-20000 K^+N, A Compilation of K^+N Reactions (1969).

53. Estimated by extrapolating cross section for $K^+p \rightarrow NK^+\pi^+$ linearly to zero at threshold. CERN/HERA 70-4, Compilation of Cross Sections III - K^+ Induced Reactions.

54. Ratios computed from the relevant cross sections taken from: M. Olson, Ph. D. Thesis, University of Maryland, Technical Report No. 379 (1964).

55. L. Hulthen and A. Sugawara, Handbuch der Physik 39, 1 (Springer-Verlag, Berlin, 1957).

56. B. R. Webber, Ph. D. Thesis, UCRL-19226 (1969), p. 39.

57. S. Marateck, V. Hagopian, W. Selove, L. Jacobs, F. Oppenheimer, W. Schultz, L. J. Gutay, D. H. Miller, J. Prentice, E. West, W. D. Walker, Phys. Rev. Letters 21, 1613 (1968).

58. W. D. Walker, J. Carroll, A. Garfinkel, and B. Y. Oh, Phys. Rev. Letters 18, 630 (1967).

59. A. H. Rosenfeld, N. Barash-Schmidt, A. Barbaro-Galtieri, L. R. Price, P. Soding, C. G. Wohl, M. Roos, and W. J. Willis, Revs. Mod. Phys. 40, 77 (1968).

60. H. Messel, A. D. Smirnov, A. A. Varfolomeev, D. F. Crawford, and J. C. Butcher, Nucl. Physics 39, 1 (1962).

61. R. Jost, J. M. Luttinger, and M. Slotnick, Phys. Rev. 80, 189 (1950).

62. W. Heitler, The Quantum Theory of Radiation, Third Ed. (Oxford, 1954).

63. H. A. Bethe and W. Heitler, Proc. Roy. Soc. A146, 83 (1934).

64. N. Barash-Schmidt, A. Barbaro-Galtieri, C. Bricman, T. Lasinski, A. Rittenberg, M. Roos, A. H. Rosenfeld, P. Soding, T. G. Trippe, C. G. Wohl, Particle Properties, April 1971 (Berkeley, 1971).

65. T. D. Lee and C. S. Wu, Ann. Rev. Nucl. Sci. 16, 511 (1966).

66. O. Nachtmann and E. De Rafael: On Radiative Corrections to the $\Delta I = 1/2$ Rule in $K_S \to \pi^+\pi^-$ and $K_S \to \pi^o\pi^o$ Decays, CERN REF.TH.1031-CERN (Geneva, 1969).

67. B. Gobbi, D. Green, W. Hakel, R. Moffett, J. Rosen, B. Goz, and D. Tycko, Phys. Rev. Letters 22, 685 (1969).

68. L. R. Price, N. Barash-Schmidt, O. Benary, R. W. Bland, A. H. Rosenfeld, and C. G. Wohl, A Compilation of K^+N Reactions, UCRL-20000 K^+N (1969).

69. A. D. Brody, W. B. Johnson, B. Kehoe, D. W. G. S. Leith, J. S. Loos, G. J. Luste, K. Moriyasu, B. C. Shen, W. M. Smart, F. C. Winkelmann, and R. J. Yamartino, Phys. Rev. Letters 26, 1050 (1971).

Table I

1.	Pion charge exchanges	10,983
2.	Detected gammas	3,781
3.	Gamma background	-60
4.	Correction for $\pi^+ D \rightarrow pp\gamma$ and $\pi^+ D \rightarrow pp\pi^o\pi^o$	-35
5.	Total gammas	3,686
6.	Single gamma detection efficiency line 5/(line 1 × 2)	16.8±0.3%
7.	Detection efficiency for $K^o \rightarrow \pi^o\pi^o$ obtained by operating on line 6 with Monte Carlo	50.8±1.1%
8.	Increase in efficiency for $K^o \rightarrow$ neutrals before 6 τ_S due to 0.6% $K^o \rightarrow \pi^o\pi^o\pi^o$	0.1%
9.	Detection efficiency for $K^o \rightarrow$ neutrals before 6 τ_S	50.9±1.1%
10.	Kaon crude C.E. sample	12,970
11.	Beam contamination (π^+ and p)	-95
12.	Measured background (due to 2 p's nonstopping)	-26
13.	Total K^o productions	12,849
14.	Events with V	4,560
15.	Beam contamination	-20
16.	Total charged mode decays	4,540
17.	Events with detected gammas	1,284
18.	Measured background gammas	-257
19.	Beam contamination	-16
20.	Unmeasured gammas	+10
21.	Total observed neutral decays	1,021

22.	K^o neutral decays before 6 τ_S (line 21/line 9)	2,006
	Analysis for $R(K_S \rightarrow \pi^+\pi^-)/R(K_S \rightarrow \pi^o\pi^o)$ to be referred to simply as BR.	
23.	Charged mode decays (brought forward from line 16)	4,540
24.	K_L charged mode decays	-112
25.	K_S charged mode decays after escaping chamber	+2
26.	Leptonic decays and $K_S \rightarrow \pi^+\pi^-\gamma$ with γ above 10 MeV energy	-22
27.	Total $K_S \rightarrow \pi^+\pi^-$	4,408
28.	K^o neutral decays before 6 τ_S (brought forward from line 22)	2,006
29.	K_L neutral decays before 6 τ_S	-14
30.	$K_S \rightarrow \pi^o\pi^o$ after 6 τ_S	+3
31.	Total $K_S \rightarrow \pi^o\pi^o$	1,995
	Analysis not assuming CPT	
32.	BR not assuming CPT (line 27/line 31)	2.21±0.11
	Analysis assuming CPT	
33.	K^o productions (brought forward from line 13)	12,849
34.	Short lifetime fraction of K^o 0.5 - Re ϵ	0.4984
35.	Number of K_S (line 33/line 34)	6404±57
36.	$K_S \rightarrow \pi^+\pi^-\gamma$ (γ above 10 MeV) and leptonic decays	-22
37.	Total $K_S \rightarrow 2\pi$ decays	6382±57
	Using only the V decay data	
38.	Computed $K_S \rightarrow \pi^o\pi^o$ (line 37 - line 27)	1974
39.	BR from V data only (line 27/line 38)	2.23±0.084
	Using only the gamma data	

40.	Computed $K_S \rightarrow \pi^+\pi^-$ (line 37 - line 31)	4387
41.	BR from gamma data alone (line 40/line 31)	2.20±0.15
	Best value for BR assuming CPT and using all data	
42.	BR assuming CPT	2.22±0.08
	Weighted average of lines 39 and 41	

Analysis for the total fraction of K^o decaying to all modes before 6 K_S mean lifetimes.

43.	Total K^o's (brought forward from line 13)	12,849
44.	Total observed charged mode decays (brought forward from line 16)	4,540
45.	Charged mode decays observed after 6 τ_S	-74
46.	Charged mode decays observed before 6 τ_S	4,466
47.	Neutral mode decays before 6 τ_S (brought forward from line 22)	2,006
48.	Total decays before 6 τ_S	6,472
49.	Fraction of K^o decaying before 6 τ_S (line 48/line 43)	0.5038±0.0075

FIGURE CAPTIONS

Fig. 1. Time-of-flight spectrum for the 620 MeV/c beam.

Fig. 2. K^+ beam range in copper.

Fig. 3. Schematic representation of the BNL 30-inch bubble chamber with γ converting cones and modified optical system.

Fig. 4. Conversion probability per radiation length. Computations were made using the Messel function for the case of iron.

Fig. 5. Ratio of Compton scatters/scatters + pair production. Compton scattering probability for free electrons was computed with the Klein-Nishina formula and multiplied by the total electron density of stainless steel. The pair production probability was computed for steel from the Messel function.

Fig. 6. Probabilities for a γ to have energy less than 25 MeV (trace a) and less than 10 MeV (trace b) after Compton scattering.

Fig. 7. Probability of positron annihilation per radiation length. These computations are for stainless steel.

Fig. 8. Gamma momentum distribution in π^o c.m. This is experimental data from the 400 MeV/c π^+ exposure. Results for observed γ conversions in the metal plates and conversions in the deuterium (or Dalitz mode decay) are displayed separately.

Fig. 9. Spatial resolution of γ's. These frequencies of occurrence of DL (solid line) and DL(X,Y) (dashed line) values were observed in the 400 MeV/c π^+ exposure. Figures 9A, 9B, 9C present the data separately for γ's observed to convert in the liquid (or Dalitz mode decay), and in the metal converters in four ranges of γ momentum. The definitions of DL and DL(X,Y) are given in the text.

Fig. 10. Limits on defined regions of acceptability of DL full line, DLXY dashed line.

Fig. 11. Momentum and angle between beam and charged secondary for K^+N scatter and for K^+N charge exchange. The computed reaction kinematics are for a 620 MeV/c K^+ beam and a free neutron.

Fig. 12. Track relative bubble densities and range. Bubble densities are computed as $1/\beta^2$ with minimum ionization = 1. Proton range is for liquid deuterium.

Fig. 13. Momentum loss in penetrating 5 mm of stainless steel.

Fig. 14. Angle between reconstructed K^o direction and V decay direction. This is experimental data from charge exchange reactions with a 620 MeV/c K^+ beam.

Fig. 15. Combined mass of $\pi^+\pi^-$ system, from a specially selected sample of events from the 620 MeV/c K^+ exposure.

Fig. 16. Phase space for $\pi^+\pi^-p$ from 600 MeV/c π^+ on n.

Fig. 17. R vs assigned proton ionization for one-prong events and two-prong events. For two-prong events, the abscissa covers all possible combinations for the two protons: SIL-3, SIL-4, SIL-5, SIL-SIL, SIL-SIP, SIP-3, SIP-4, SIP-5, SIP-SIL, SIP-SIP, both protons non-stopping (SIL means proton stopping in liquid while SIP means proton stopping in the metal γ converters). For two-prong events, the data in some categories has been combined, as indicated, for increased statistical weight. R vs radius of interaction. The parameter R is defined in the text as the ratio of events with no V decay to all charge exchanges.

Fig. 18. R vs momentum of fast proton (all events).

R vs dip of fast proton (all events).

R vs momentum of the K^o (all events).

R vs dip of K^o (all events).

The parameter R is defined in the text as the ratio of events with no V decay to all charge exchanges.

Fig. 19. Angular distribution of the π^o in the reaction center of mass. The experimental data is for the charge exchange reactions in the 400 MeV/c π^+ exposure.

Fig. 20. Z dependence of γ's. The experimental data from observed γ conversions in the 400 MeV/c π^+ exposure (points with error bars) is compared with Monte Carlo generated data (solid line). Cases of γ conversion in each of the two cones are displayed separately.

Fig. 21. PHI dependence of γ's. The experimental data from observed γ conversions in the 400 MeV/c π^+ exposure (points with error bars) is compared with Monte Carlo generated data (solid line). Cases of γ conversion in each of the two cones are displayed separately.

Fig. 22. Production momentum distribution of γ's observed. Reconstructed π^o parameters and observed γ angle was used to compute actual γ momentum. The experimental data from the 400 MeV/c π^+ exposure (points with error bars) is compared with Monte Carlo generated data (solid line).

Fig. 23. Charged mode decay lifetime. Decay time distribution from observed length of flight of K^o's before V decay is presented. Three typical error bars are shown. The data is compared with $\frac{1}{\tau_S} e^{-t/\tau_S}$ and $\frac{1}{\tau_S} e^{-t/\tau_S} + \frac{1}{\tau_L} e^{-t/\tau_L}$.

Fig. 24. Experimentally observed distribution of the DL parameter for detected γ's in the 620 MeV/c K^+ exposure. Clear distribution is for γ's associated with K^+ charge exchanges when no V decay was

present. Hatched distribution is for γ's associated with K^+ charge exchanges when a V decay was present. The units for the abscissa are the limit of acceptability in the processing program.

Fig. 25. Experimentally observed distribution of the DL parameter for detected γ's in the 620 MeV/c K^+ exposure. Clear distribution is for γ's associated with K^+ charge exchanges when no V decay was present. Hatched distribution is for γ's associated with K^+ charge exchanges when a V decay was present. The units for the abscissa is the limit of acceptability in the processing program.

Fig. 26. Gamma momentum in π^o center of mass for γ's assigned to $K_{\pi 2}$ decays.

Fig. 27. K^o lifetime distribution determined from the detected γ's.

Fig. 28. Apparent combined mass of γ's for events with more than one detected γ. All possible pairings of γ's are included. Data from the 620 MeV/c K^+ exposure (points with error bars) is compared with Monte Carlo generated data (solid line).

Fig. 29. Emerging electron energy for γ's assigned to main K^o decay. Experimental data from the 620 MeV/c K^+ exposure (points with error bars) is compared with Monte Carlo generated data (solid line).

Fig. 30. Polar angle in fiducial plane of γ's assigned to main K^o decay. Experimental data from the 620 MeV/c K^+ exposure (points with error bars) is compared with Monte Carlo generated data (solid line).

Fig. 31. Schematic representation of the beam line.

Fig. 32. 632 MeV/c pion beam profile at first mass slit taken with 1/16-inch wide counter.

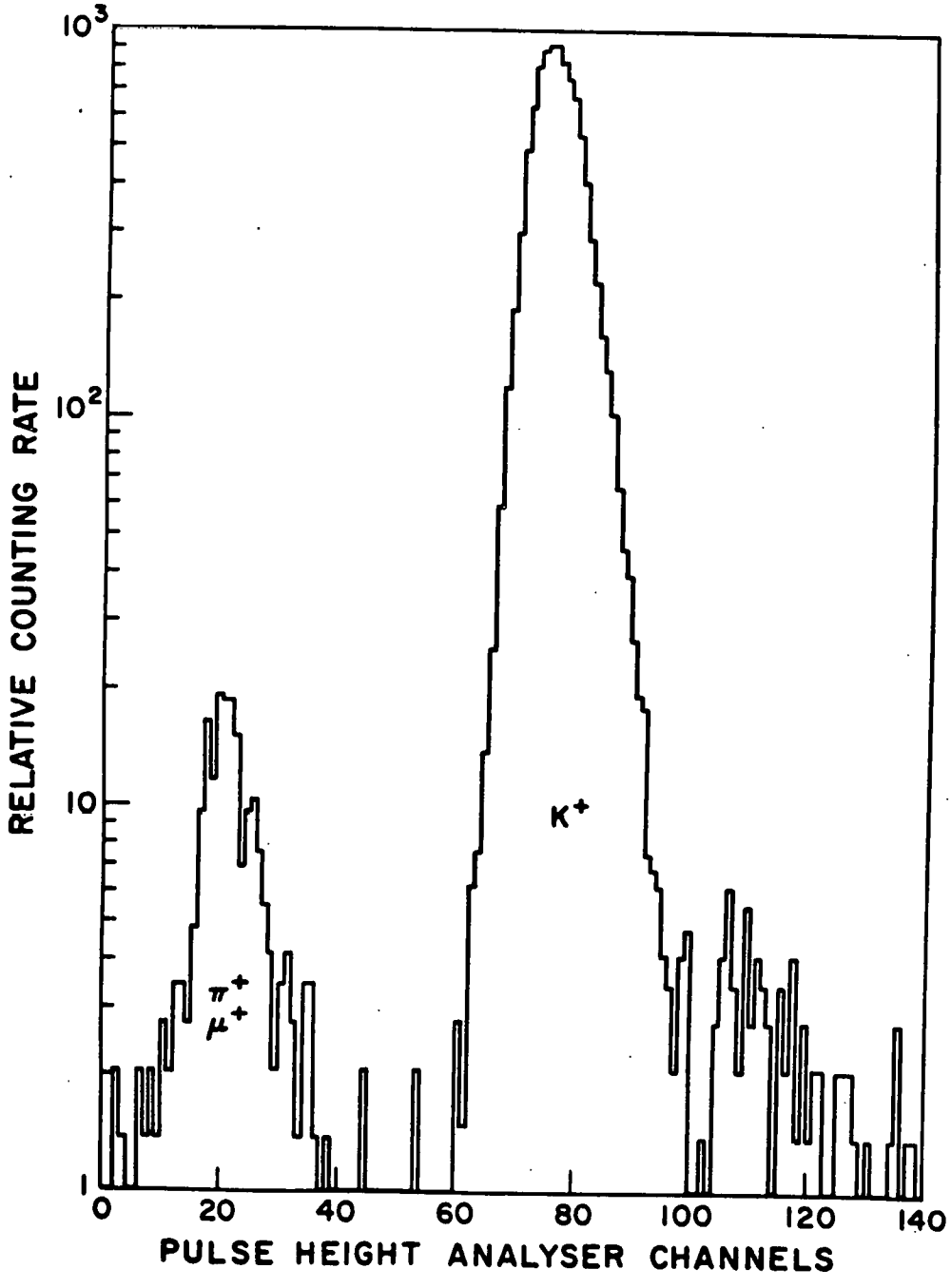

Figure 1 TIME OF FLIGHT SPECTRUM

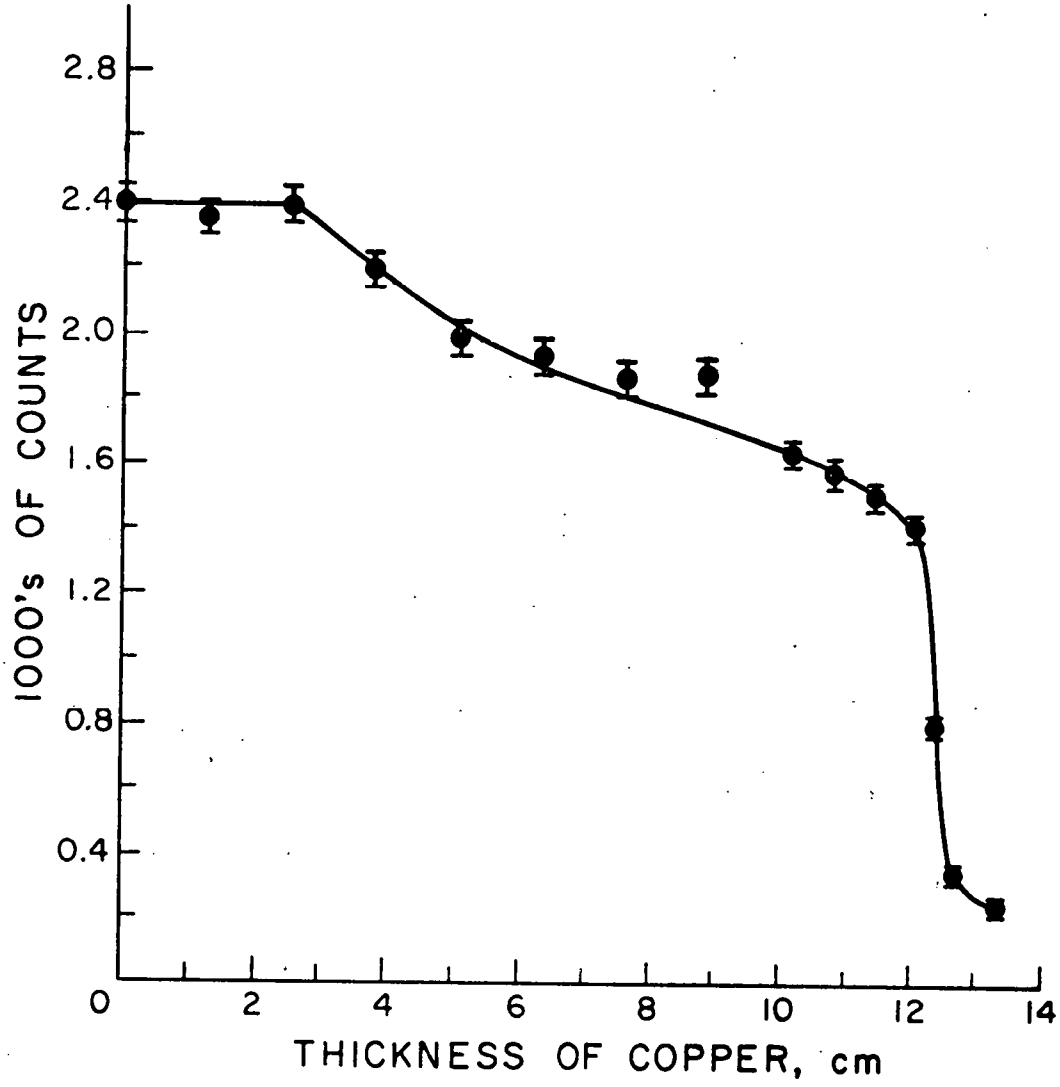

Figure 2 K^+ BEAM RANGE IN COPPER

EXPERIMENTAL ARRANGEMENT

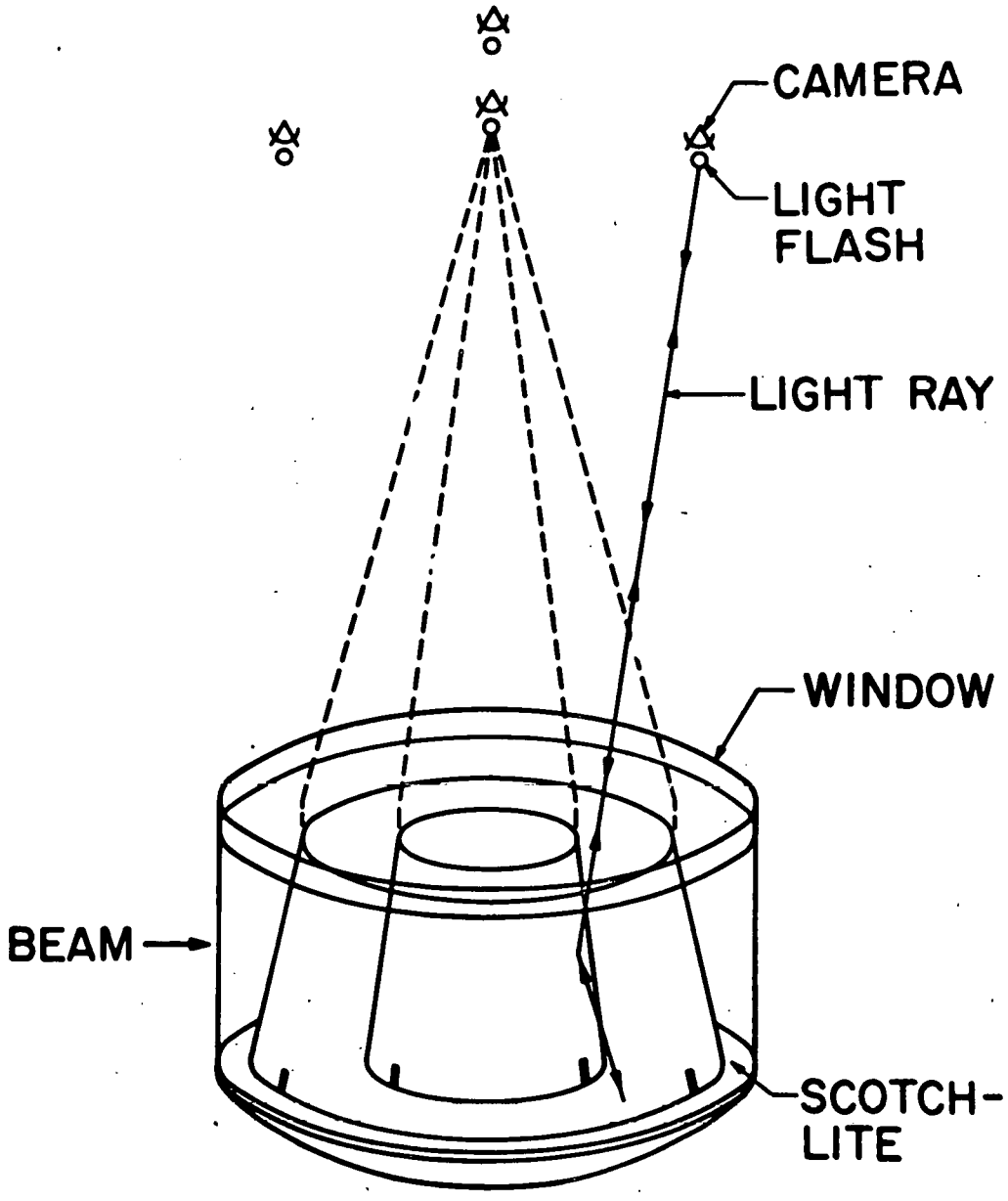

Fig. 3

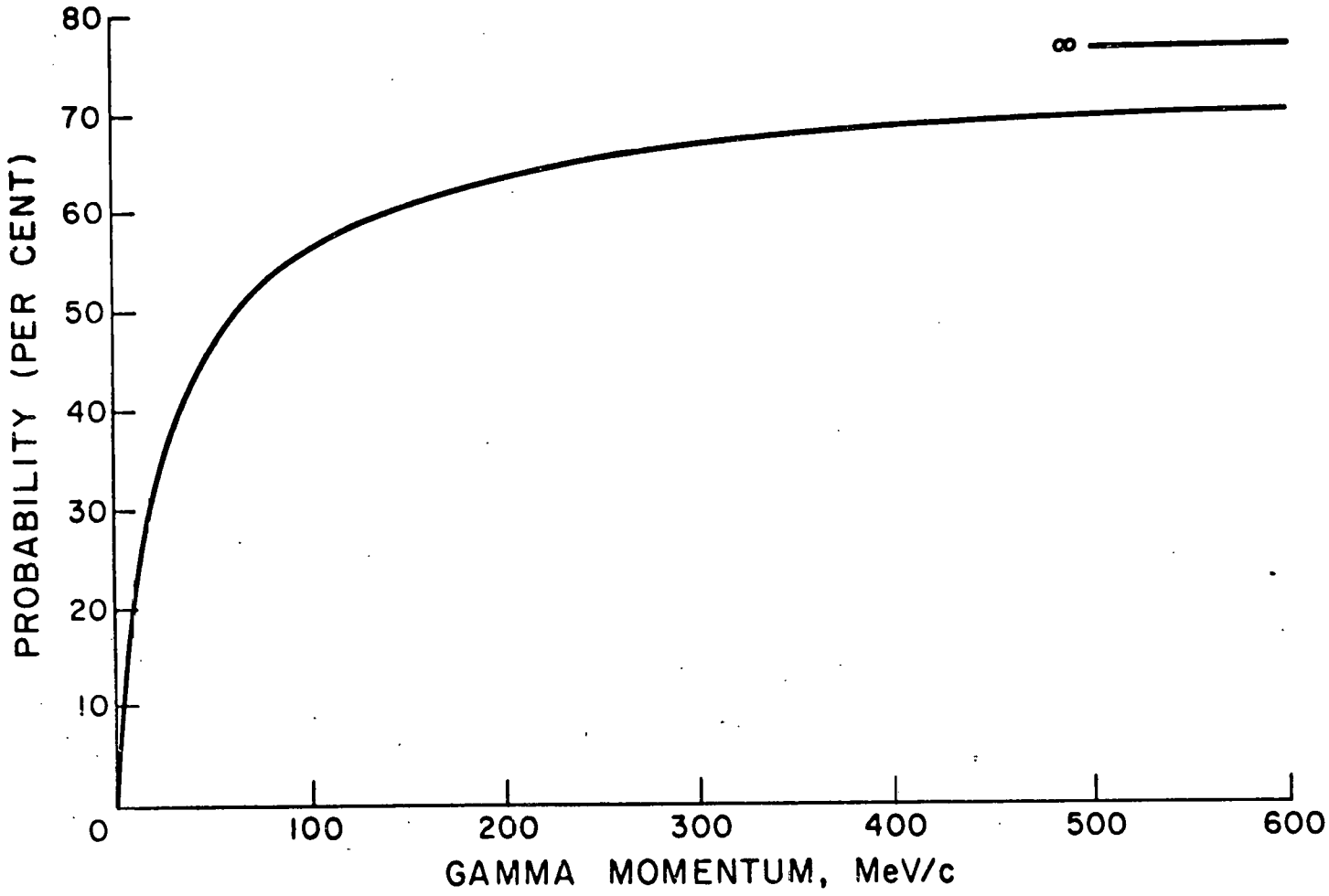

Figure 4 CONVERSION PROBABILITY PER RADIATION LENGTH

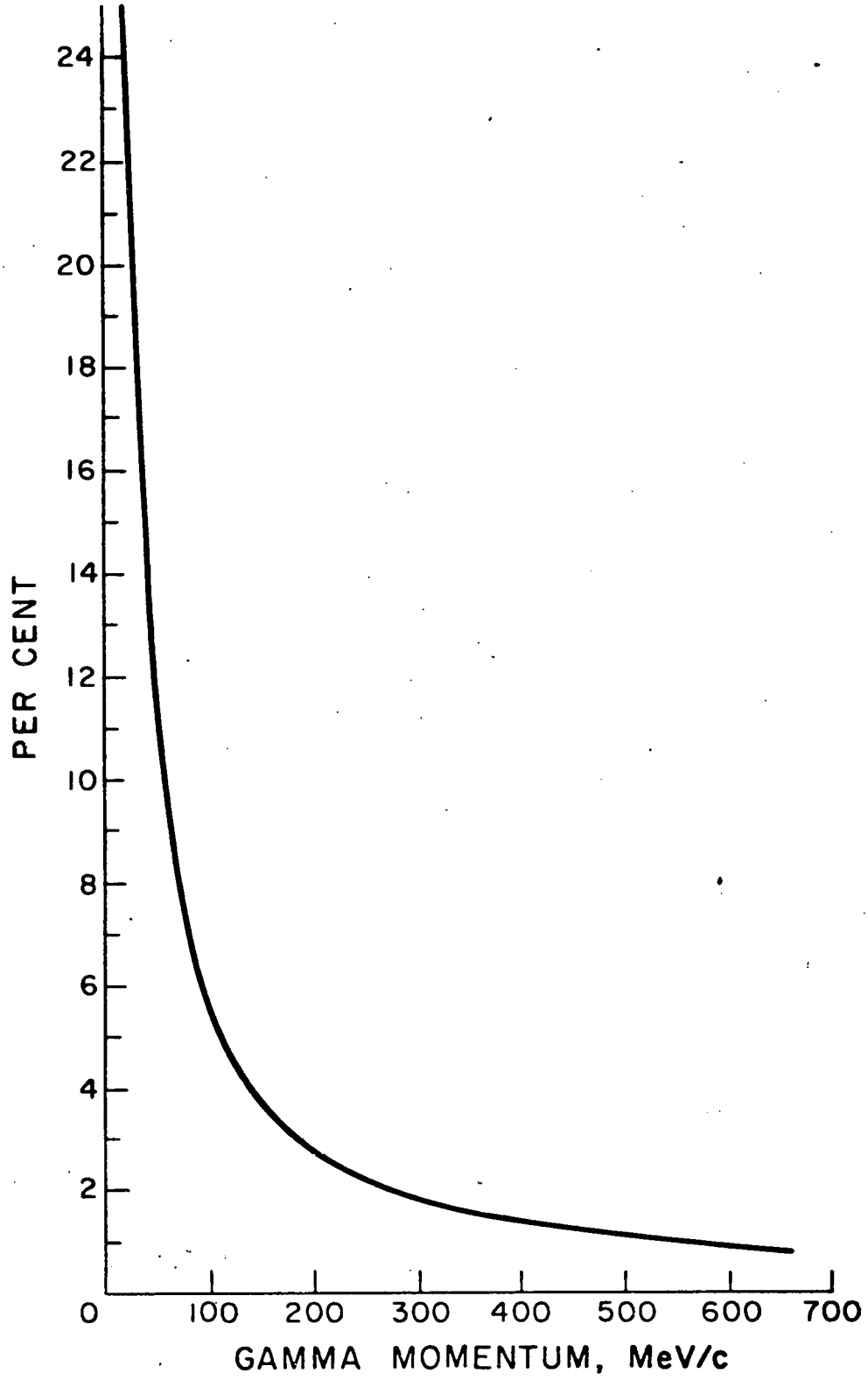

Figure 5 RATIO $\frac{\text{COMPTON SCATTERS}}{\text{SCATTERS+PAIR PRODUCTION}}$

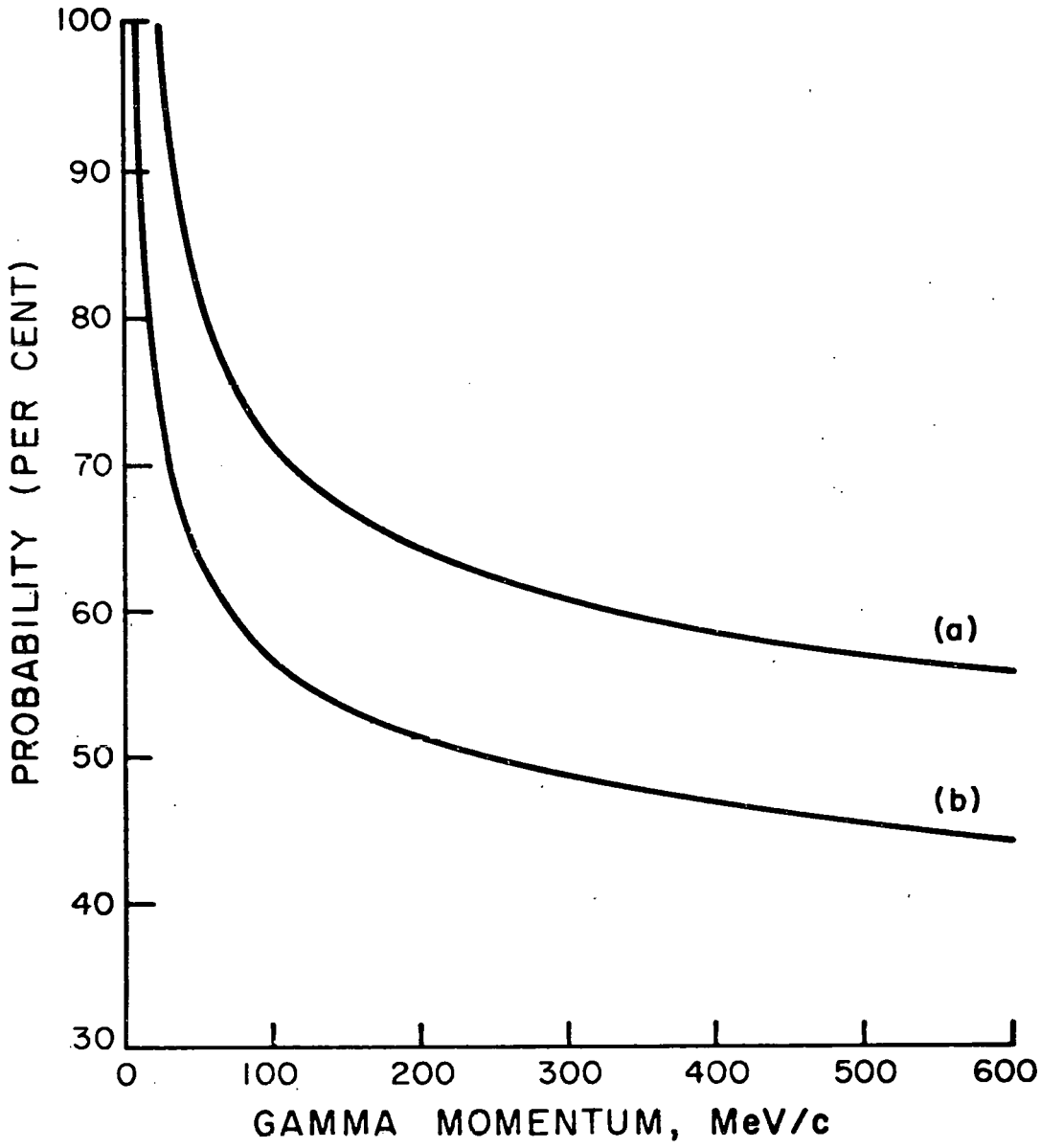

Figure 6 PROBABILITIES FOR A GAMMA TO HAVE ENERGY LESS THAN (a) 25 MeV AND (b) 10 MeV AFTER COMPTON SCATTERING

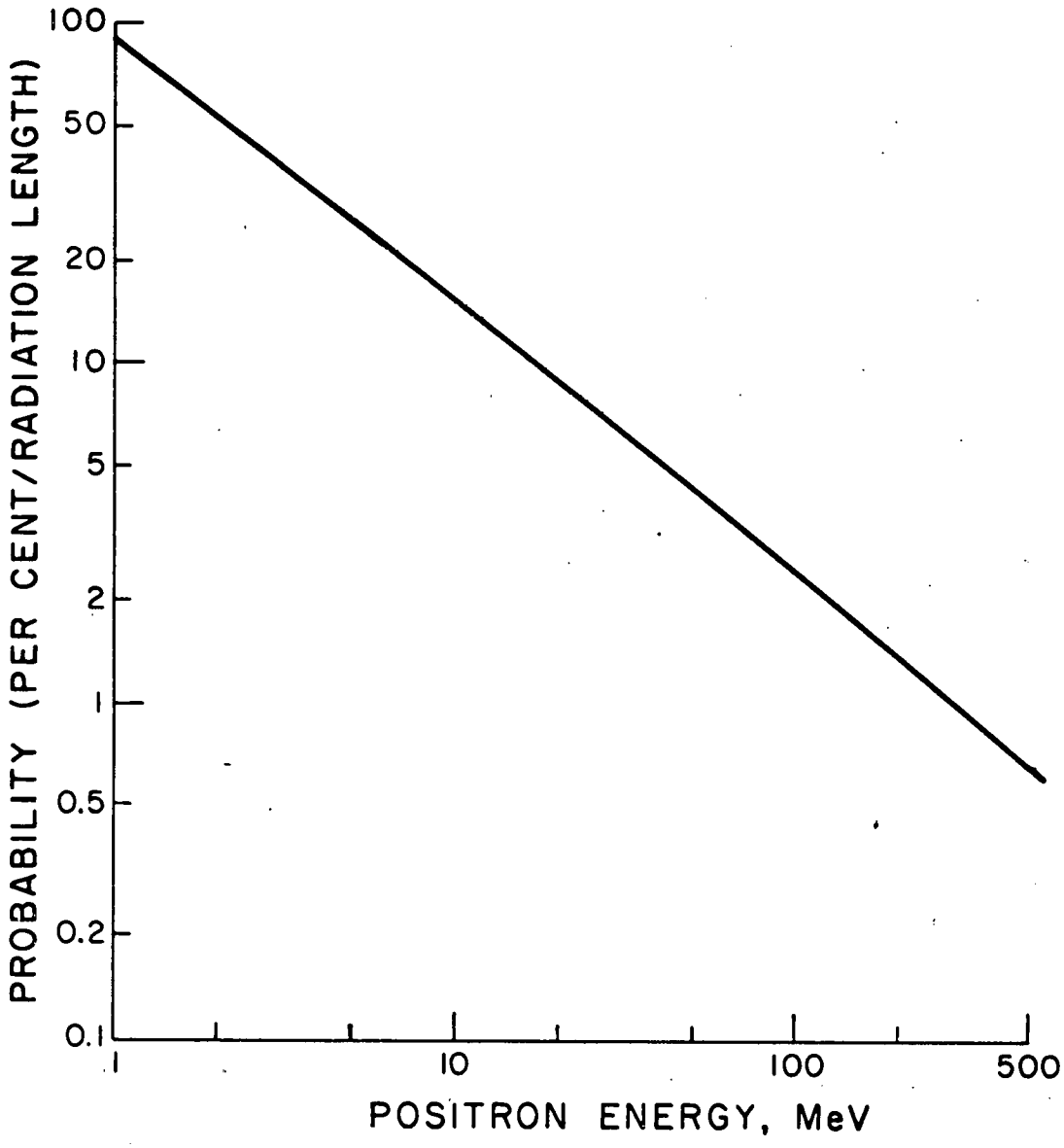

Figure 7 PROBABILITY OF POSITRON ANNIHILATION PER RADIATION LENGTH

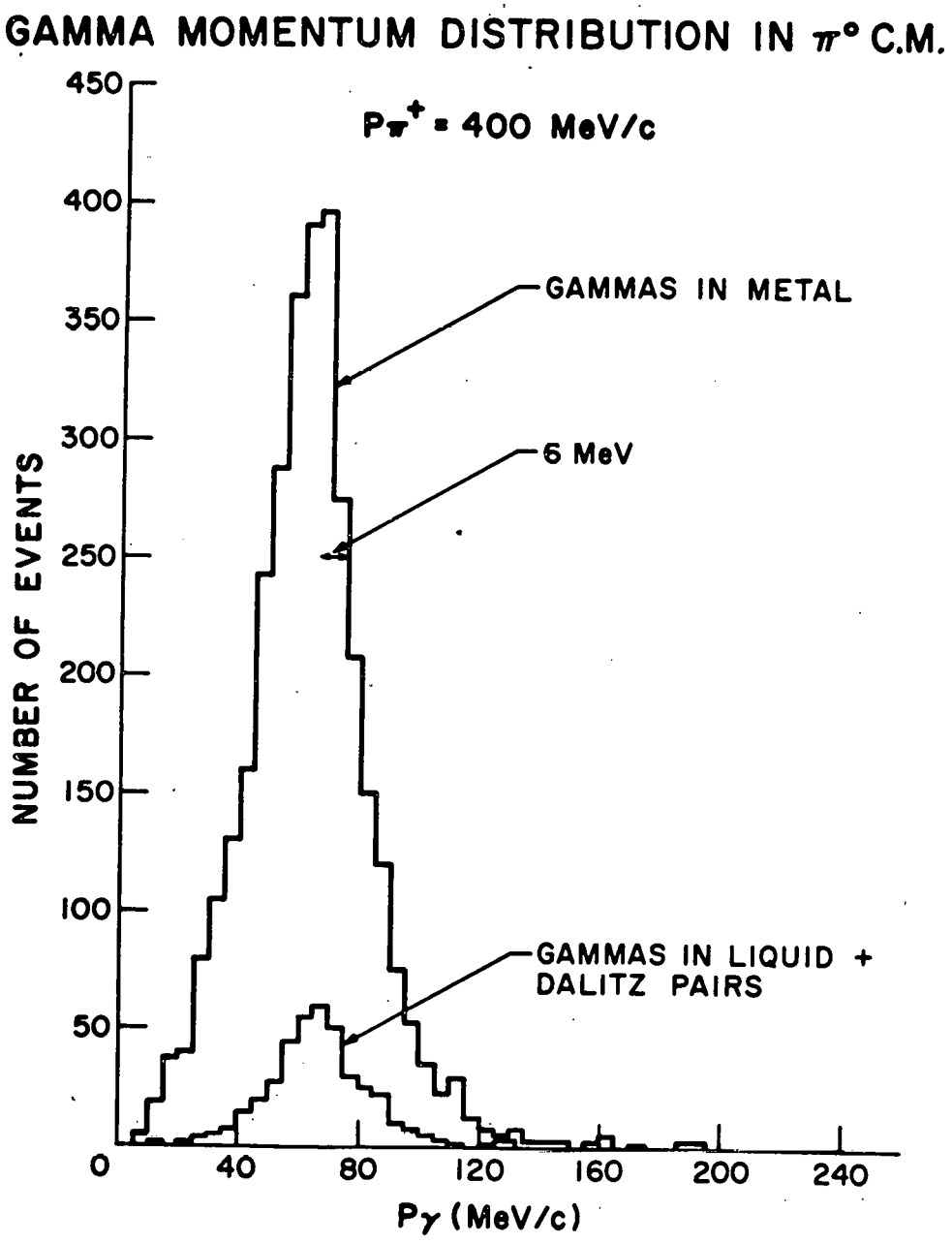
GAMMA MOMENTUM DISTRIBUTION IN π° C.M.
Pπ+ = 400 MeV/c
GAMMAS IN METAL
6 MeV
GAMMAS IN LIQUID + DALITZ PAIRS
NUMBER OF EVENTS
Pγ (MeV/c)
0
40
80
120
160
200
240
50
100
150
200
250
300
350
400
450

Fig. 8

SPATIAL RESOLUTION OF GAMMAS

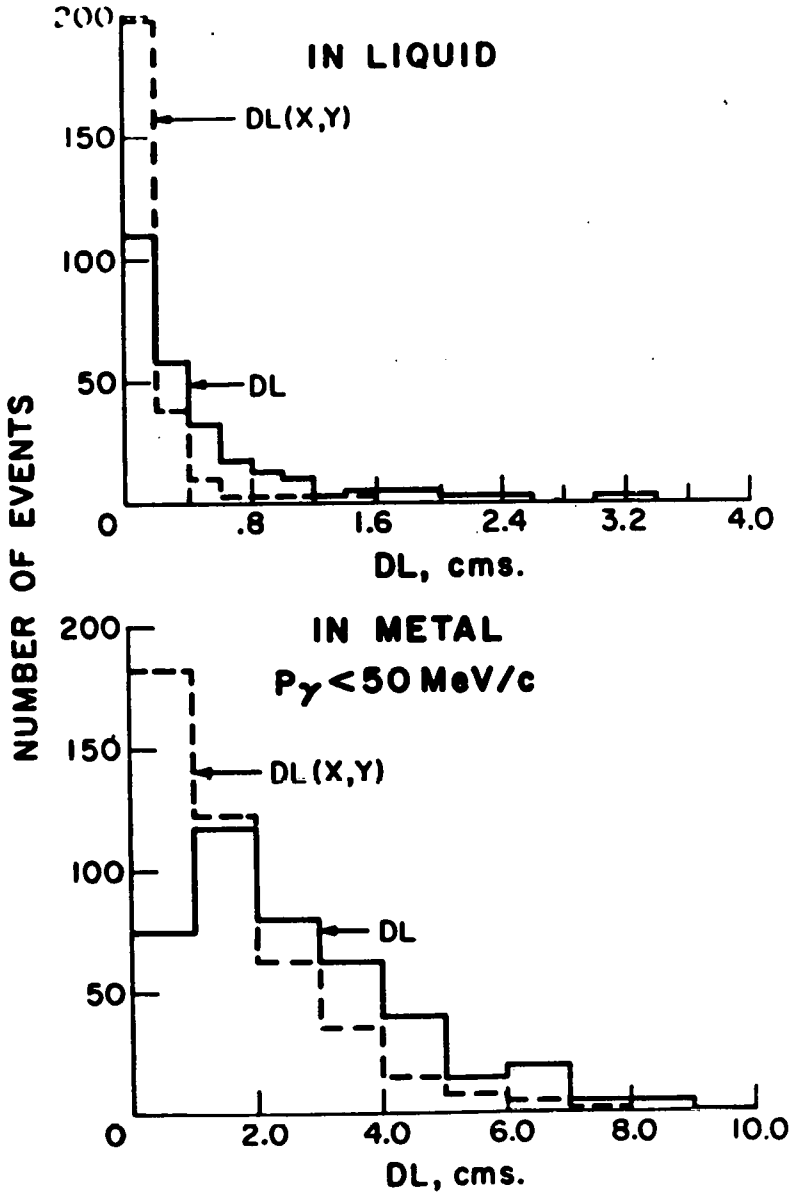

Fig. 9A

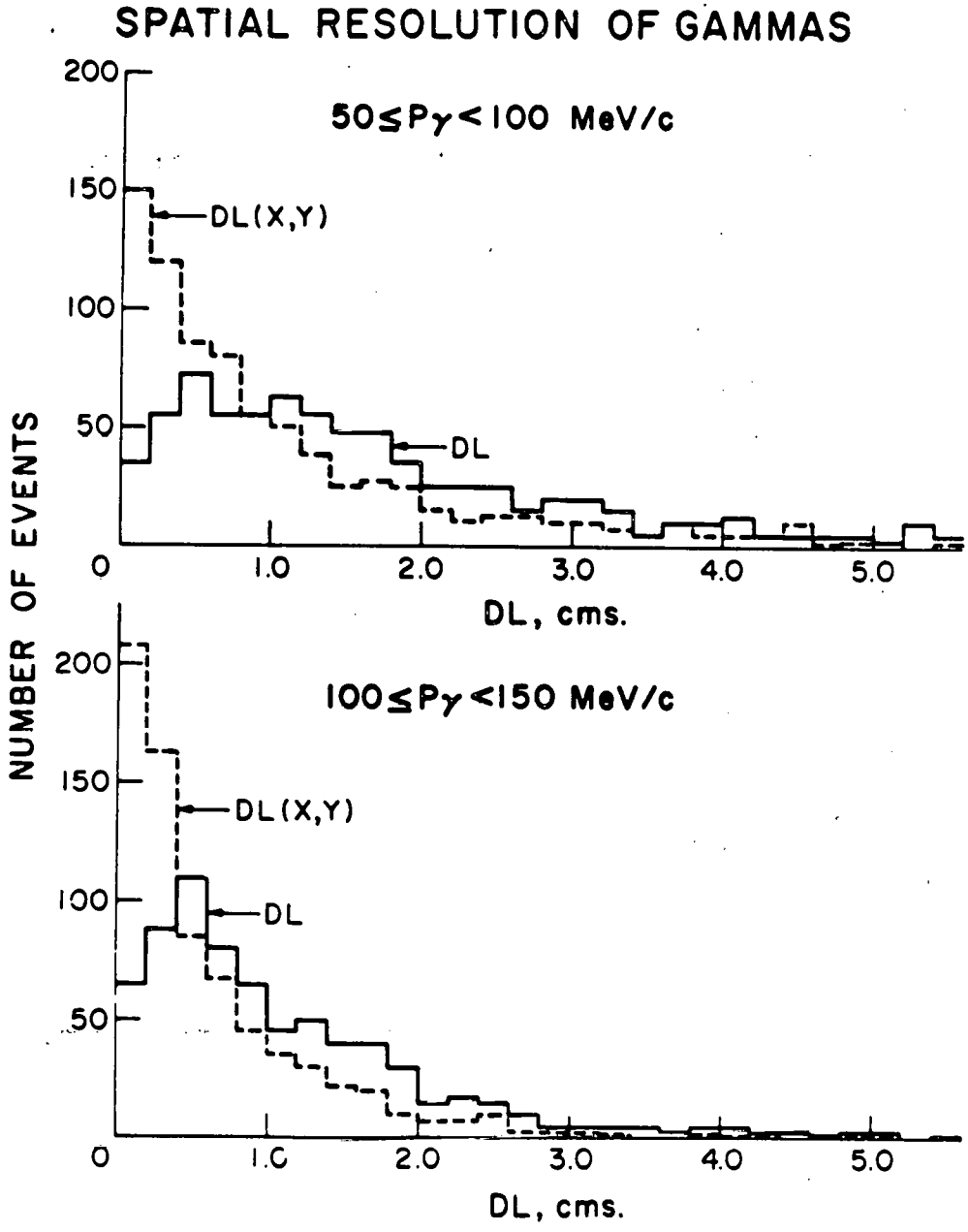
SPATIAL RESOLUTION OF GAMMAS
50≤Pγ<100 MeV/c
DL(X,Y)
DL
NUMBER OF EVENTS
200
150
100
50
0
1.0
2.0
3.0
4.0
5.0
DL, cms.
100≤Pγ<150 MeV/c
DL(X,Y)
DL
200
150
100
50
0
1.0
2.0
3.0
4.0
5.0
DL, cms.

Fig. 98

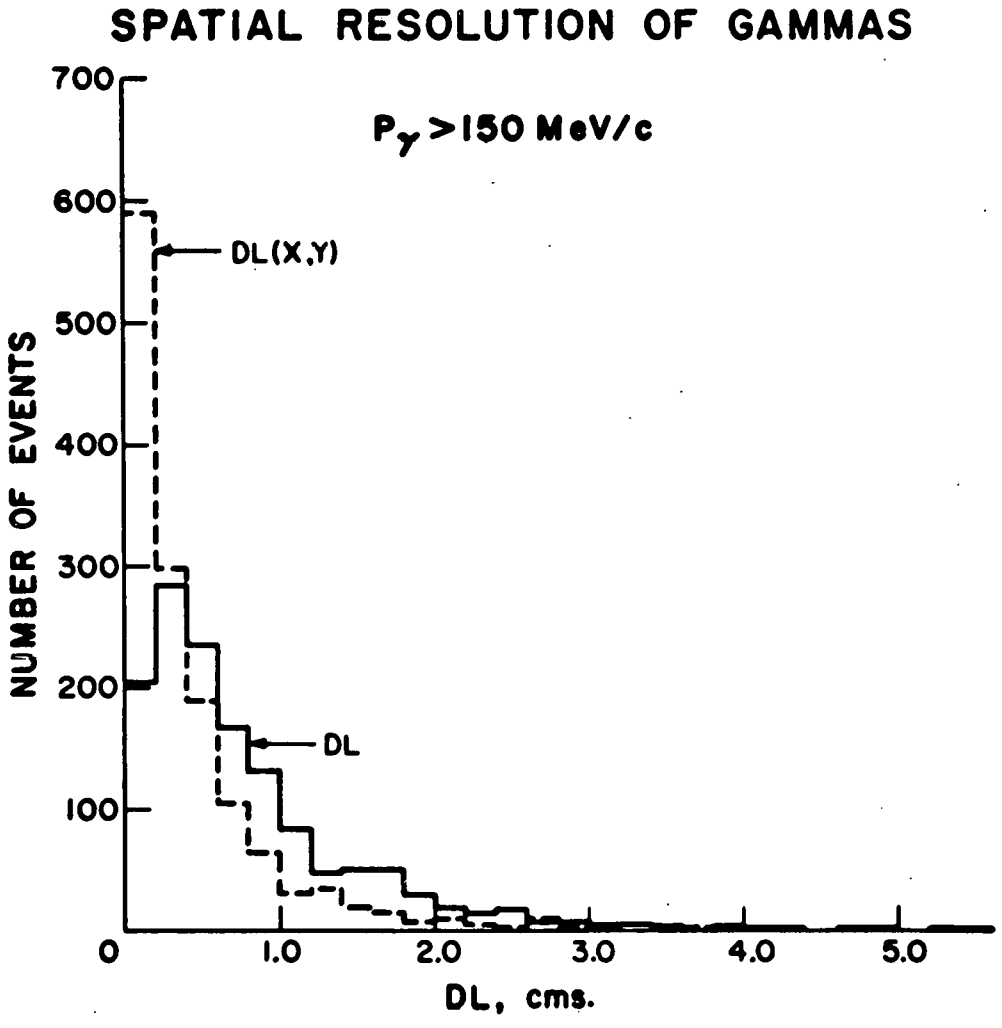
SPATIAL RESOLUTION OF GAMMAS
$P_\gamma > 150$ MeV/c
NUMBER OF EVENTS
700
600
500
400
300
200
100
0
DL(X,Y)
DL
1.0
2.0
3.0
4.0
5.0
DL, cms.

Fig. 9C

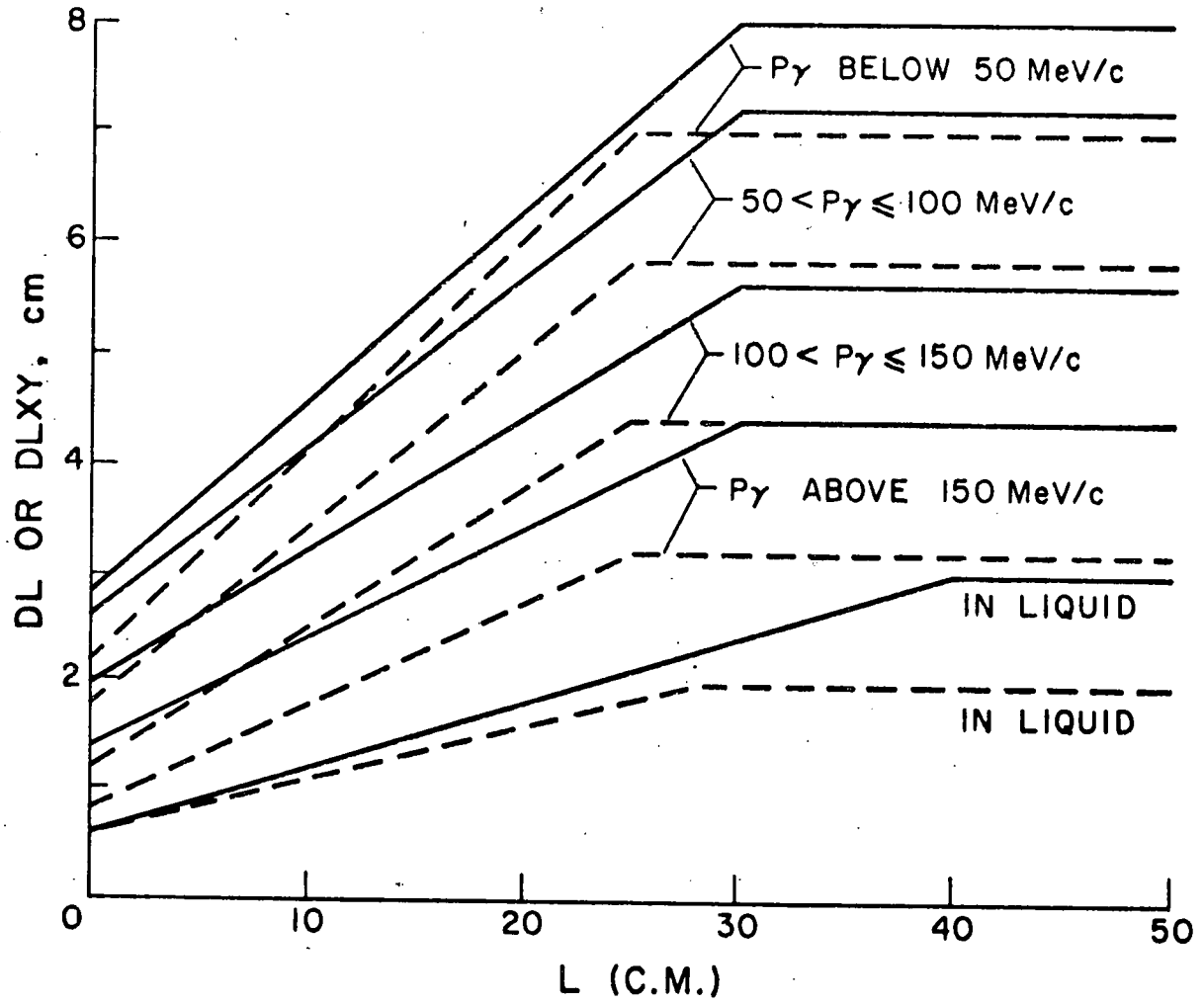

Figure 10 LIMITS ON DEFINED REGIONS OF ACCEPTABILITY OF, DL FULL LINE, DLXY DASHED LINE

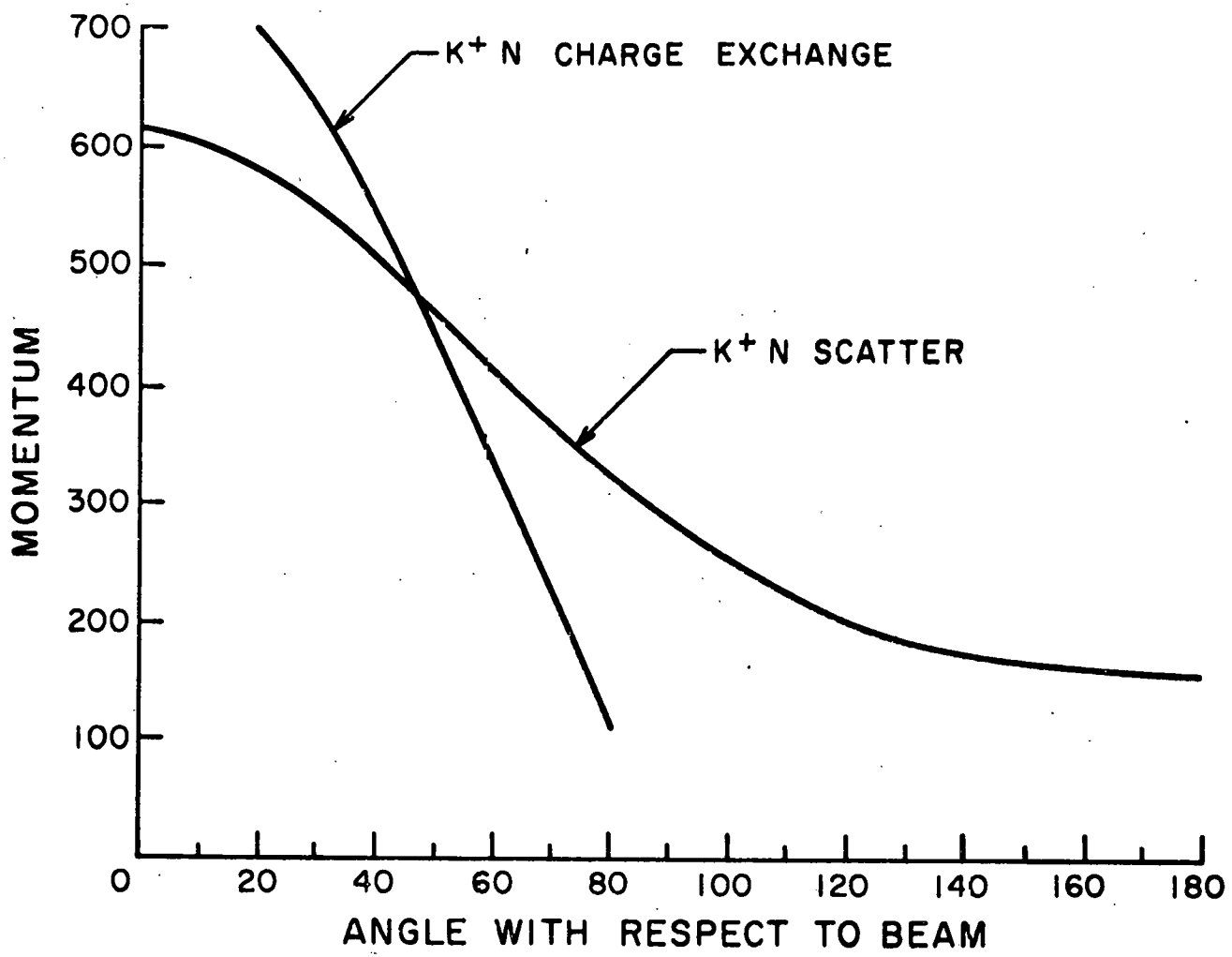

Figure 11 MOMENTUM AND ANGLE BETWEEN BEAM AND CHARGED SECONDARY FOR K^+N SCATTER AND FOR K^+N CHARGE EXCHANGE

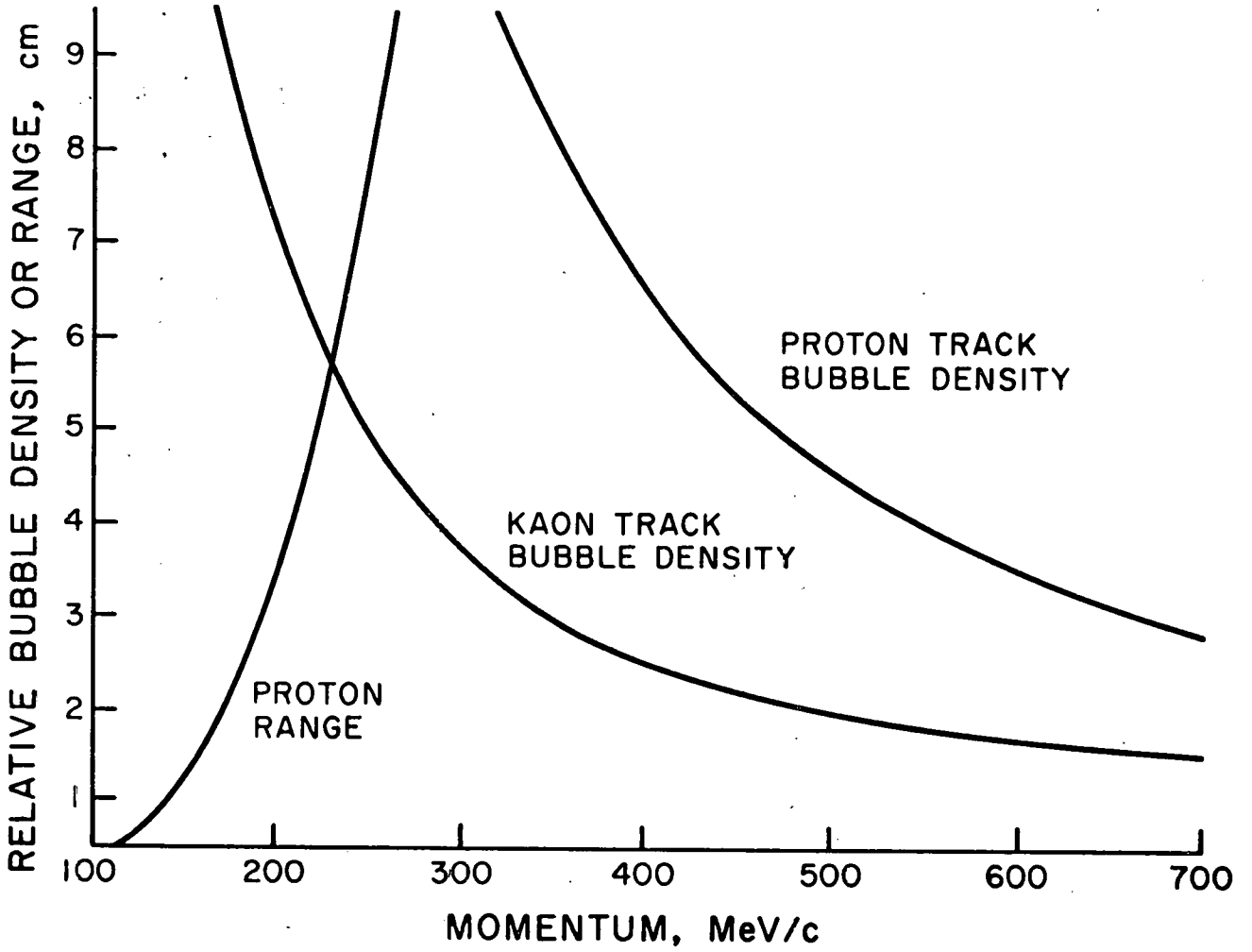

Figure 12 TRACK RELATIVE BUBBLE DENSITIES AND RANGE

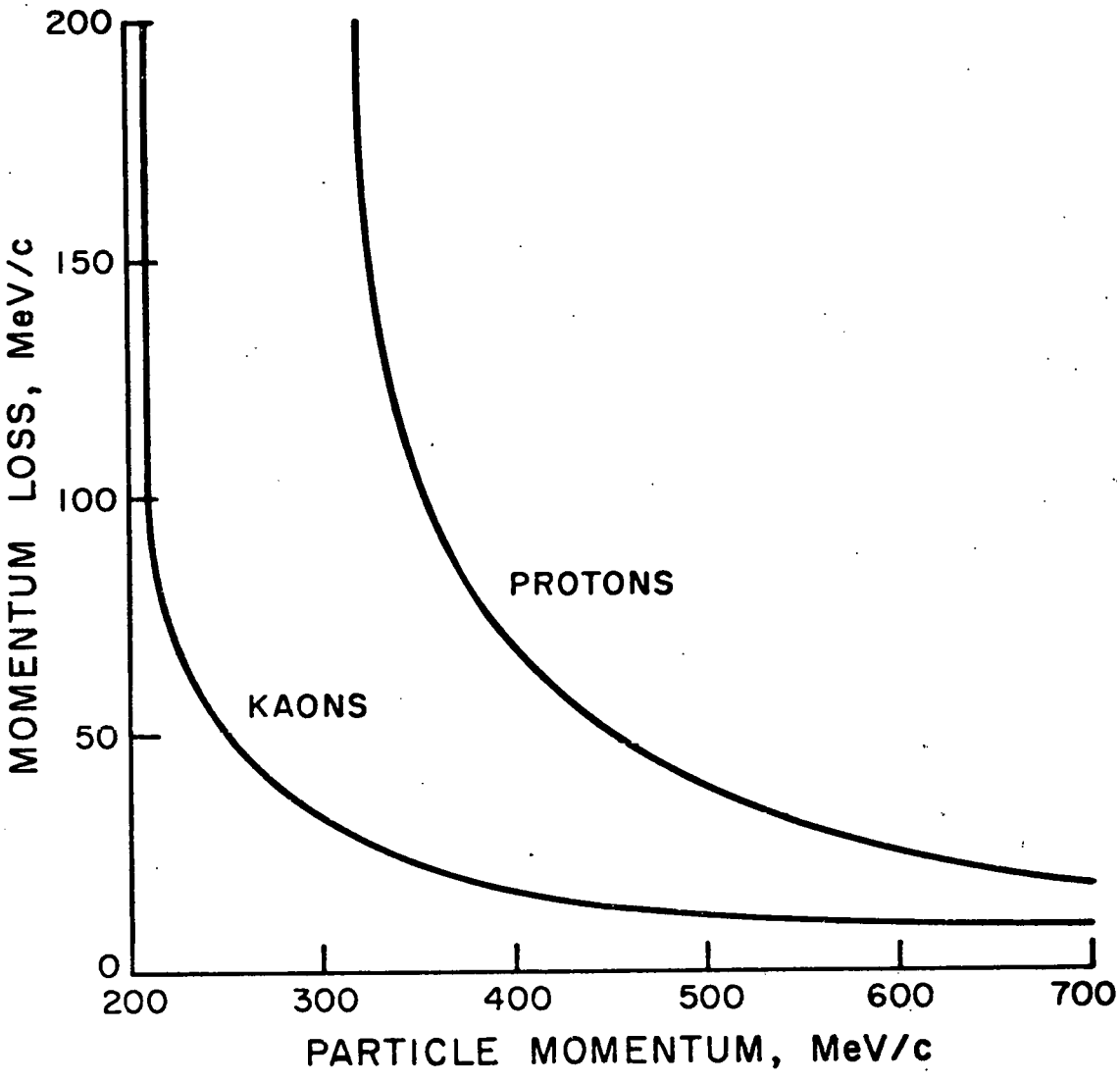

Figure 13 MOMENTUM LOSS IN PENETRATING 5mm OF STAINLESS STEEL

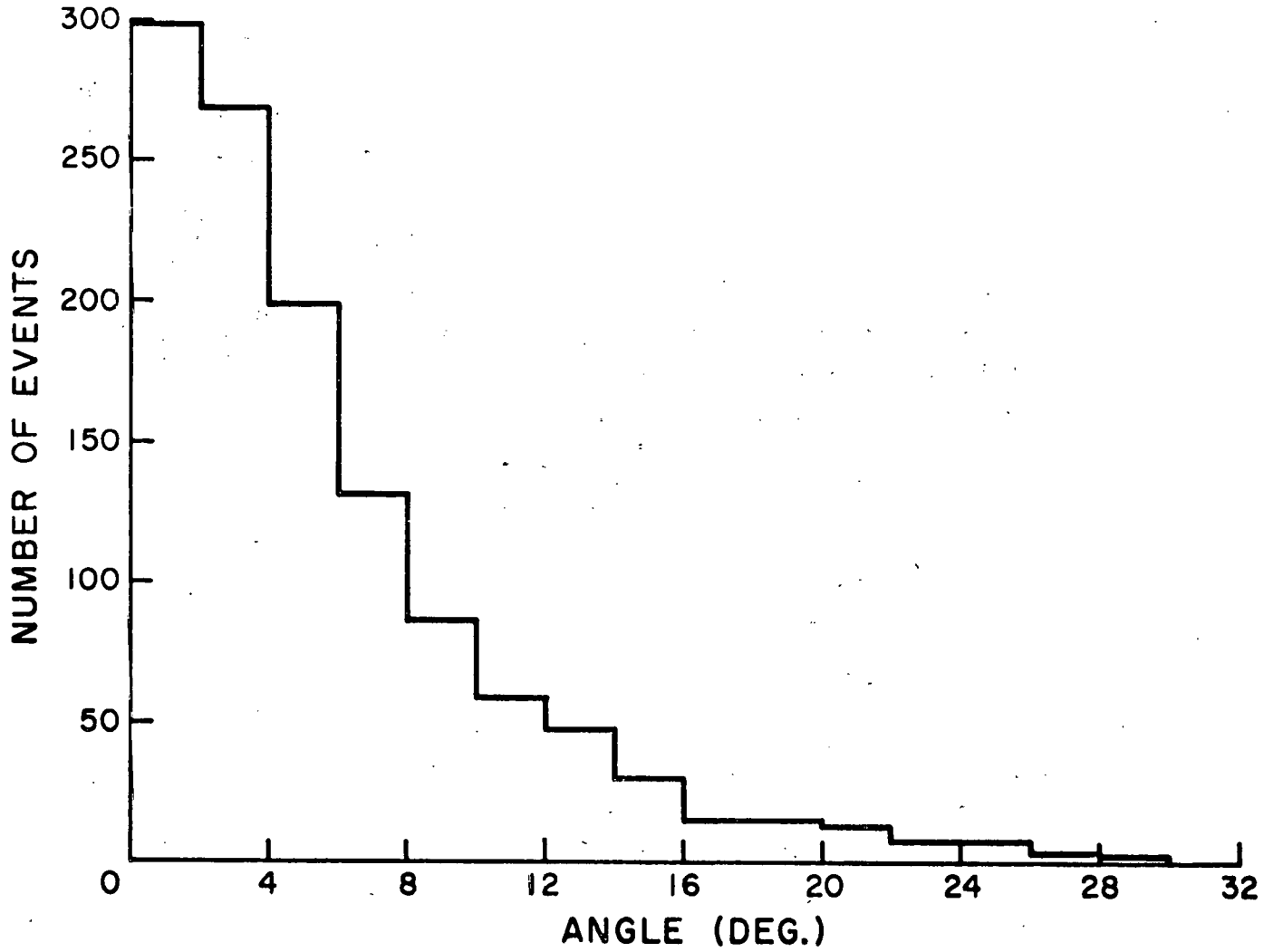

Figure 14 ANGLE BETWEEN RECONSTRUCTED KO DIRECTION AND V DECAY DIRECTION

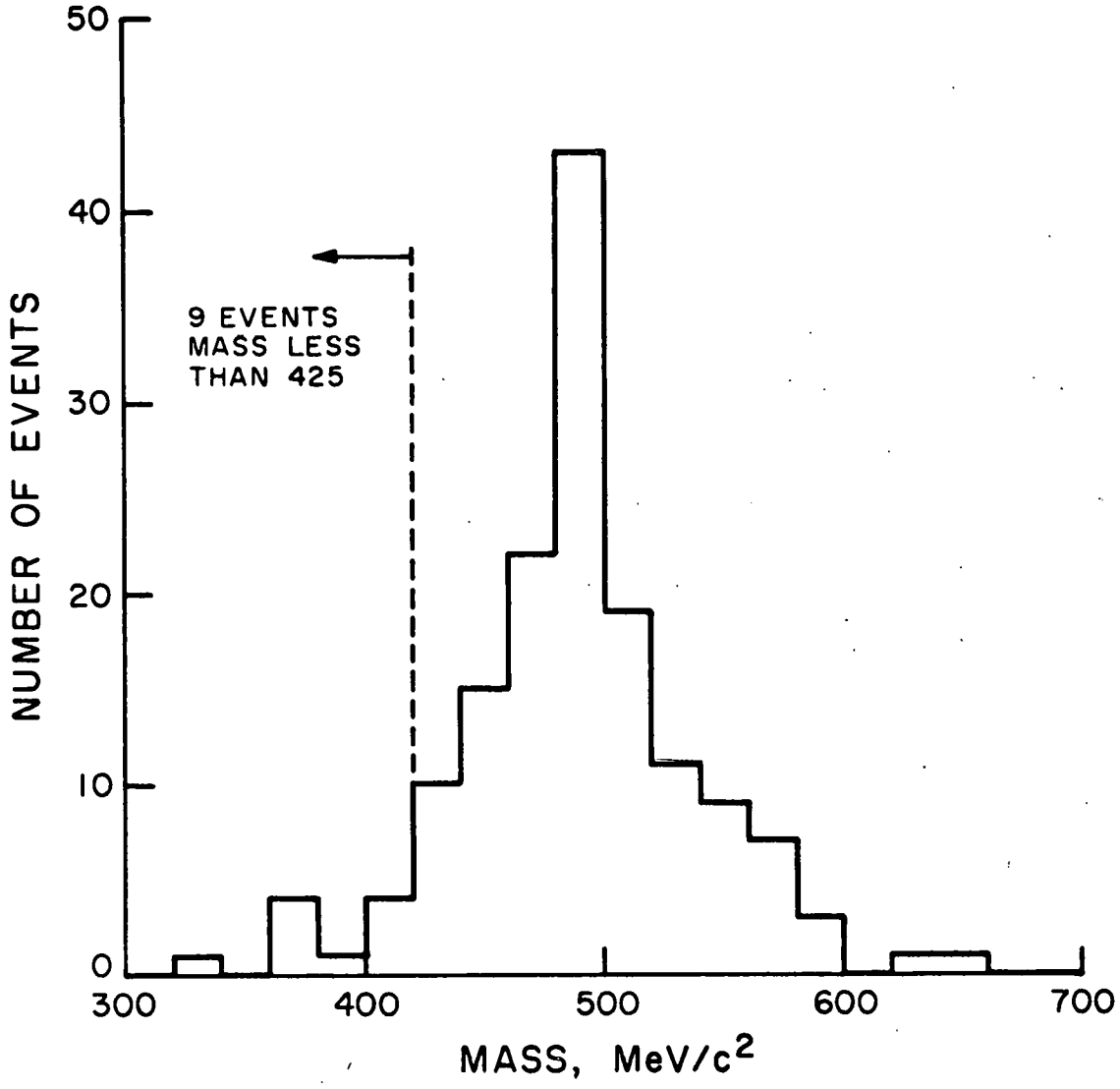

Figure 15 COMBINED MASS OF $\pi^+ \pi^-$ SYSTEM

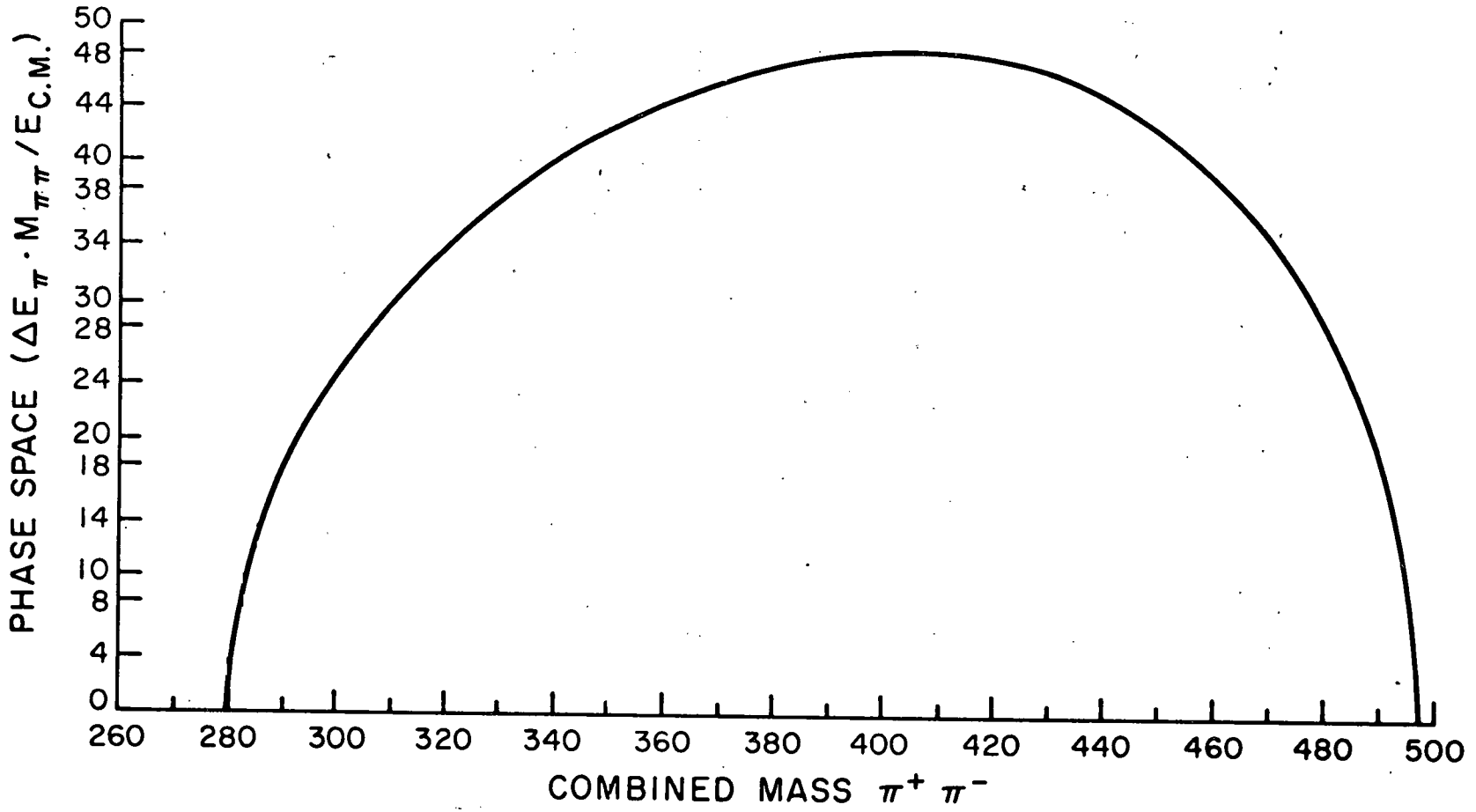

Figure 16 PHASE SPACE FOR $\pi^+ \pi^- p$ FROM 600 MeV/c π^+ ON n

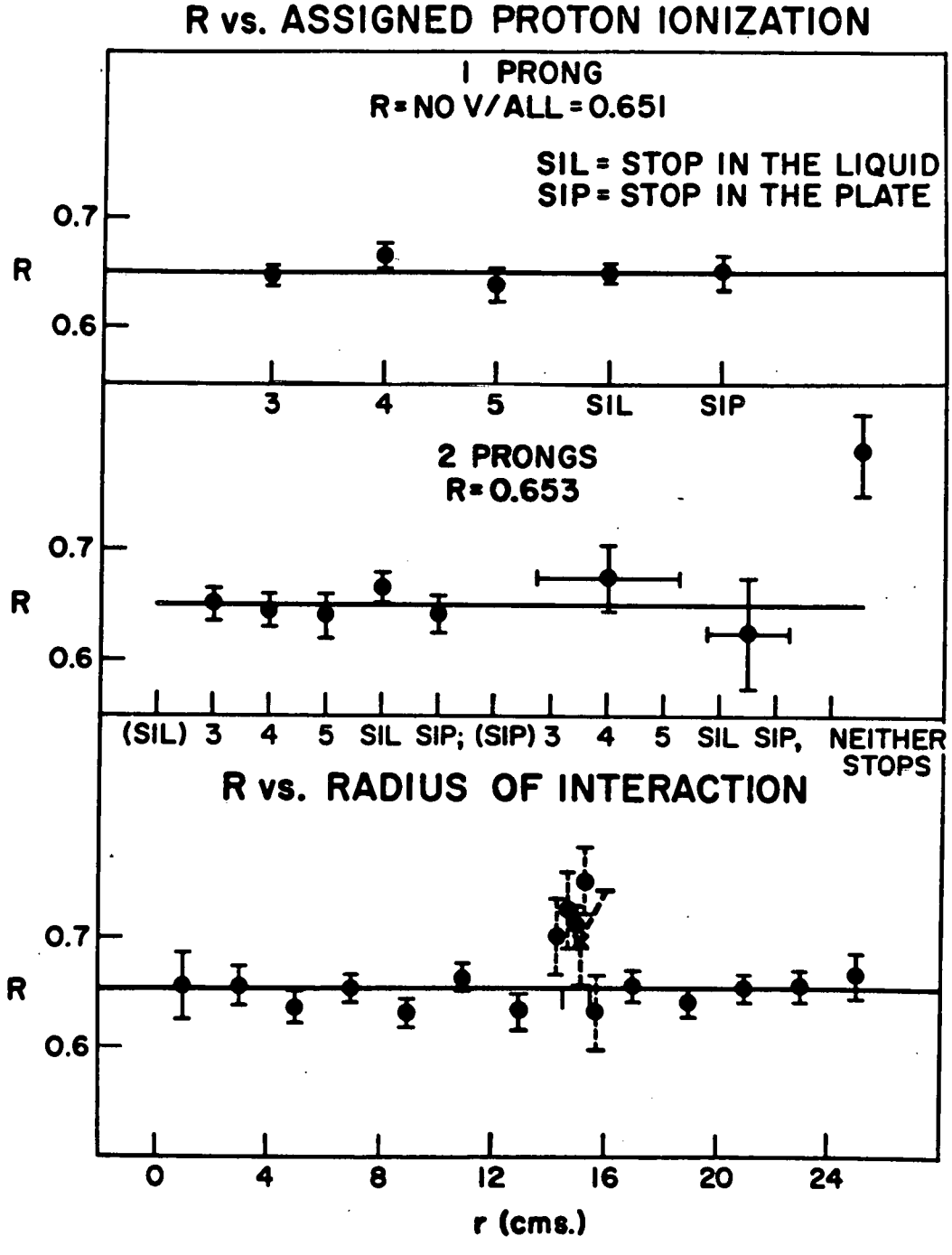
R vs. ASSIGNED PROTON IONIZATION
1 PRONG
R = NO V/ALL = 0.651
SIL = STOP IN THE LIQUID
SIP = STOP IN THE PLATE
0.7
R
0.6
3
4
5
SIL
SIP
2 PRONGS
R = 0.653
0.7
R
0.6
(SIL) 3 4 5 SIL SIP; (SIP) 3 4 5 SIL SIP, NEITHER STOPS
R vs. RADIUS OF INTERACTION
0.7
R
0.6
0
4
8
12
16
20
24
r (cms.)

Fig. 17

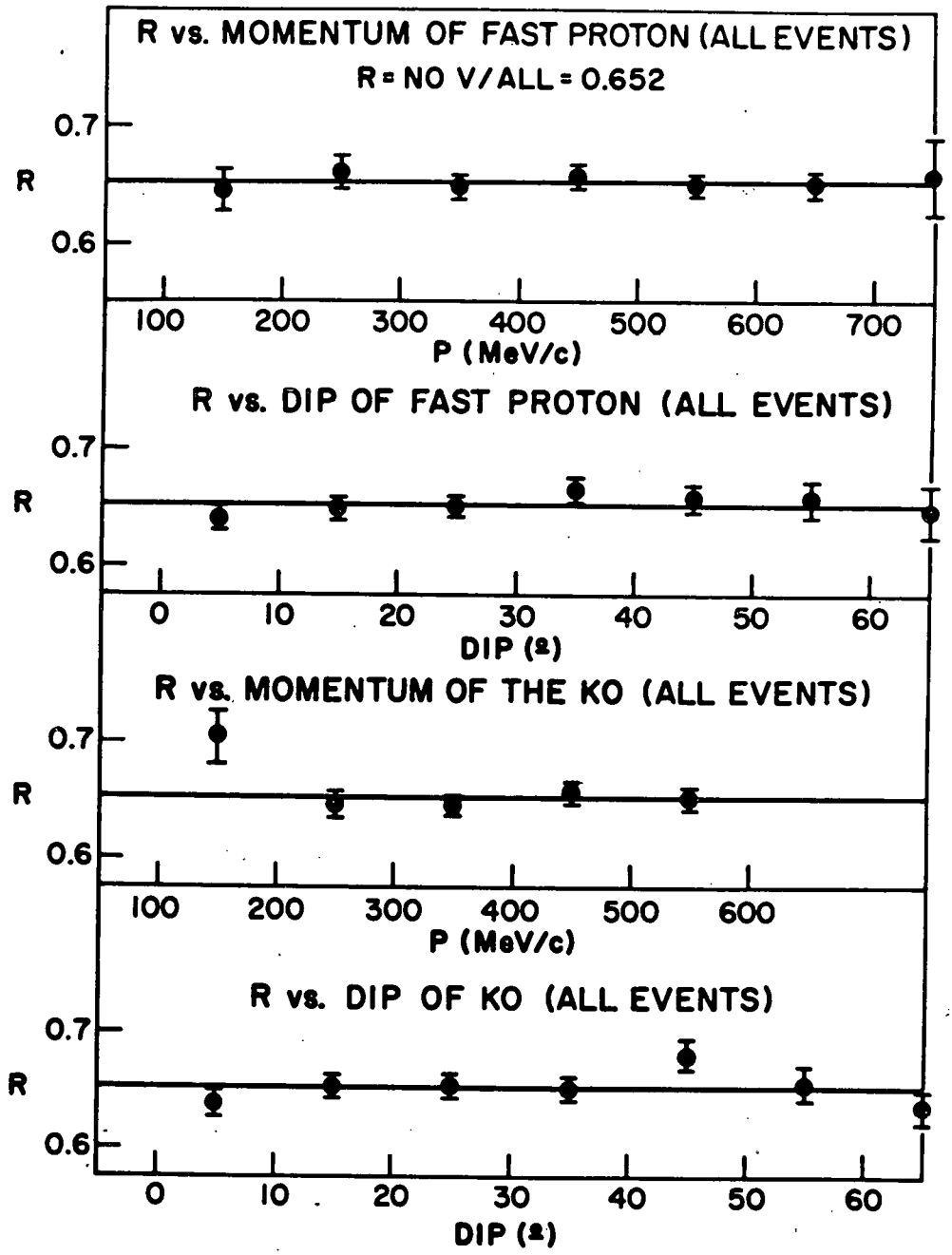
R vs. MOMENTUM OF FAST PROTON (ALL EVENTS)
R = NO V/ALL = 0.652
R
0.7
0.6
100
200
300
400
500
600
700
P (MeV/c)
R vs. DIP OF FAST PROTON (ALL EVENTS)
R
0.7
0.6
0
10
20
30
40
50
60
DIP (Ω)
R vs. MOMENTUM OF THE KO (ALL EVENTS)
R
0.7
0.6
100
200
300
400
500
600
P (MeV/c)
R vs. DIP OF KO (ALL EVENTS)
R
0.7
0.6
0
10
20
30
40
50
60
DIP (Ω)

Fig. 18

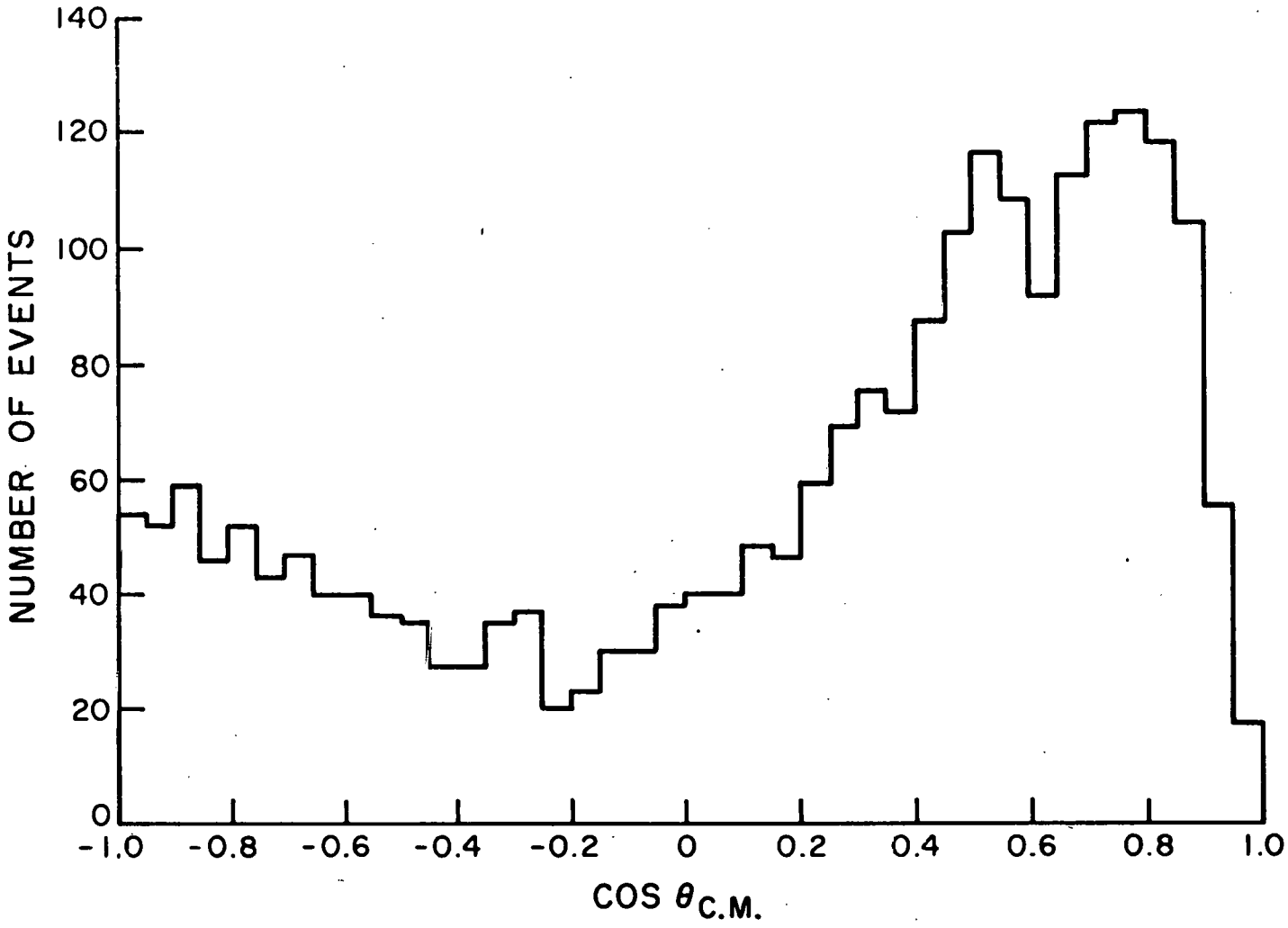

Figure 19 ANGULAR DISTRIBUTION OF THE π^0 IN THE REACTION CENTER OF MASS

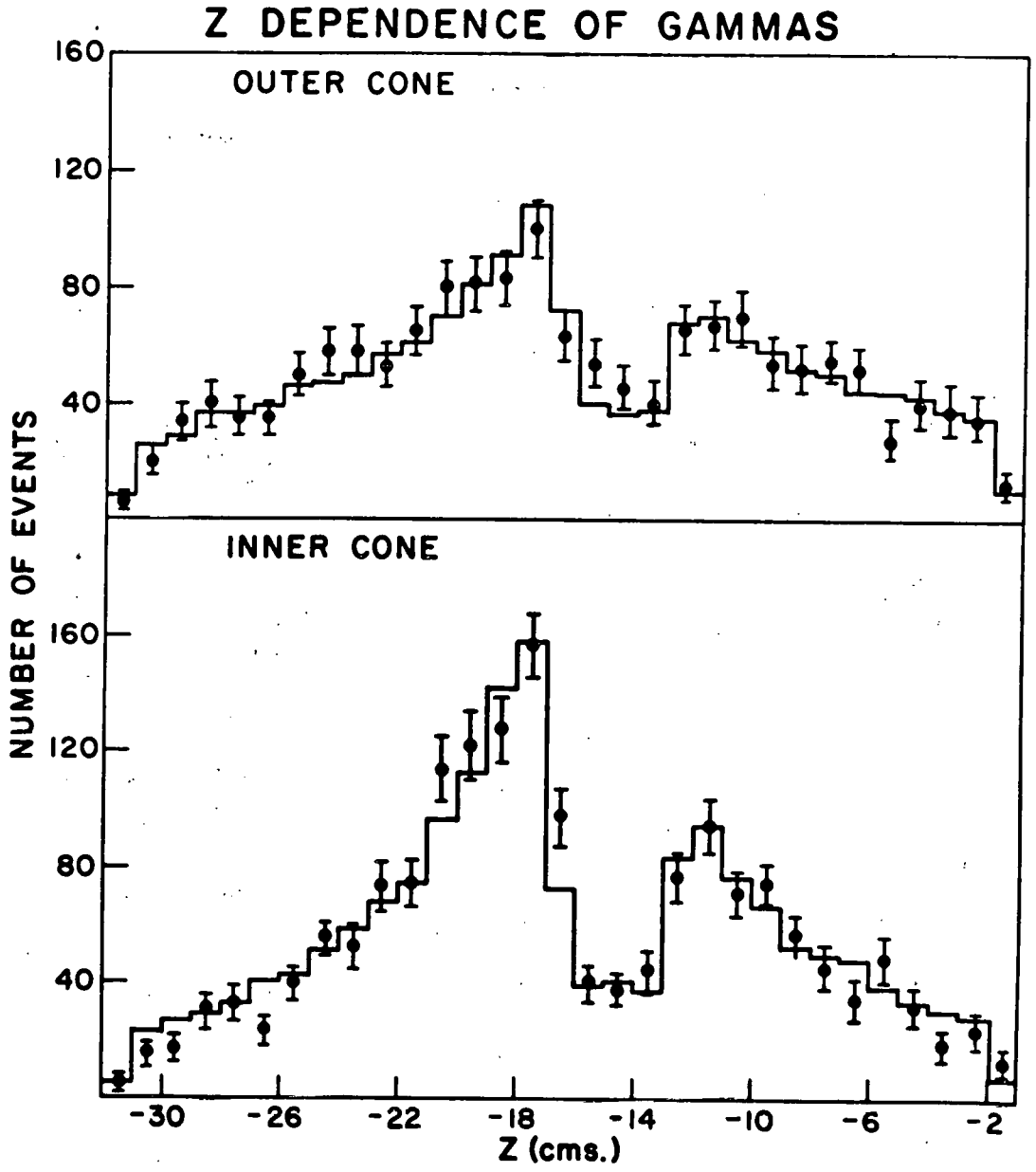
Z DEPENDENCE OF GAMMAS
OUTER CONE
INNER CONE
NUMBER OF EVENTS
160
120
80
40
160
120
80
40
-30
-26
-22
-18
-14
-10
-6
-2
Z (cms.)

Fig. 20

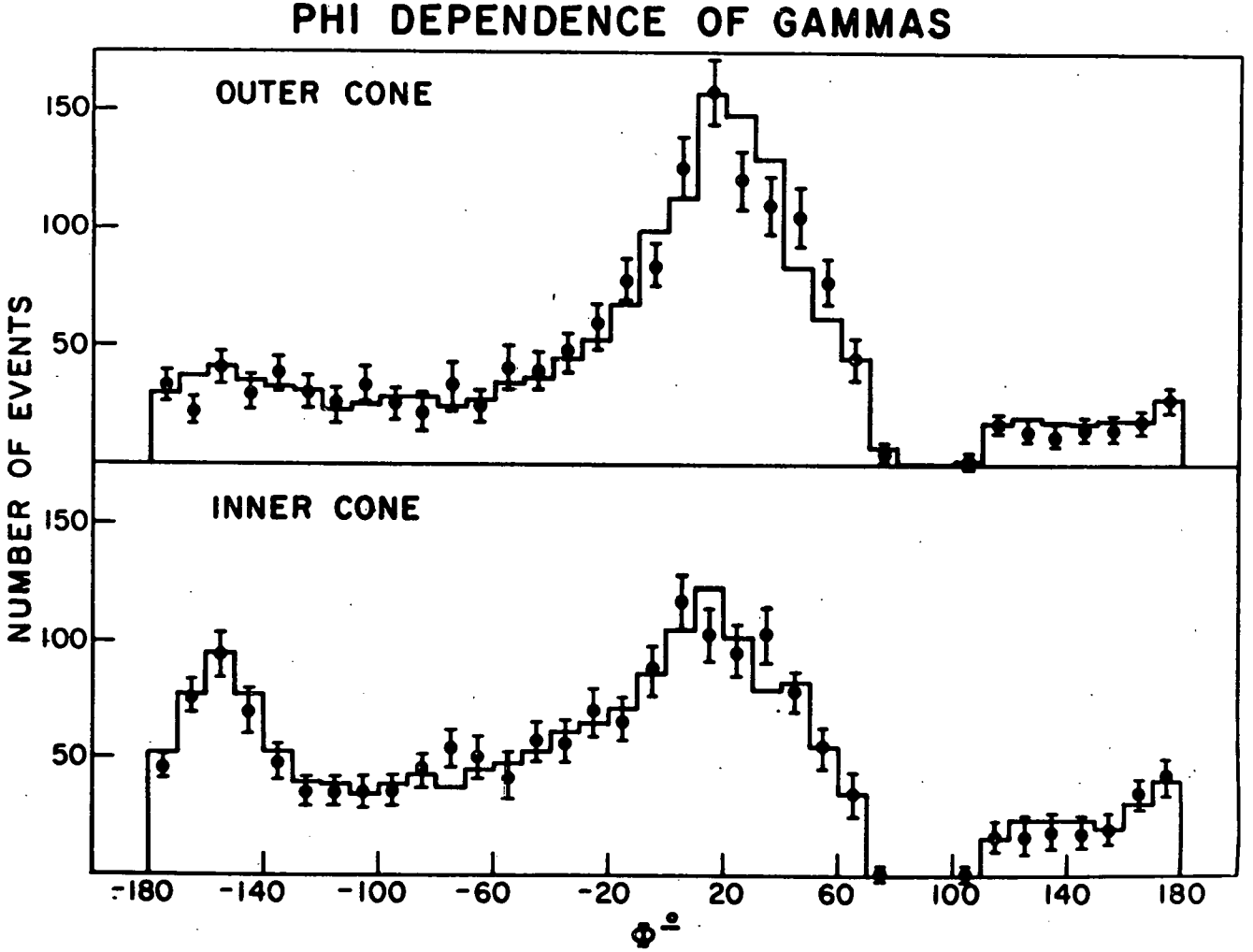
PHI DEPENDENCE OF GAMMAS
OUTER CONE
INNER CONE
NUMBER OF EVENTS
150
100
50
150
100
50
-180
-140
-100
-60
-20
20
60
100
140
180
Φ°

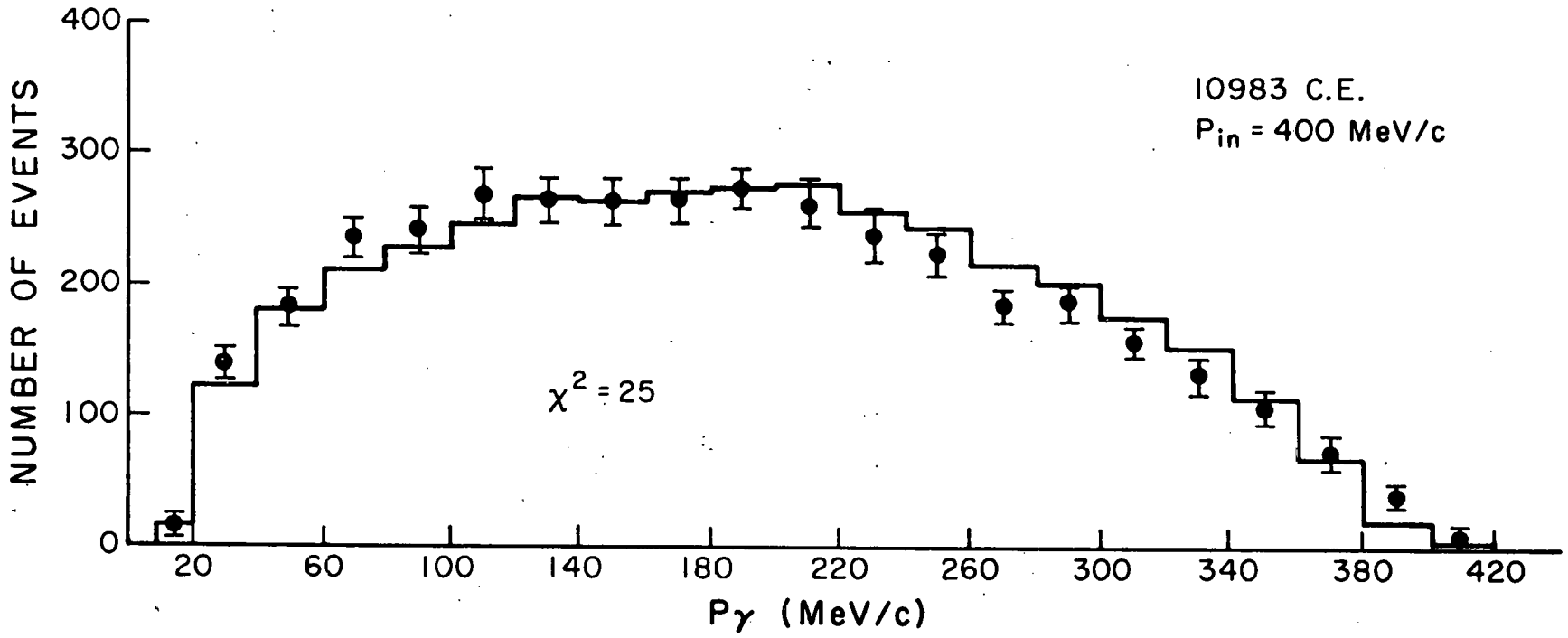

Figure 22 PRODUCTION MOMENTUM DISTRIBUTION OF GAMMAS OBSERVED

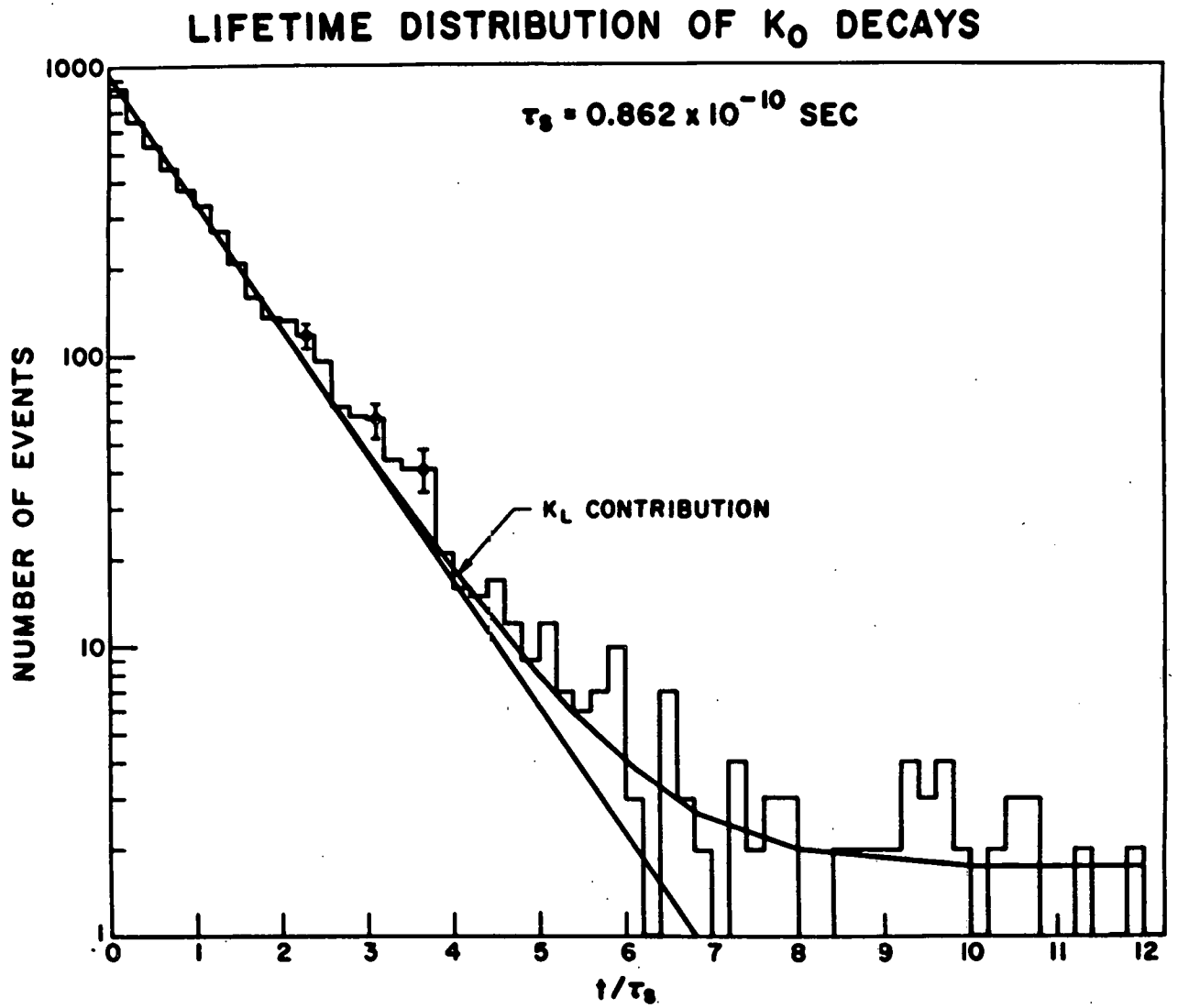

Fig. 23 CHARGED MODE DECAY LIFETIME

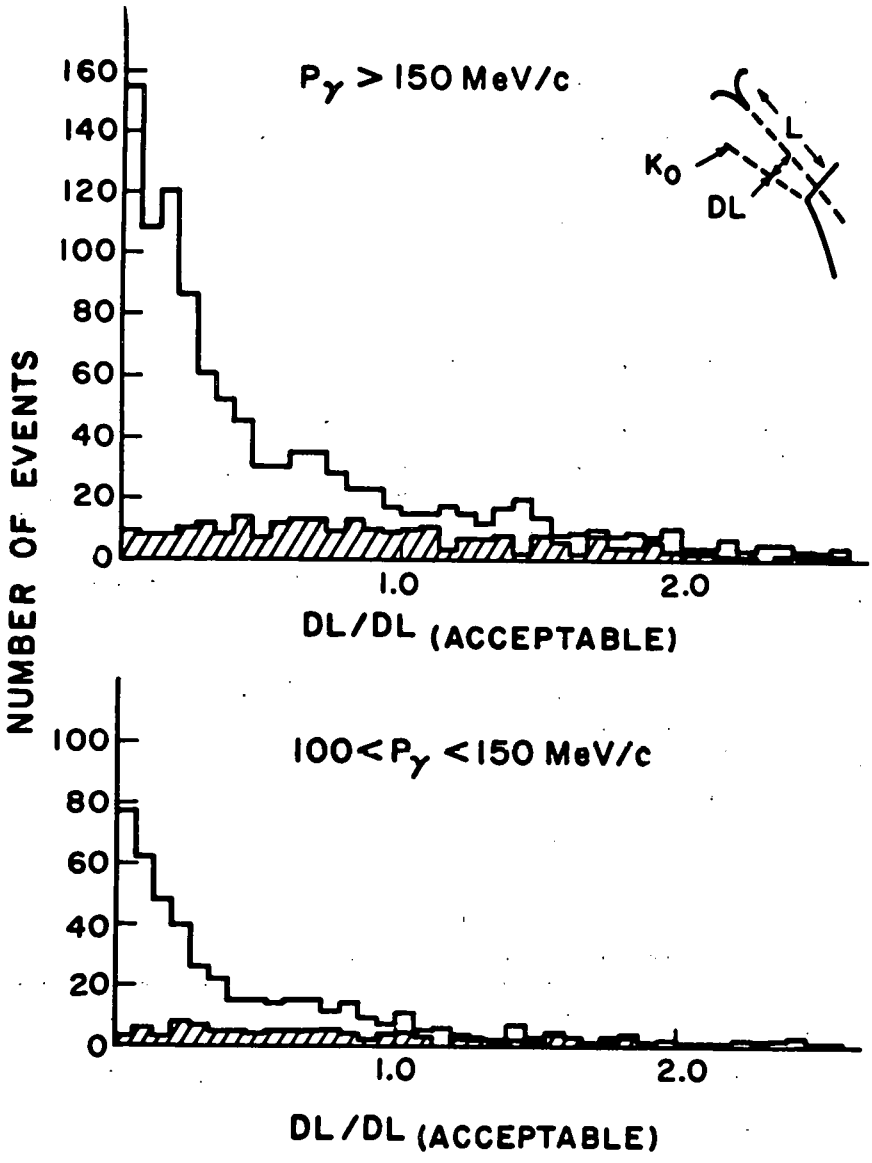
$P_\gamma > 150$ MeV/c
K_0
L
DL
NUMBER OF EVENTS
160
140
120
100
80
60
40
20
0
1.0
2.0
DL/DL (ACCEPTABLE)
$100 < P_\gamma < 150$ MeV/c
100
80
60
40
20
0
1.0
2.0
DL/DL (ACCEPTABLE)

Fig. 24

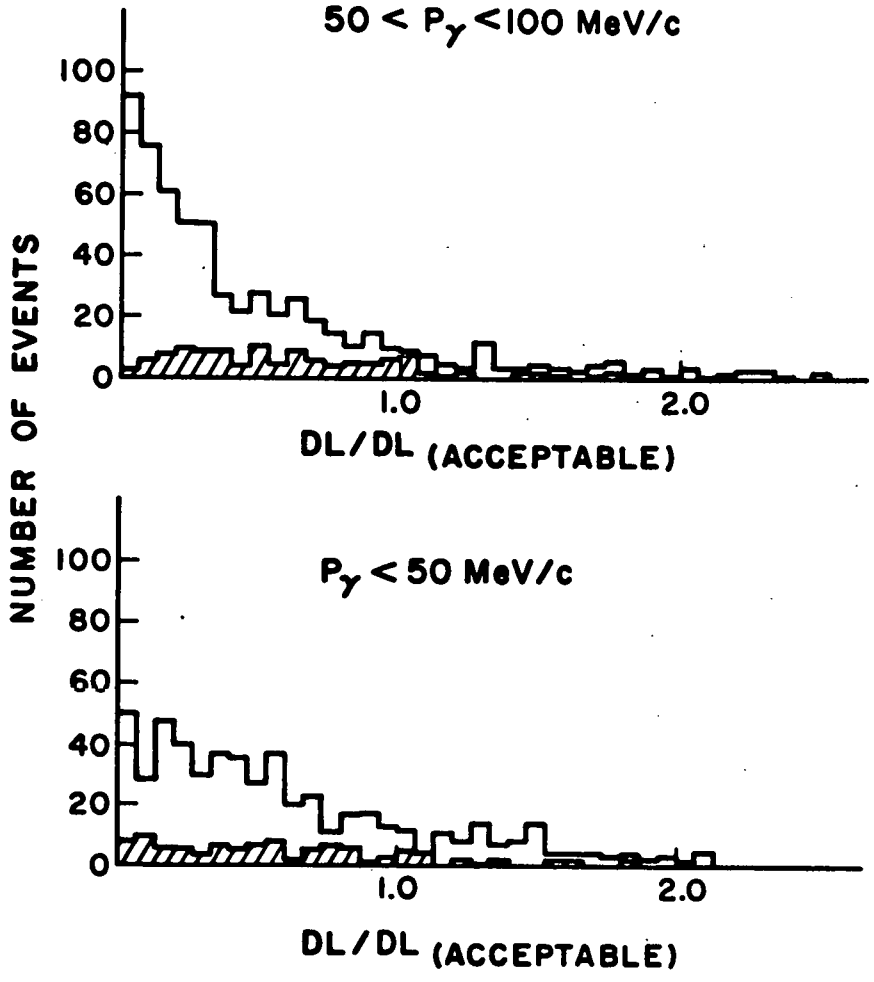
50 < P_γ <100 MeV/c
100
80
60
40
20
0
1.0
2.0
DL/DL (ACCEPTABLE)
NUMBER OF EVENTS
P_γ < 50 MeV/c
100
80
60
40
20
0
1.0
2.0
DL/DL (ACCEPTABLE)

Fig. 25

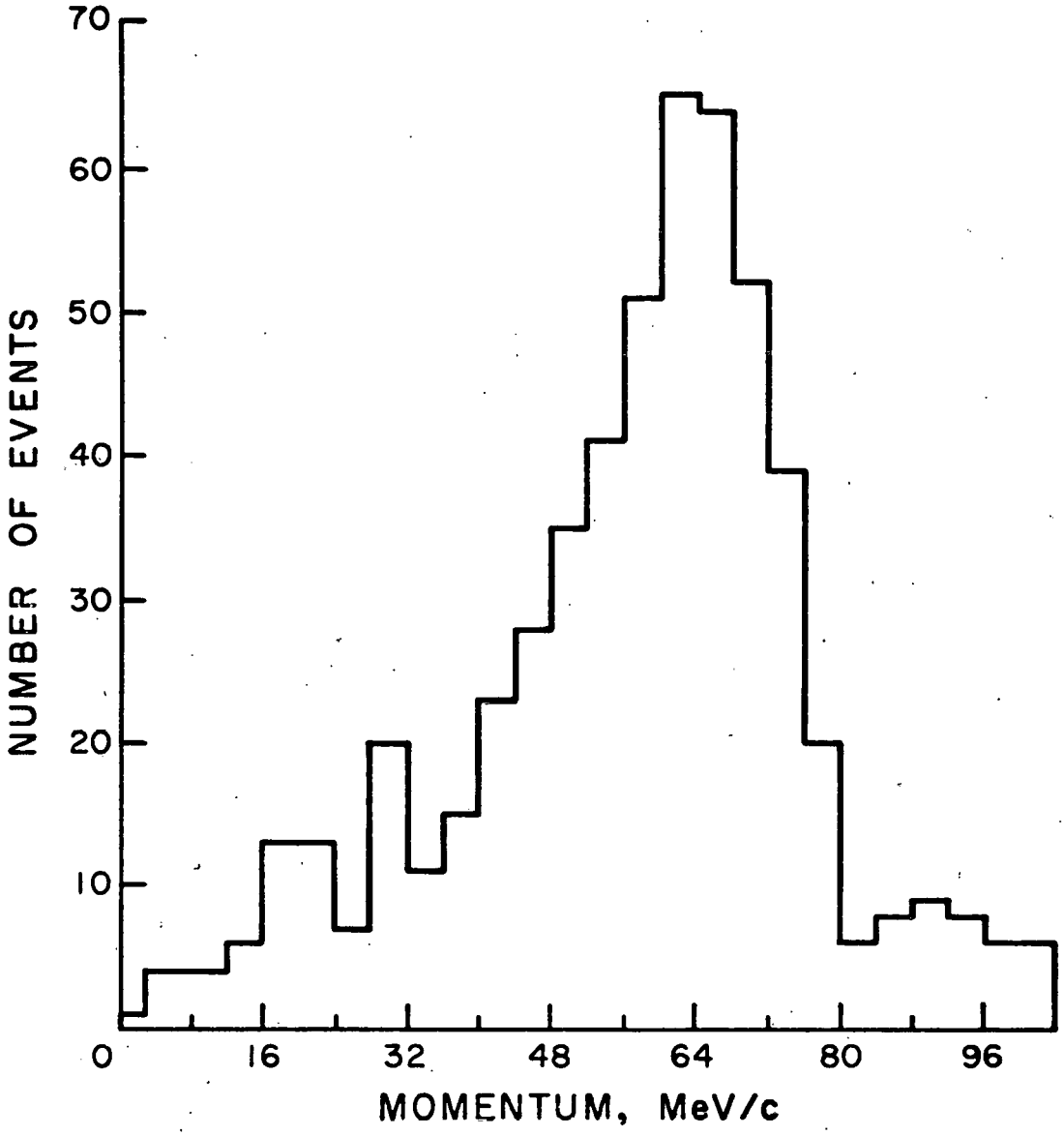

Figure 26 GAMMA MOMENTUM IN π^0 CENTER OF MASS FOR GAMMAS ASSIGNED TO $K\pi_2$ DECAYS

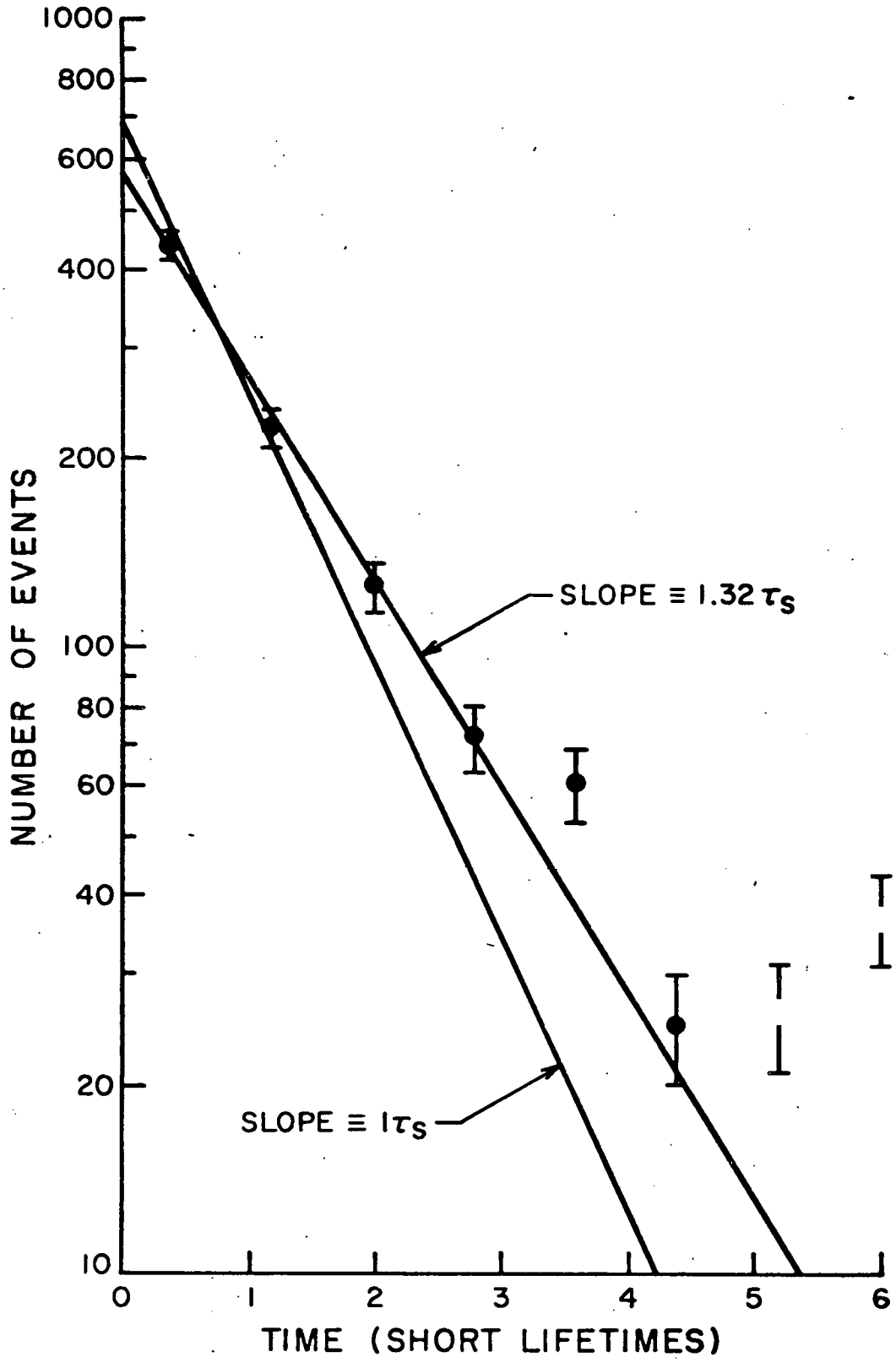

Figure 27 KO LIFETIME DISTRIBUTION DETERMINED FROM THE DETECTED GAMMAS

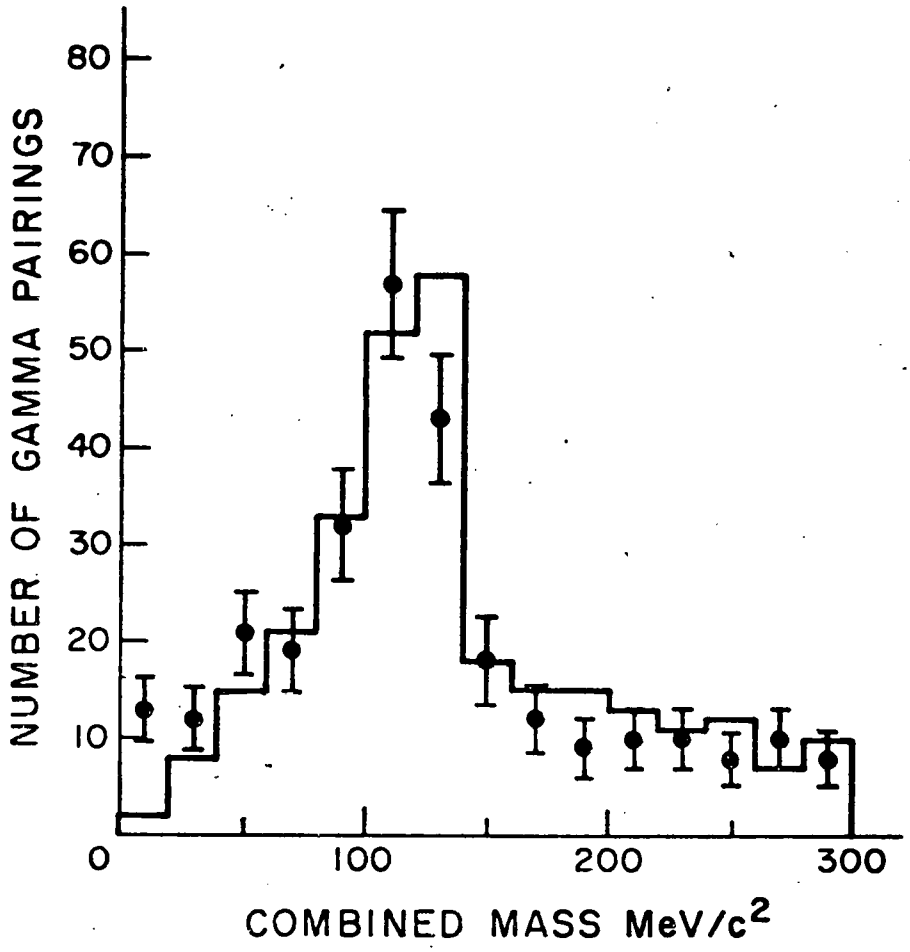

Fig. 28 APPARENT COMBINED MASS OF GAMMAS FOR EVENTS WITH MORE THAN ONE DETECTED GAMMA

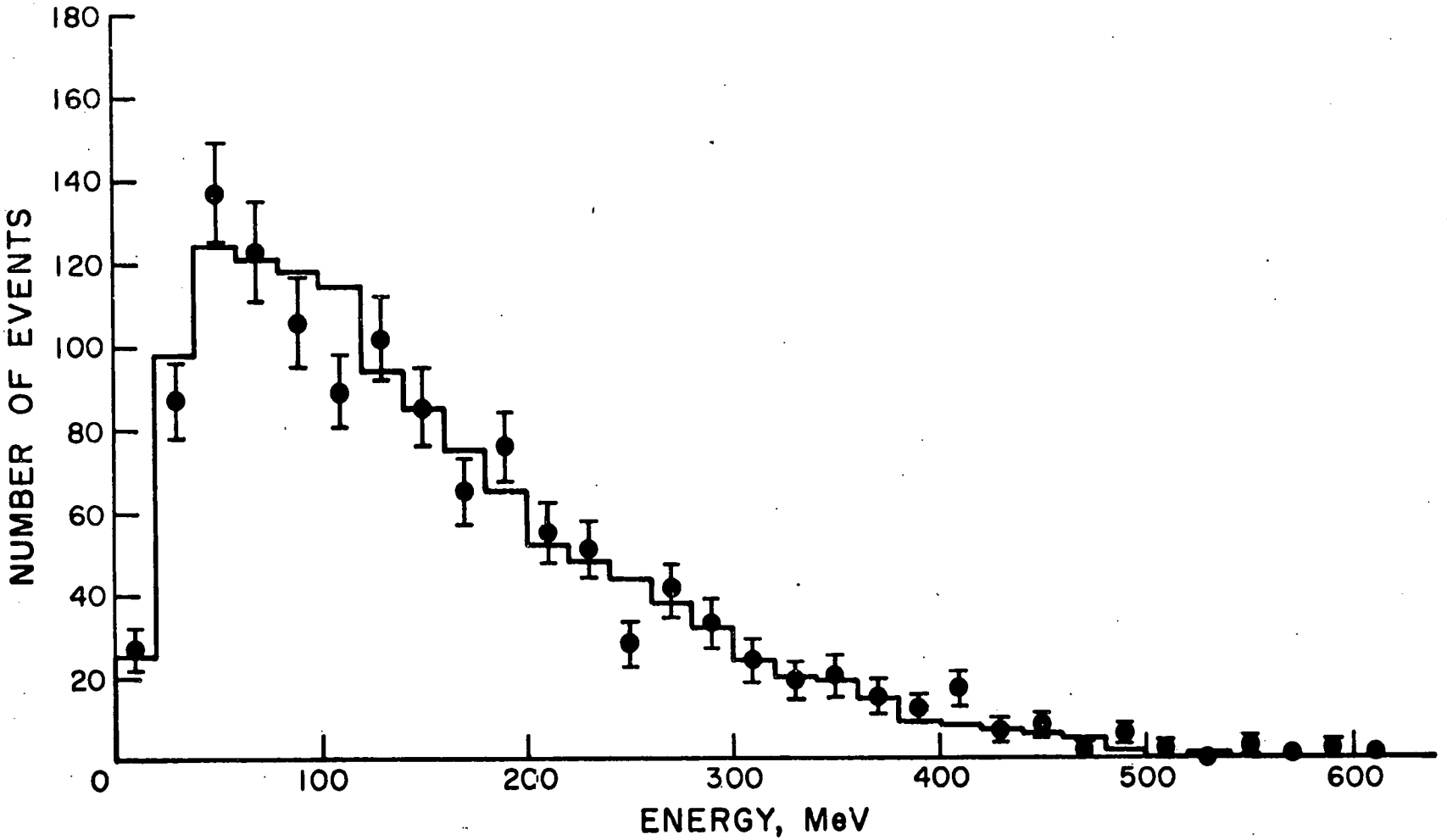

Figure 29 EMERGING ELECTRON ENERGY FOR GAMMAS ASSIGNED TO MAIN KO DECAY

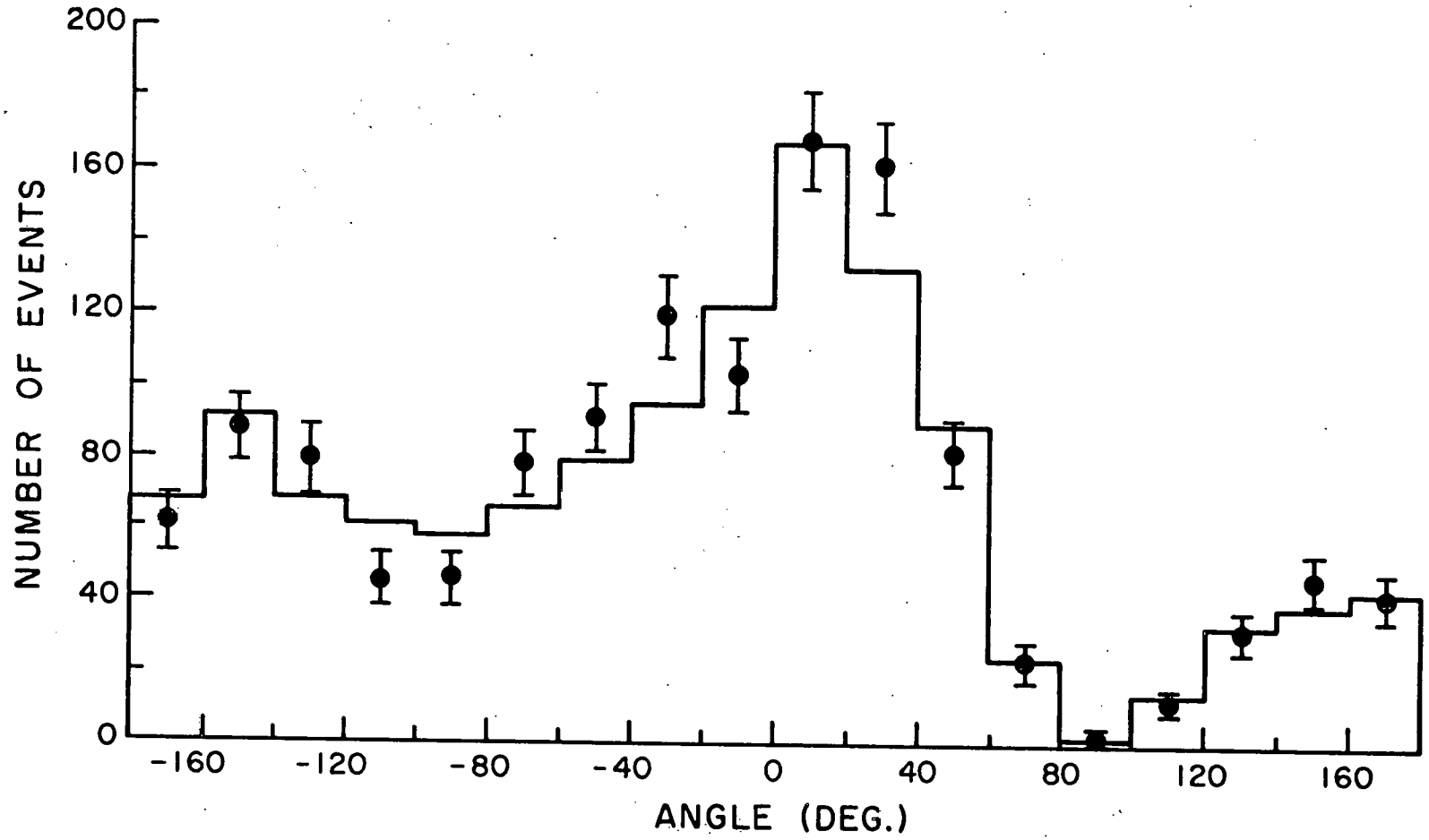

Figure 30 POLAR ANGLE IN FIDUCIAL PLANE OF GAMMAS ASSIGNED TO MAIN KO DECAY

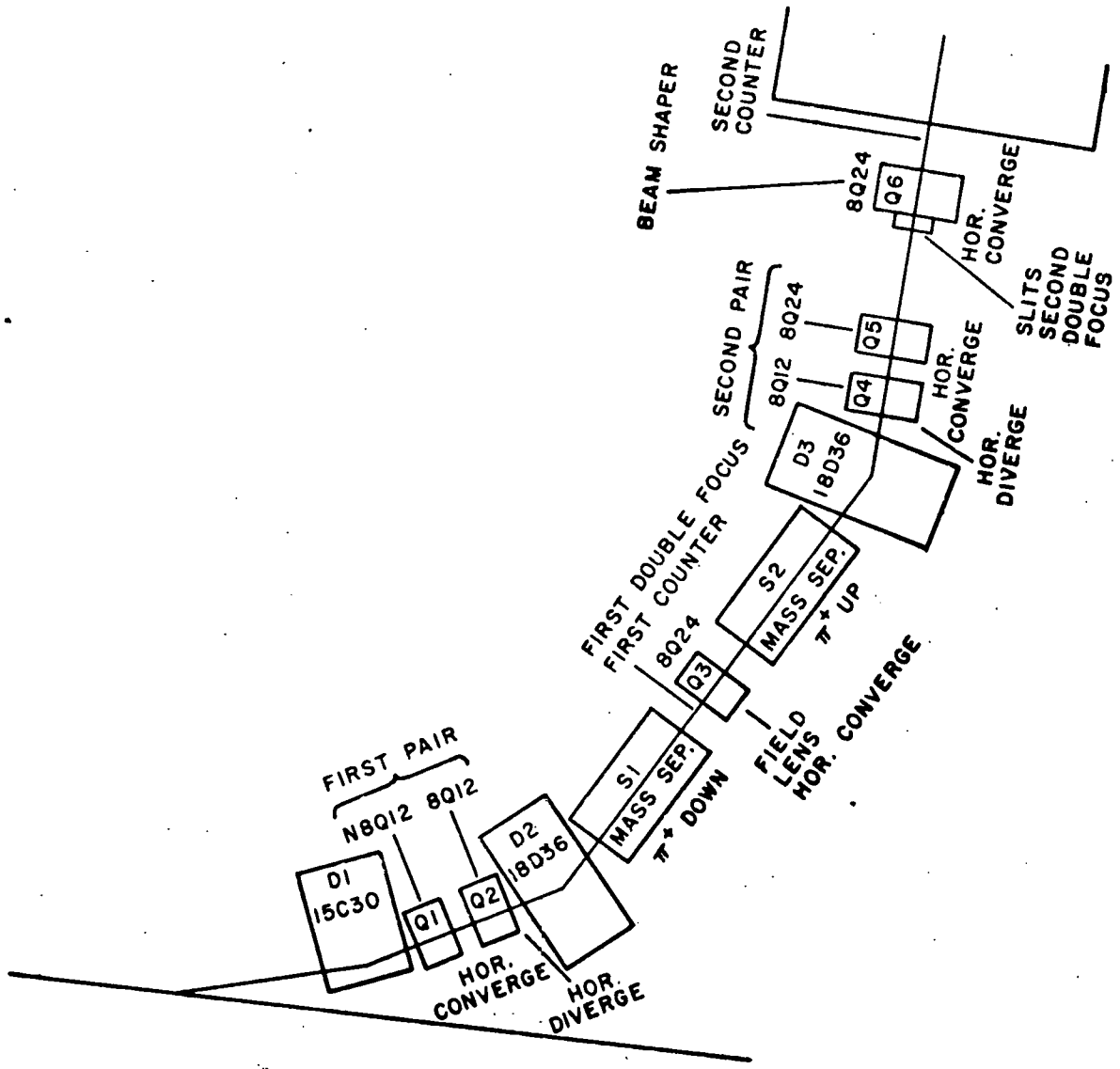

DISTANCE BETWEEN COUNTERS ≈ 400 Inches

Figure 31

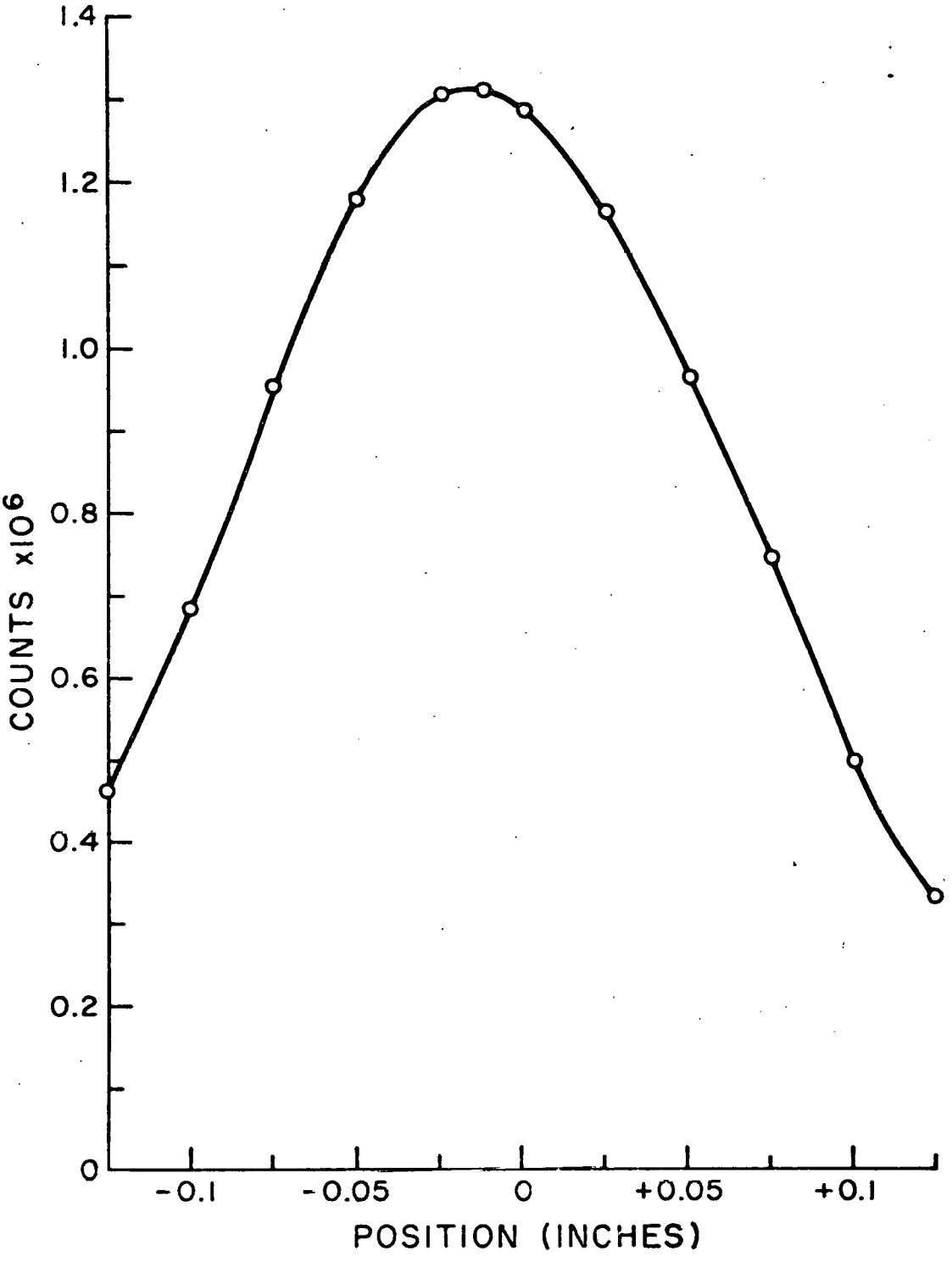

Fig. 32 632 MeV/c PION BEAM PROFILE AT FIRST MASS SLIT TAKEN WITH 1/16" WIDE COUNTER